Structural studies on the von Willebrand Factor A1 and A3 domains

Binding to GpIbα and collagen

Structurele studies over de von Willebrand Factor A1 en A3 domeinen
Binding aan GpIbα en collageen

(met een samenvatting in het Nederlands)

Proefschrift ter verkrijging van de graad van doctor aan de Universiteit Utrecht op gezag van de Rector Magnificus Prof. Dr. W.H. Gispen, ingevolge het besluit van het College voor Promoties in het openbaar te verdedigen op dinsdag 1 oktober 2002 des namiddags te 12.45 uur

door

Roland Antonius Paulus Romijn

geboren op 12 februari 1971 te Tiel

1e Promotor: Prof. Dr. J.J. Sixma
Laboratorium voor Thrombose en Haemostase,
Faculteit Geneeskunde, Universiteit Utrecht

2e Promotor: Prof. Dr. P. Gros
Sectie Kristal- en Structuurchemie, Faculteit Scheikunde, Universiteit Utrecht

Co-promotor: Dr. E.G. Huizinga
Laboratorium voor Thrombose en Haemostase,
Faculteit Geneeskunde en
Sectie Kristal- en Structuurchemie, Faculteit Scheikunde, Universiteit Utrecht

ISBN 90-393-3113-8

The research described in this thesis was supported by the Nederlandse Organisatie voor Wetenschappelijk Onderzoek (grand 902.26.193).

Aan Monique en onze kinderen

Contents

Get Acrobat Reader

Chapter 1

General introduction on von Willebrand Factor

List of abreviations

a.u.	asymmetric unit
CR	Complement receptor
CD	Cluster of Differenciation
EC	Endothelial Cells
iC3b	inactivated Complement 3b
ICAM	Intercellular Adhesion Molecule
LFA-1	Leukocyte Function-associated Antigen 1
LRR	Leucine-rich repeat
Mac-1	Macrophage antigen alpha polypeptide-1
MIDAS	Metal Ion Dependent Adhesion Site
TTP	Thrombotic Thrombocytopenic Purpura
VCAM-1	Vascular Cell Adhesion Molecule-1
VLA	Very Late Antigen
VWF	von Willebrand Factor
vWFcp	von Willebrand Factor cleaving protease, also known as ADAMTS13
ADAMTS	A Desintegrin And Metalloprotease with Thrombospondin Motives

Chapter 1 Introduction

Discovery of Von Willebrand Factor

In 1926 the Finnish Internist Eric A. von Willebrand reported a case of patients from the Åland Islands with "hereditary pseudohaemophilia" [1]. Elongated bleeding and clotting times were manifested. It was not real haemophilia, because both male and female were affected. In 1953 it was found that patients with von Willebrand Disease also lacked factor VIII. In 1972 von Willebrand Factor was purified and the protein was sequenced by Edman degradation in 1986 [2]. The cDNA was cloned and sequenced in 1985 [3; 4]. The last decades, von Willebrand factor (vWF) is intensively studied and slowly the secret of its action becomes clear.

Normal haemostasis is dependent on vWF

Haemostasis can be divided in two different processes, i) staunching, which is the process that stops the bleeding due to the formation of a platelet plug and ii) coagulation, which is the process of fibrin formation that stabilises the platelet plug. Coagulation is dependent on the presence of coagulation proteins, calcium and the negatively charged phospholipid phosphatidyl serine. The latter two compounds are provided by platelets that become adhered at the site of vascular damage. Platelet plug formation is dependent on von Willebrand Factor and adhesive compounds from the vascular matrix [5].

Upon damage of the vessel wall, contents of the vessel wall are exposed to the blood. *In vitro* it has been shown that vWF can bind to fibrillar collagen types I, III and IV [6]. *In vivo*, however, vWF is co-localised with collagen types I, III and VI in the subendothelium [7; 8] and not with collagen type IV [9]. When vWF is immobilised to the subendothelium, it can bind to platelet glycoprotein (Gp) Ibα via its A1 domain [10]. The interaction of the A1 domain with GpIbα has relative high association- and dissociation rate constants, thereby preventing permanent arrest of the platelet [11-13]. In other words, the platelets tether and or roll over the surface. However, tethering platelets do slow down via interactions of platelet receptor GPVI with collagen [14]. Due to the interaction of GpVI with collagen, the platelet becomes activated (the activation process involves many signal transduction pathways and will not be discussed here) that results in binding of integrin $\alpha_2\beta_1$ to collagen and binding of integrin $\alpha_{2b}\beta_3$ to the RGD sequences of fibrinogen and vWF [15]. The latter event results in platelet-platelet interactions leading to platelet plug formation. The adhered platelets spread, release their granular contents (calcium, ADP and coagulation factors) and the negatively charged phospholipid

phosphatidyl serine becomes exposed. Now coagulation starts and the thrombus obtains it final strength.

Biosynthesis of vWF

The vWF gene is located on chromosome 12p13.3 and spans approximately 178 kilo basepairs. It contains 52 exons which code for 2813 amino acid residues [2; 4]. A pseudogene is located on chromosome 22q11.1, is 21-29 kbp in length and spans exons 23-34 [16]. The overall homology between the vWF gene and pseudogene is 96.9 %. There is slight divergence between the sequences corresponding to the exons (97.5 %) and slightly more divergence for the introns (96.8 %).

VWF is synthesised as pre-pro-vWF in megakaryocytes [17] and endothelial cells (EC) [18; 19]. After synthesis, the 22 amino-acid residues of the vWF pre-peptide are cleaved off in the endoplasmatic reticulum, vWF is dimerised at the C-terminus and partially glycosylated [20; 21]. VWF-dimers are transported to the Golgi apparatus and multimerisation takes place in the trans Golgi network [22]. Sorting to the Golgi-apparatus does not require the propeptide, also known as vWF-Ag II [23], whereas multimerisation does [24]. For multimerisation the propeptide does not have to be covalently linked to the protein [25]. The protease furin cleaves the pro-peptide but the peptide remains non-covalently associated with mature vWF [22; 26]. Any uncleaved propeptide is removed from the multimer in the plasma, but the enzyme responsible for this process remains unknown [27]. Additional *N*-linked and *O*-linked glycosylation [28; 29] and sulfation [22] occurs. VWF is *N*-glycosylated at asparagine residues 94, 384, 468, 752, 811, 1460, 1527, 1594, 1637, 1783, 1822 and 2027. *O*-linked glycosylation sites are threonine residues 485, 492, 493, 705, 714, 724, 916 and 1535 and serine 500 and 723 [2].

After synthesis, vWF is partitioned between two pathways. Approximately 95 % is constitutively secreted. The remainder is stored in the tubular structures in α-granula of megakaryocytes [29] and in Weibel-Palade bodies of endothelial cells [29; 30]. Weibel-Palade bodies are not formed in vWF deficient cells, whereas α-granula are still present, but these granula lack the tubular systems [31]. Sorting of vWF to storage granules requires the propeptide, and Arg^{416} has been shown to be essential [23; 32]. This implies that the propeptide functions as a catalyst in multimerisation and as a molecular chaperone in translocation to storage granules. The stoichiometry of the propeptide and mature vWF is 1:1 in the Weibel-Palade bodies.

In vivo, vWF and propeptide plasma levels are 10 and 1 µg/ml, respectively. Half-lifes are 12 h and 2 h, respectively [33]. VWF plasma levels depent on the blood group [34]. Blood group AB persons have an average plasma level of 12.2 µg/ml, blood groups A and B 10.6 µg/ml and blood group O 8.8

µg/ml. Propeptide levels are not blood group type sensitive, because the propeptide does not contain the A and B oligosaccharides whereas mature vWF does [35; 36]. Increased plasma levels can result from stimulation of endothelial cells by for example 1-desamino-8-D-arginine vasopressin (DDAVP) [37].

Functional domains of mature vWF

Mature, monomeric vWF consists of 2050 amino acid residues in twelve domains (figure 1) [38]. VWF multimerises upto 80 monomers in a multimer [39]. The D3 domain contains cysteins that form the N-terminal intermolecular disulfide bridges. Intermolecular disulfide bridges are formed involving Cys^{379} [40], and at least one cysteine of triplet Cys^{459}-Cys^{462}-Cys^{464} [40; 41]. The CK domain, residues 1961 – 2050, contains cysteins that are involved in C-terminal intermolecular disulfide bridges probably requiring Cys^{2008}, Cys^{2010} and Cys^{2048} [42]. Intra-molecular disulfide bridges are formed between Cys^{1961}-Cys^{2011}, Cys^{1987}-Cys^{2041}, Cys^{1991}-Cys^{2043} and Cys^{1976}-Cys^{2025} within the CK domain [42]. The D´ and the D3 domains are involved in binding clotting factor VIII [43-45] thereby preventing factor VIII from binding to membrane surfaces and activation and degradation by a variety of serine proteases [46]. Factor VIII binding affinity decreases when vWF is bound to collagen [47]. The A1 domain binds GpIbα [10], heparin [10], collagen type III and VI [8; 48-50] and sulfatides [50-52]. The linker between the A1 and A2 domains is involved in binding to leukocytes [53]. The A2 domain contains the proteolytic cleavage site for the vWF protease [54]. The A3 domain contains the collagen binding site [48; 55]. No specific function has been assigned for the D4 and B domains. The C domains contain the recognition sequence RGD at residues 2507-2509, which bind to platelet integrin $\alpha_{2b}\beta_3$ [56]. The vWF multimeric structure is essential for its function [57; 58]. In collagen binding, multimeric vWF displays an apparent K_d of 1 – 7 nM [59], while monomeric, recombinant A3 binds collagen with a K_d of 2 µM [60]. In contrast, factor VIII binding only requires N-terminal dimers.

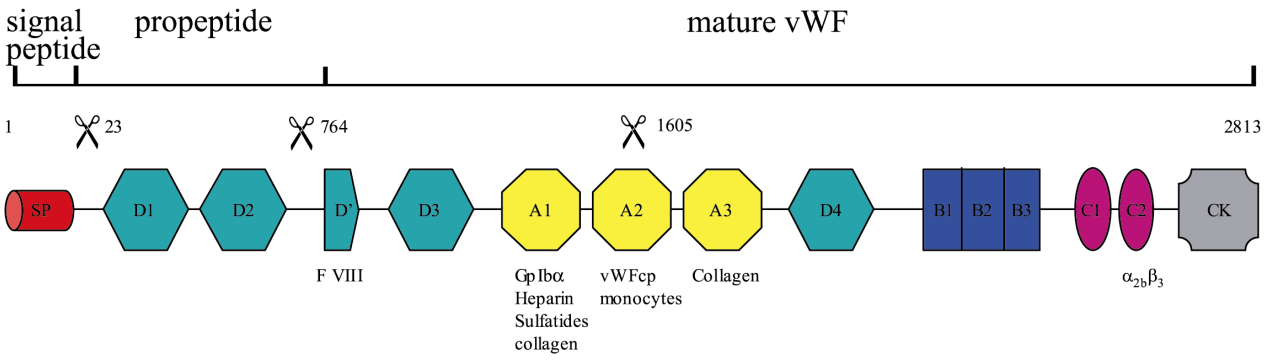

Figure 1: Schematic representation of the pre-pro-vWF domain organisation. Scissors indicate sites where vWF is cleaved during synthesis (before Ala^{23} and Ser^{764}) or in plasma in the A2 domain (after Tyr^{1605}) by the vWFcp. Of note, the diagram is not on scale.

A-type domains

A-type domains (and homologous integrin I- or inserted domains) are recognized in vWF A1, A2 and A3 domains, integrins of the β_1 family, $\alpha_1\beta_1$, $\alpha_2\beta_1$, $\alpha_{10}\beta_1$, $\alpha_{11}\beta_1$, integrins of the β_2 family, $\alpha_L\beta_2$, $\alpha_X\beta_2$, $\alpha_M\beta_2$, integrins α_D, $\alpha_E\beta_7$, different collagen subtypes, complement components [61] and other proteins. A brief summary of A type domains is given in Table I and figure 2.

A-type domains adopt a so-called Rossman or di-nucleotide binding fold that consists of a central hydrophobic β-sheet, flanked on both sides by amphipathic α-helices (figure 3). The top face consists of loops connecting the α-helices and the β-strands and contains the metal-ion-dependent-adhesion-site (MIDAS) motive. The MIDAS motive will be discussed below. The bottom face consists of loops connecting the α-helices and the β-strands and contains a disulfide bridge.

Table I
vWF domains and integrin receptors containing A- or I-type domains

Receptor	Alternative name(s)	Ligand(s)	References
vWF-A1		GpIbα, collagen type III and VI, botrocetin, ristocetin, heparin, sulfatides, bitiscetin	10; 41; 62-66
vWF-A2		vWFcp	67; 68
vWF-A3		collagen type I and III, bitiscetin	55; 69
$\alpha_1\beta_1$	VLA-1, CD49a/CD29	collagen, laminin-1	56; 70
$\alpha_2\beta_1$	VLA-2, GpIa/IIa, CD49b/CD29	collagen I and III	56; 71-75
$\alpha_{10}\beta_1$		echovirus, laminin-1 collagen II	76
$\alpha_{11}\beta_1$		collagen	56; 77
$\alpha_D\beta2$	CD11d/CD18, ADB2, leucointegrin alpha D	VCAM1	78
$\alpha_E\beta7$	CD103, mucosal lymphocyte-1 antigen	E-Cadherin	56
$\alpha_L\beta_2$	CD11a/CD18, LFA-1 lymphocyte function-associated antigen 1	ICAM-1, -2, -3, -4, -5	56; 79 80
$\alpha_M\beta_2$	Mac-I, CR3 CD11b/CD18, Mo1	iC3b, Factor X, ICAM-1, neutrophil inhibitory factor	56; 81 80; 82
$\alpha_X\beta_2$	Leukocyte adhesion-receptor p150,95, CD11c/CD18	iC3b	56

```
                                  β1                  α1                        β2        β3        α2
vWF-A1    498 DISEPPLHDFYCSRLLDLVFLLDGSSRLSEAEFEVLKAFVVDMMERLRISQKWVRVAVVEYHDGSHAYIGLKDRKRPSEL
vWF-A2    722 VSTLGPKRN---SMVLDVAFVLEGSDKIGEADFNRSKEFMEEVIQRMDVGQDSIHVTVLQYSYMVTVEYPFSEAQSKGDI
vWF-A3    922 ----------DCSQPLDVILLLDGSSSFPASYFDEMKSFAKAFISKANIGPRLTQVSVLQYGSITTIDVPWNVVPEKAHL
Alpha 1   131 -----------CSTQLDIVIVLDGSNSIYP--WDSVTAFLNDLLERMDIGPKQTQVGIVQYGENVTHEFNLNKYSSTEEV
alpha 2   137 --------RSSCPSLIDVVVVCDESNSIYP--WDAVKNFLEKFVQGLDIGPTKTQVGLIQYANNPRVVFNLNTYKTKEEM
Alpha 10  159 --------AQRCPTYMDVVIVLDGSNSIYP--WSEVQTFLRRLVGKLFIDPEQIQVGLVQYGESPVHEWSLGDFRTKEEV
Alpha 11  157 ---------QRCQTYMDIVIVLDGSNSIYP--WVEVQHFLINILKKFYIGPGQIQVGVVQYGEDVVHEFHLNDYRSVKDV
Alpha D   142 --------PECPHQEMDIVFLIDGSGSIDQNDFNQMKGFVQAVMGQFEGT--DTLFALMQYSNLLKIHFTFTQFRTSPSQ
Alpha E   194 --------EEEEEAGTEIAIILDGSGSIDPPDFQRAKDFISNMMRNFYEKCFECNFALVQYGGVIQTEFDLRDSQDVMAS
alpha L   125 ----------CIKGNVDLVFLFDGSMSLQPDEFQKILDFMKDVMKKLSN--TSYQFAAVQFSTSYKTEFDFSDYVKRKDP
Alpha M   134 ---------GCPQEDSDIAFLIDGSGSIIPHDFRRMKEFVSTVMEQLK--KSKTLFSLMQYSEEFRIHFTFKEFQNNPNP
Alpha X   143 --------QECPRQEQDIVFLIDGSGSISSRNFATMMNFVRAVISQFQRP-S-TQFSLMQFSNKFQTHFTFEEFRRTSNP

                                 α3                  β4                        α4        β5
vWF-A1          RRIASQVKYAGSQVASTSEVLKYTLFQIFSKI--DRPEASRIALLLMASQEPQRMSRNFVRYVQGLKKKKVIVIPVGIG-
vWF-A2          LQRVREIRYQGGNRTNTGLALRYLSDHSFLVSQGDREQAPN-LVYMVTGNPASD---EIKR-LPG----DIQVVPIGVG-
vWF-A3          LSLVDVMQREGG-PSQIGDALGFAVRYLTSEMHGARPGASKAVVILVTDVSVDS----VDAAADAARSNRVTVFPIGIG-
Alpha 1         LVAAKKIVQRGGRQTMTALGIDTARKEAFTEARGARRGVKKVMVIVTDGESHDNH--RLKKVIQDCEDENIQRFSIAILG
alpha 2         IVATSQTSQYGGDLTNTFGAIQYARKYAYSAASGGRRSATKVMVVVTDGESHDGS--MLKAVIDQCNHDNILRFGIAVLG
Alpha 10        VRAAKNLSRREGRETKTAQAIMVACTEGFSQSHGGRPEAARLLVVVTDGESHDGE--ELPAALKACEAGRVTRYGIAVLG
Alpha 11        VEAASHIEQRGGTETRTAFGIEFARSEAF-Q-KGGRKGAKKVMIVITDGESHDSP--DLEKVIQQSERDNVTRYAVAVLG
Alpha D         QSLVDPIVQLKG-LTFTATGILTVVTQLFHHKNGARKSAKKILIVITDGQKYKDPL-EYSDVIPQAEKAGIIRYAIGVG-
Alpha E         LARVQNITQVGS-VTKTASAMQHVLDSIFTSSHGSRRKASKVMVVLTDGGIFEDPL-NLTTVINSPKMQGVERFAIGVG-
alpha L         DALLKHVKHMLL-LTNTFGAINYVATEVFREELGARPDATKVLIIITDGEATDS------GNIDAAK--DIIRYIIGIG-
Alpha M         RSLVKPITQLLG-RTHTATGIRKVVRELFNITNGARKNAFKILVVITDGEKFGDPLGY-EDVIPEADREGVIRYVIGVG-
Alpha X         LSLLASVHQLQG-FTYTATAIQNVVHRLFHASYGARRDATKILIVITDGKKEGDSL-DYKDVIPMADAAGIIRYAIGVG-

                α5'          α5              β6      α6          (α7)
vWF-A1          -----PHAN---LKQIRLIEKQAPENKAFVLSSVDELEQQRD---EIVSYLCDLAPEAPPPT
vWF-A2          -----PNAN---VQELERIGWP---NAPILIQDFETLPREAP---DLVLQRCCSGEGLQIPT
vWF-A3          -----DRYD---AAQLRILAGPAGDSNVVKLQRIEDLPTMVTLGNSFLHKLCSG--------
Alpha 1         SYNRGNLSTEKFVEEIKSIASEPTEKHFFNVSDELALVTIVK---TLGERIFALEATADQSA
alpha 2         YLNRNALDTKNLIKEIKAIASIPTERYFFNVSDEAALLEKAG---TLGEQIFSIEGGT----
Alpha 10        HYLRRQRDPSSFLREIRTIASDPDERFFFNVTDEAALTDIVD---ALGDRIFGLEGSHAENE
Alpha 11        YYNRRGINPETFLNEIKYIASDPDDKHFFNVTDEAALKDIVD---ALGDRIFSLEGTN-KNE
Alpha D         ----HAFQGPTARQELNTISSAPPQDHVFKVDNFAALGSIQK---QLQEKIYAVEGTQSRAS
Alpha E         ----EEFKSARTARELNLIASDPDETHAFKVTNYMALDGLLS---KLRYNIISMEGTVG---
alpha L         -KHFQTKES---QETLHKFASKPASEFVKILDTFEKLKDLFT---ELQKKIYVIEG------
Alpha M         -DAFRSEKS---RQELNTIASKPPRDHVFQVNNFEALKTIQN---QLREKIFAIEG------
Alpha X         ----LAFQNRNSWKELNDIASKPSQEHIFKVEDFDALKDIQN---QLKEKIFAIEGTETTSS
```

Figure 2: Alignment of vWF-A and integrin-I domains**.** The domains were pre-aligned using ClustalW 1.81 at the EBI website (http://www.ebi.ac.uk/clustalw/). Alignments of domains with known crystal structures were optimised based on a superposition of the models. The alignment of domains with unknown crystal structure were adjusted to the crystal-structure optimised alignment. Residues in *Bold* form the MIDAS motive, α-helices and β-strands are indicated by the *dark* and *blue* boxes, respectively.

click on this link for rotating image

Figure 3: Structure of the A- or I-type domains. The vWF-A1 domain is shown. A-type domains contain a so-called dinucleotide binding or Rossmann fold that consists of a central β-sheet which is flanked on both sides by α-helices (colour coded in *red* and *blue*, respectively). The top- and bottom faces contain loops connecting the α-helices and β-sheet. The bottom-face contains the disulfide bridge and in integrin I-domains the top face contains the MIDAS motif. In the vWF-A1 domain vWD type 2B mutations cluster at the bottom of the domain and vWD type 2M mutations scatter all over A1.

A1 domain

The vWF-A1 domain spans residues 509 – 695 and contains the GpIbα binding site [10; 41; 63]. The crystal structure has been solved [83; 84]. It binds to GpIbα [10], collagen [48 48; 64], ristocetin [66], botrocetin [65], bitiscetin [85], sulfatides [50-52] and heparin [10; 50; 86]. The sulfatide- and heparin-binding sites probably do not overlap [52]. The N- and C-termini are linked by a disulfide bridge. The formation of this disulfide bridge is an absolute requirement for a proper function of the vWF-A1 domain. In the absence of the disulfide bridge, the GpIbα binding affinity is strongly reduced [87-90]. Moreover, the function of the A1 domain is modulated by the number of residues in the N- and C-terminal peptides [91] and the presence of *O*-linked glycans. The number of residues in the flanking peptides required for a proper modulation of the A1-domain is still a matter of debate (table II). Removal of the *O*-linked glycans [89; 92] or desialisation [93] pro-activates the A1 domain. The antibiotic ristocetin A and the snake toxins botrocetin and bitiscetin bind to specific sequences in A1 resulting in activation of A1.

The A1 domain does not bind spontaneously to GpIbα, therefore it needs to be activated. Activation can be achieved via vWF-immobilisation to a surface (for example the vessel wall), although it is not clear whether activation occurs due to a conformational change in vWF or because the local vWF-concentration is increased. Additionally, vWF can be activated due to vWD type 2B mutations and activators like ristocetin or botrocetin and will be discussed below. The strucure of the A1•GpIbα complex and conformational changes in the A1 domain that result in GpIbα binding are the subject of chapters five and six of this thesis.

Table II
Effect of the length of the N- and C-terminal flanking peptides on the activation-state of A1

Construct	Origin	Effect in GpIb binding	References
plasma vWF	human	No spontaneous binding to GpIb, ristocetin and botrocetin activate binding	94; 95
441-730	CHO/COS-7	No spontaneous binding to GpIb, ristocetin activates	87
481-718	human	No spontaneous binding to platelets, ristocetin and botrocetin activate	87
481-718 Δsialic acid	human	Bit spontaneous binding to platelets, ristocetin does not activate, botrocetin activates	89
475-709	COS-7	No spontaneous binding to GpIb, ristocetin activates	96
441-704	*E. coli*	Little bit spontaneous binding to platelets, botrocetin activates	89
475-709	*E. coli*	No spontaneous binding to GpIb, less ristocetin required for activation	90
508-704	*E. coli*	Binds spontaneous to platelets, less platelets bind to A1-coated surface at high shear stress and the platelets that become attached to the surface do not tether	96
508-733	*E. coli*	Spontaneous binding to platelet, botrocetin activates	

A2 domain

Defining the borders of the A2 domain is not straightforward, because the A2 domain does not contain a disulfide bridge connecting the N- and C-termini. Based on sequence homology with other A-type domains, we define the borders between residues Ser^{731} and Cys^{907} (figure 2). The A2 domain contains the cleavage site for the von Willebrand Factor cleaving protease (vWFcp) that is also known as ADAMTS13 [54; 97; 98]. The gene for the vWFcp is located on chromosome 9q34. This enzyme cleaves the A2 domain between residues Tyr^{842} and Met^{843} resulting in lower vWF multimers [99; 100]. The A2 domain contains a disulfide bridge at the bottom of the domain, but this disulfide bridge does not connect the N- and C-terminal flanking peptides. The disulfide bridge is formed between two consecutive residues. The aberrant disulfide bridge is essential, because otherwise a proteolytic cleavage within the A2 domain does not decrease the multimeric size of vWF.

A number of mutations in the A2 domain (and also some in the A1 domain), so-called vWD type 2A mutations, have been identified in patients that make vWF more sensitive towards the vWFcp [101]. Most likely, these mutations partially unfold the A2 domain thereby making the A2 domain more susceptible to the protease. As a result, these patients lack the high-molecular-weight multimers in their plasma. The partial unfolding (or sensitisation) of vWF is probably required for efficient proteolysis for several reasons. i) Based on homology with other A-type domains it is most likely that the Tyr^{842}-Met^{843} peptide bond is located in the interior of the domain (figure 4), ii) *in vivo* application of shear increases the proteolysis [102], iii) *In vitro* low ionic strength buffers and denaturating agents are required for proteolysis [100]. A deficiency in vWFcp-activity results in the presence of ultra-large vWF multimers that may cause thrombotic thrombocytopenic purpura (TTP), which is manifested by thrombocytopenia, microangiophatic hemolytic anemia, bleedings and other symptoms [103].

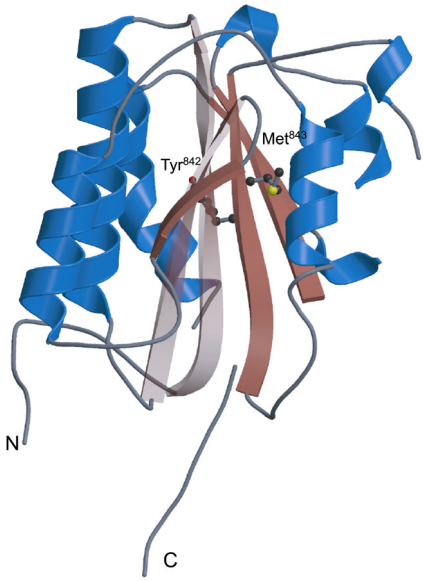

Figure 4: Model of the A2 domain. This hypothetical model of the A2-domain has been constructed based on the homologous vWF-A1 domain (PDB accession code 1auq), which, based on amino-acid sequence, is the most closely related A-type domain and has been prepared by the internet 3dpssm server (**http://www.sbg.bio.ic.ac.uk/servers/3dpssm**). Of note, the connectivity of the model is not complete, which is most significant for helix α4 that is absent in A2. Strand β2 is drawn transparent for clarity. The von Willebrand Factor cleaving protease cuts between residues Tyr^{842} and Met^{843}, which are shown in ball-and-stick representation and are located at the centre of the β-sheet in the interior of the domain.

A3 domain

The A3 domain spans residues 923 to 1109 and contains the binding site for fibrillar collagen types I and III [55; 60]. The multimeric structure of vWF is important for vWF binding to collagen. The K_d of monomeric A3 and multimeric vWF for the binding to collagen is 2 μM and 4 nM, respectiviely [59; 60; 104]. Crystal structures have been solved by two groups independently [105; 106]. The putative vWF-A3 MIDAS motif at the top-face of A3 is formed by residues Asp^{934}, Ser^{936}, Ser^{938}, Ser^{1005} and Thr^{1038} (figure 2). The latter two residues are threonine and aspartic acid in I-domains. In A3 however, the aspartic acid (Asp^{1039}) has been shifted by one residue and the hydroxyl group of Thr^{1038} is not able to coordinate to the metal ion. In addition, the side chain of Asp^{1039} (which is glycine in the case of integrin I-domains) prevents a metal-ion from entering the MIDAS motive. The MIDAS motif of integrin I-domains usually contains a magnesium or manganese ion [75; 79; 82; 107] which is absolutely required for ligand binding [108-110]. The MIDAS motif of A3 does not contain a metal-ion and the binding of A3 to collagen type I and III is metal-ion independent [105; 106; 111].

The collagen-binding site of integrin α_2 I-domain, and most likely also of the I-domain of integrins $\alpha_1\beta_1$ [70], $\alpha_{10}\beta_1$ [76], $\alpha_{11}\beta_1$ [77], is located at the top-face of the domain [74; 112]. A divalent cation, either Mg^{2+} or Mn^{2+} [108; 109], bound to the MIDAS motif is involved in collagen binding [71; 74] and the protruding additional helix determines the specificity towards certain collagen subtypes [75; 113]. The top face of the vWF-A3 domain is not involved in collagen binding [59;106; 114] and therefore the collagen-binding site on A3 must be located somewhere else. Two other studies on the collagen-binding site were conducted. Cruz *et al.* constructed an A1/A3 chimer, spanning residues 475-598/1018-1114 [104]. Collagen binding of this chimer was similar compared to wt-A3. Based on a cyanogen bromide digestion of vWF, Roth *et al.* localized a collagen-binding site within residues 948-998. An additional collagen binding site, however, was identified within residues 542-662 in A1 [48] sugesting that the collagen binding affinity of the A1/A3 chimer may also originate from residues 479-598 of the A1 domain. The exact location of the collagen-binding site in the A3 domain is the subject of chapters two, three and four of this thesis.

The nature of the collagen triple helix interacting with vWF has been studied by Verkleij *et al.* [115]. A collagen type III related-peptide from the α1 chain containing residues 541 – 558 (in sequence GAA GRP^* GPP^* GSA GTP^* GLQ (P^* = hydroxyproline)) was able to bind vWF directly. However, in a perfusion system platelets also adhered to a collagen-related-peptide spanning residues 511 – 540 in a vWF dependent manner. This discrepancy was also observed for collagen type IV that does not bind vWF directly, but platelet adhesion to a collagen type IV coated surface is vWF dependent [55; 62; 116]. In analogy to the α_2 I-domain, it seems likely that vWF binds to multiple collagen sequences with different affinities [70].

Glycoprotein Ib-IX-V complex

The glycoprotein Ib-IX-V complex contains the proteins GpIbα, GpIbβ, GpIX and GpV in stoichiometry 2:2:2:1 (figure 5) and it is the platelet receptor for vWF, α-thrombin, P-selectin and $\alpha_M\beta_2$ (reviewed in [117] and [118]). Approximately 20,000 copies of the complex are present per platelet. GpIbα associates covalently with GpIbβ outside the cell via a disulfide bridge close to the trans-membrane helices of both proteins. GpIbβ non-covalently associates with GpIX [119]. Via GpIbα, two GpIbα-GpIbβ-GpIX trimers associate non-covalently with one GpV molecule. Within the cell, GpIb-IX-V associates with actin-binding protein, phosphatidylinositol 3-kinase [120] and the signalling protein 14-3-3ζ [120; 121]. It has been hypothesised that upon vWF- or thrombin-binding to the GpIb-IX-V complex, 14-3-3ζ delivers phosphatidylinositol 3-kinase to the cytoskeleton [120] and thereby keeps integrin $\alpha_{2b}\beta_3$ in its phosphorylated, active conformation [122]. All extra-cellular members of the GpIb-IX-V complex contain so-called leucine-rich repeats (LRRs). GpIbα and GpV contain a heavily glycosylated stalk. The glycosylated stalk of GpIbα is extremely long and positions the vWF binding-site at 45 nm from the platelet surface. Expression of the GpIbα-GpIbβ-GpIX trimeric complex at the platelet membrane requires all three components, whereas GpV is not required [123]. Impaired expression of the GpIb-IX-V complex results in a not well developed demarcation membrane of megakaryocytes resulting in giant platelets and low platelet numbers [124]. It has been suggested that GpV enhances the avidity of the GpIb-IX complex and thereby strengthens the interaction of vWF with the platelet [125]. GpV also binds to collagen type I [126].

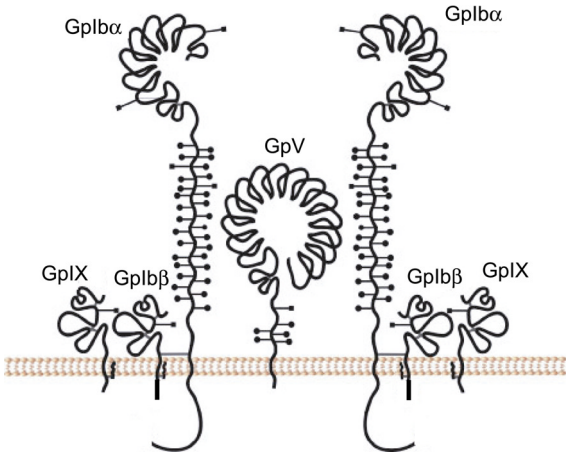

Figure 5: Model of the GpIbα-Ibβ-V-IX complex. At the platelet surface, GPIbα is disulphide-linked to GPIbβ that is associated in a non-covalent manner with GPIX. GpIbα is also non-covalently associated with GPV. The stoichiometry of the complex is 2:2:2:1. All members of the complex are linked to the platelet membrane via a transmembrane helix. *O*- and *N*-linked glycosylation sites are indicated by circles and squares, respectively. (adapted from Berndt *et al.* [118])

GpIbα contains the vWF-binding site. The binding site is located in the N-terminal 293 residues of the GpIbα that contains several distinguishable domains:

- Residues 1-35: N-terminal flanking sequence.
- Residues 36-200: seven leucine-rich repeats (LRRs).
- Residues 201-268: double-loop- or C-terminal flanking sequence.
- Residues 269-282: anionic region.

It is not clear whether the N-terminal flanking sequence interacts directly with A1, because botrocetin induced vWF binding is not dependent on this loop whereas the loop appears to be involved in ristocetin-induced vWF binding [127].

Leucine-rich repeats, which are found in numerous proteins involved in hormone-receptor interactions, enzyme inhibition and cell adhesion processes (reviewed in [128]), contain 20-29 amino-acid residues repeating sequences. The LRRs of the GpIb-IX-V complex belong to the "typical" LRR subfamily with the repeating sequence LxxLxxLxLxxN/CxLxxLpxxoFx-x, in which "x" is any residue, "o" is any non-polar residue and "–" is a possible insertion site. Within a protein the different LRRs typically contain the same number of residues. An alignment of LRRs from human GpIbα is given in figure 6A. A LRR forms a "U"-shaped structure in which one leg is a β-strand and the other leg a helical structure (figure 6B). The type of helical structure depends on the type of protein; in ribonuclease inhibitor it is an α-helix, in internalin B it is a 3_{10}-helices and in U2B"-U2A' it contains α-helices, 3_{10}-helices and short loops [128]. A number of consecutive LRRs form a horseshoe-like structure, with on the inner-face a parallel β-strand and on the outer-face the helical structures that determine the curvature of the horse-shoe. Conserved asparagine (or cysteine) residues at the base of the LRR form hydrogen bonds with the preceding LRR. The parallel β-strands and the β-α loops form the interaction surface with other proteins, although sequences outside the LRRs may contribute in ligand binding [128]. The LRR is flanked on both sides by structures that protect the hydrophobic core of the ``U``-shaped structure. These flanking sequences are typically amphipathic α-helices or cysteine-rich structures.

A

```
LRR1          46   PKDTTILHLSENLLYTFSLATLMP  69
LRR2          70   YTRLTQLNLDRCELTKLQVDG-T-  91
LRR3          92   LPVLGTLDLSHNQLQSLPLLGQT- 114
LRR4         115   LPALTVLDVSFNRLTSLPLGALRG 138
LRR5         139   LGELQELYLKGNELKTLPPGLLTP 162
LRR6         163   TPKLEKLSLANNNLTELPAGLLNG 186
LRR7         187   LENLDTLLLQENSLYTIPKGFFGS 210
"typical" LRR      LxxLxxLxLxxNxLxxLpxxoFx-x
```

B

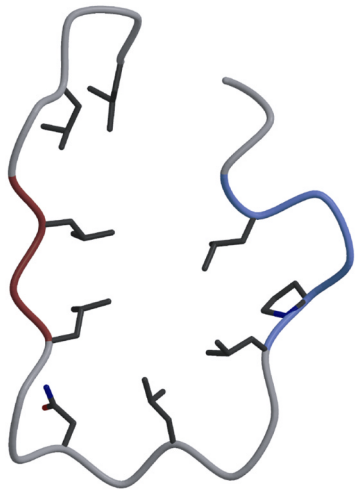

Figure 6: The GpIbα leucine rich repeats. A: The GpIbα leucine rich repeats were aligned using the program ClustalW 1.81 and adopts the consensus sequence of the so-called "typical" sub-family of LRR-proteins, except for the phenylalanine residue after the non-polar residue that is absent in LRRs 1-6. Residues that form the β-strand and helical-like structure are underlined and in *bold*, respectively. The indicated numbering starts at the ATG of the 16-residue signal peptide. B: The seven GpIb-LRRs form a horseshoe like structure [129]. GpIbα-LRR 5 (see chapter 5 of this thesis) is shown as a typical example. Residues that form the β-strand and α-helix are colour-coded *red* and *blue*, respectively.

The LRRs of human, canine and mouse GpIbα have been modelled using the known crystal structure of internalin B [129]. The inner face of the hypothetical GpIbα-LRRs model contain β-sheets, whereas the outer face most likely contains 3_{10} helices. It has been suggested that the LRRs interact with the vWF-A1 domain for several reasons. Firstly, LRRs in other proteins are known to form a structural framework required for protein-protein interactions [128]. Secondly, human vWF does not bind to GpIbα containing canine GpIbα LRRs 2-4 [127]. Thirdly, a number of Bernard-Soulier syndrome mutations are located in the LRRs (Table III). However, since these mutations involve buried residues in the hydrophobic core, these mutations most likely alter the conformation of the LRR that is most likely the underlaying cause of the observed reduced A1 binding.

The double-loop domain is essential for the interaction with A1. Its function has been investigated in only one, recent study [130]. It contains two disulfide bonds between Cys^{209}-Cys^{248} and Cys^{211}-Cys^{264}. It has been proposed that the first disulfide loop and its N-terminal flanking peptide up to residue Phe^{201} interacts with LRR-6 and this interaction is required for proper binding to A1. Disruption of this interaction results in a loss-of-function phenotype. All platelet-type vWD mutations are located in the first disulfide loop. The second disulfide loop is required for the interaction of botrocetin but not ristocetin with GpIbα. These findings confirm the hypothesis that ristocetin and botrocetin do not share the same binding-site on GpIbα. Replacement of the second double-loop by canine sequences results in a gain-of-function phenotype. The second disulfide loop

of human and canine differ only at five residues; charge alternations at positions Asp249Val, Asp252Lys, Lys253Asn, Lys258Thr and Gly263Asp. The mechanism by which these mutations activate GpIbα is not understood.

The anionic region contains ten aspartic and glutamic acid residues and three sulphated tyrosines at positions 276, 278 and 279. Although no consensus sequence exists for sulfation, negative charged residues at both sides of the tyrosines are required for a proper sulfation [131]. When the tyrosines are not sulfated, shear induced rolling of platelets over vWF or ristocetin- or botrocetin induced binding of vWF to GpIbα are strongly reduced [125; 132; 133]. Interestingly, mutation of the tyrosines to glutamic acid abolishes botrocetin induced vWF binding, but does not have an effect in ristocetin-induced vWF binding and shear-induced rolling of cells. This suggests that just negative charges are satisfactory for ristocetin- or shear induced binding [133]. Neutralising or charge reversal mutations of the negatively charged aspartic and glutamic acid residues in the anionic region decreases botrocetin- and ristocetin induced binding [134] [131]. The negative charges between residues 251-279 are essential for both ristocetin- and botrocetin induced binding, whereas the negative charges between residues 280-302 are also required for botrocetin induced vWF binding [134].

Table III
Bernard-Soulier and platelet-type vWD mutations

Syndrome	Protein	Mutation	Consequences	Reference
Bernard-Soulier Syndrome	GpIbα	K19R	frameshift and premature stop	135
		S39STOP	frameshift and premature stop	136
		L57F	compound hetrozygote with Y492C	137
		C65R	compound hetrozygote with W98STOP	138
		L76R	frameshift and premature stop	139
		A80STOP	frameshift and premature stop	140
		L129P		141
		A156V		142
		L179Δ		143
		C209S		144
		N226V	identified by scanning	145
		K231V	identified by scanning	145
		Q232V	identified by scanning	145
		A238V	identified by scanning	145
		T240V	identified by scanning	145
		A244V	identified by scanning	145
		V295S	frameshift and premature stop	146
		W343STOP		147
		S444I		146
		S444STOP		148
		K451STOP	frameshift and premature stop	146; 149
		Y492C	frameshift and premature stop. Might be compound hetrozygote with S39STOP	136; 150; 151
		W498STOP	might be compound hytrozygote with C65R	138; 152
	GpIbβ	absent protein		153-155
		R17C		156
		P74R		157
		Y88C		158; 159
		A108P		158
	GpIX	C8R		160
		D21G	compound hetrozytote with N45S	161-163
		L40P		164
		N45S	compound hetrozytote with D21G	161-163; 165
		F55S		166
		C73Y		167
		W127STOP		149
		A139T		168
Platelet-type vWD	GpIbα	G233V		169; 170
		V234G		171
		D235V		145
		K237V		145
		M239V		172; 173

Numbering starts at the first residue of the mature peptide.

Modulators of the collagen–vWF–GpIbα axis

In vitro vWF functions can be influenced by several modulators. A number of molecules have been described that interfere with the binding of vWF to collagen or to GpIbα. These modulators act either by a loss-of-function or a gain-of-function mechanism (Table IV).

Table IV
Modulators of the collagen-vWF-GpIbα axis

Modulation	Modulator	Isolated from	Family	Function	Reference
Gain-of-function	Ristocetin	*Nocardia lurida*	antibiotics	activates A1	174-176
	Botrocetin	*Bothrops jararaca*	C-type lectin	activates A1	177-179
	Jararhagin	*Bothrops jararaca*	metalloproteinase-desintegrin	activates A1	180
	Bitiscetin	*Bitis arientans*	C-type lectin	activates A1 but binds to A1 and A3 domain	69; 85; 181; 182
	Jaracetin	*Bothrops jararaca*	metalloproteinase desintegrin	activates A1	180
Loss-of-function	Heparin		poly glycan	blocks A1	50; 86; 183; 184
	Flavocetin-A/B	*Trimeresurus flavoviridis*	C-type lectin	Blocks GpIb	185-187
	Alboaggregin-B		C-type lectin	Blocks GpIb	188
	Mamushigin	*Agkistrodon halys blomhoffii*	C-type lectin	Blocks GpIb	189
	Agkistin	*Agkistrodon acutus*	C-type lectin	Blocks GpIb	190
	Echicetin	*Echis carinatus*	C-type lectin	Blocks GpIb	191-193
	Jararaca GpIb-BP	*Bothrops jararaca*	C-type lectin	Blocks GpIb	194; 195
	Tocaracetin	*Trimeresurus tokarensis*	C-type lectin	Blocks GpIb	196
	Heparin		glycosamineglycan	Blocks A1	86; 184
	Aurintricarboxylic acid			Blocks A1	197

These modulators belong to the C-type lectin super-family (although they do not possess lectin activity), metalloproteinase desintegrin family, glycopeptide antibiotics or aromatic chemical compounds. Botrocetin and ristocetin-A are relevant to the work described in this thesis and will be described in more detail.

Botrocetin

Botrocetin belongs to the C-type lectin super-family [179]. It is a hetero-dimeric molecule containing a 133 amino-acid (15 kDa) α-subunit and a 125 amino-acid (14.5 kDa) β-subunit, each containing three intra-chain disulfide bonds and one inter-chain disulfide bond. Also a one-chain botrocetin variant (32 kDa) has been isolated, but this variant is less active in vWF activation and belongs to the metalloproteinase desintegrin family [178]. The crystal-structure of botrocetin has been solved (figure 7) [198]. A large loop protrudes from each of the subunits and interacts with its

counterpart. One magnesium ion is bound to the α-chain of the botrocetin hetrodimer. A distinctive negatively charged region at the centre of the molecule is hypothesized to interact with positive charges on A1. Binding of botrocetin to A1 does not introduce conformational changes within A1. Mutagenesis and crystallographic studies identified residues in helices α4A, α4B and α5 of A1 that are essential for botrocetin binding [199;200]. These residues are close to Lys[599], which is involved in GpIbα binding, indicating that botrocetin binds close to the GpIbα binding site. Botrocetin also interacts directly with GpIbα, see above. It has been hypothesized that botrocetin binds to A1 and thereby provides additional surface that interacts with GpIbα [200].

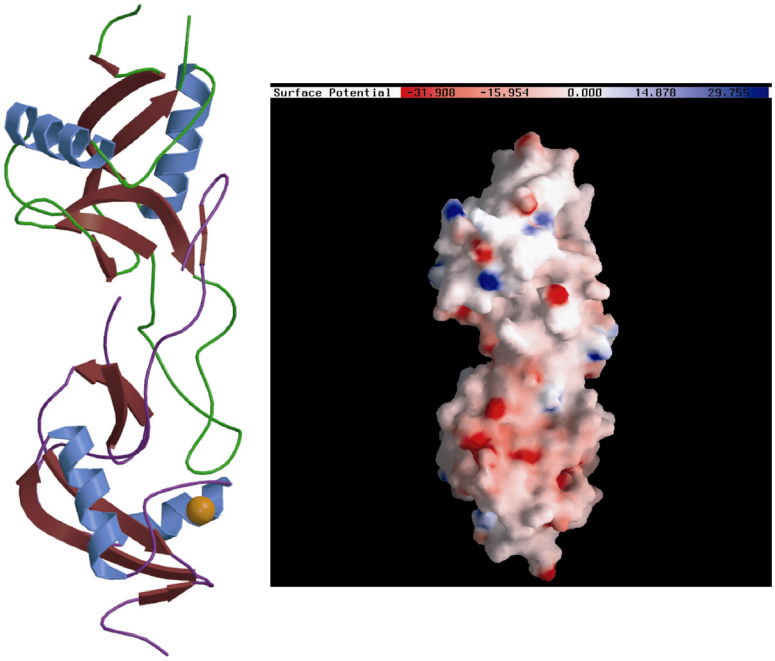

Figure 7: Structure of A1 activator botrocetin. Botrocetin activates the vWF-A1 domain that leads to GpIbα binding. A: The botrocetin crystal structure is shown. The botrocetin α (*pink)* and β (*green)* chains tightly interact via a large protruding loop. B: Surface potential of botrocetin. Positive- and negative potentials are coloured *blue* and *red*, respectively. It is hypothesised that the major negatively charged surface at the centre of botrocetin interacts with positive charges on A1.

Ristocetin

Ristocetin-A belongs to the glycopeptide antibiotics. It contains a poly-tyrosine backbone in which the aromatic rings are linked to each other via ether bonds. It also contains several glycan residues (figure 8) [174]. The glycan residues are probably essential for the activation of A1, because removal of rhamnose residues results in an inactive form of ristocetin [175].

The ristocetin-binding site on A1 is different from the botrocetin binding site [176]. Based on peptide inhibition studies it has been suggested that residues Cys[474]-Pro[488] in the N-terminal flanking peptide and residues Ser[692]-Pro[708] in the C-terminal flanking peptide are involved in ristocetin binding [176; 201]. A1 in which Pro[702-703-704] were mutated could not be activated by ristocetin, suggesting that these residues are essential for ristocetin binding [94]. In contrast to botrocetin,

ristocetin-induced vWF binding to GpIbα correlates with shear-induced binding [202]. Ristocetin does not only bind to A1, but also interacts with GpIbα, see above.

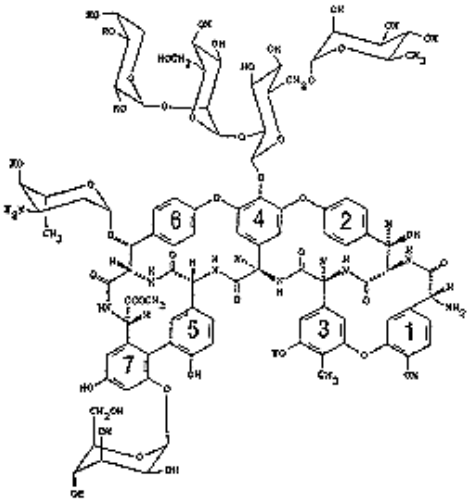

Figure 8: Strucutre of A1 activator ristocetin. Ristocetin is a glycopeptidic antibioticum and is homologous to vancomycin. Most likely a ristocetin dimer binds to specific sequences within the N- and C-terminal flanking peptides at the bottom of A1 via its modified tyrosine backbone. There is some evidence that ristocetin also may bind to the N-terminal part of GpIbα. (adapted from J.P. Scott *et al.* [174])

Malfunction of the Von Willebrand Factor–GpIb axis

Von Willebrand Disease (vWD) is the most common inherited bleeding disorder and can be divided in three different subtypes [101].

- Type I vWD refers to a partial quantitative deficiency of vWF.
- Type II vWD refers to a qualitative deficiency of vWF.
- Type III vWD refers to a total quantitative deficiency of vWF.

Type II vWD is divided in four subtypes.

- Type II A refers to a decreased platelet-dependent function, associated with absence of high molecular weight (HMW) multimers.
- Type IIB refers to an increased GpIbα affinity and are so-called gain-of-function mutations.
- Type IIM refers to a decreased GpIbα affinity, without absence of HMW and are so-called loss-of-function mutations.
- Type IIN refers to a decreased affinity for factor VIII.

An extensive database with all known mutations in the vWF gene available on the World-Wide-Web, http://www.shef.ac.uk/vwf/. A summary of vWD type IIB and 2M mutations, both found in patients and identified by site directed mutagenesis, is given in appendix I.

Type 2B mutations are scattered throughout the A1 domain and its N- and C-terminal flanking peptides. In the three dimensional structure of A1 these residues are spatially close together and are located in a region at the bottom of the domain (figure 3). It is hypothesized that amino acid residues susceptible for vWD type 2B mutations involve interactions with the N-terminal flanking peptide [84]. In contrast, type 2B mutation I546V induces a conformational change in hair-pin β2-β3 as has been shown in a crystallographic study [203].

Type 2M mutations scatter over the domain (figure 3). Several residues are buried and are essential for the conformation of the A1 domain. Mutation of these residues most likely results in a missfolded domain that is not capable to bind to GpIbα. Other residues causing type 2M vWD are solvent exposed.

Other bleeding disorders affecting the vWF-GpIbα axis occur in the GpIb-IX-V complex and are platelet-type vWD (gain-of-function) [204], that consernce mutations in the first loop of the GpIbα C-terminal flanking sequence, and Bernard-Soulier syndrome mutations [205] (loss-of-function) (Table III).

Scope of the Thesis

Von Willebrand Factor is essential for platelet adhesion and thrombus formation. Mechanisms at a molecular level involved in this process are only partially understood. Therefore we conducted several studies in which we investigated i) the binding of the vWF-A3 domain to collagen, ii) the complex formation of the A1 domain with its platelet receptor GpIbα and iii) conformational changes that activate the vWF-A1 domain.

Chapters **two and three** describe the identification of the collagen-binding site in the vWF-A3 domain using a combination of protein crystallography and site-directed mutagenesis. We have identified the collagen-binding site at the front face of A3.

Chapter **four** concerns mutation Ser968Thr in the A3 domain that has been found in a patient. The effect of the mutation on collagen binding and platelet adhesion has been studied and the crystal structure of Ser968Thr-A3 has been solved. We suggest that the collagen-binding site of the vWF-A3 domain undergoes a conformational change upon collagen binding.

Chapter **five** describes the complex of the vWF-A1 domain with platelet receptor GpIbα. The structure explains at a molecular level the effect of vWD type 2B and 2M mutations that have been identified in patients. The results of this study may be of great interest in the development of anti-arterial thrombotic drugs.

Chapter **six** was conducted to identify conformational changes in the vWF-A1 domain that result in vWF to GpIbα binding. Six crystal structures of wt-A1 and gain-of-function mutant Arg543Gln-A1 were solved and compared to A1 in the A1•GpIbα complex. The structures suggest that the N and C-terminal flanking peptides shield the GpIbα binding site on A1. Shear stress or gain-of-function mutations change the conformation of the peptides that results in GpIbα binding.

APPENDIX I

Effect of mutations in the vWF-A1 domain and flanking peptides in GpIbα binding

Mutation(s)[1,2] and Type		RIPA[3,4]	vWF:RCo[3,5]	Botrocetin aggregatie[3,6]	Botrocetin binding[3,7]	SIPA[3,8]	Shear adhesion[3,9]	Heparin binding[3,10]	Reference
463-465 (2A) (S)		normal		normal	norrmal				206
472-476 (2A) (S)		normal		normal	normal				206
D486A (S)		normal		normal	normal				206
497-498-501-3A (S)	2B	increased		normal	normal				206
P503L	2B	Requires less risto	reduced						207; 208
H505D	2B	requires less risto, increased		• requires less botro • partial increased • normal	normal				208; 209
505-506-2A (S)	2B	increased		normal	normal				206
C509G (S)	2B 2A	• normal • spontaneous			not active				210; 211
C509R (S)	2B 2A	• strong reduced • normal • spontaneous			not active			partial reduced	210 211-213
C509,695A (S)	2M	Strong red.							88
C509,695S (S)	2M	not active							89
R511A (S)	2B	increased		normal	normal				206
L513P	2M								208
D514A (Ab) (S)	2M	not active		not active	not active				206
V516I	2M	reduced in plasma	reduced in plasma						214
L519R	2M	reduced in plasma	reduced in plasma						214
D520A (S) (Ab)	2M								199
520-524(2A) (S) (Ab)	2M	not active		normal	normal				206
S522F	2M	reduced in plasma	reduced in plasma						214
R524S (S)	2M	reduced					not active		215
R524A (S)		• normal • partial reduced		normal	reduced			normal	199; 216
S526R (S)	2M	reduced					not active		215
E527A (S)		normal		normal	normal				206
527-531(2A) (S)	2M	not active		normal	normal				206
E529A (S)		normal		normal	normal				199
E531A (S)	2M	reduced		normal	normal				199
L533P	2M	reduced in plasma	reduced in plasma						214
K534A (S)	2M	• reduced • not active		normal	partial reduced			normal	206; 216
D539G	2M	reduced in plasma	reduced in plasma						214
539-542-543 (3A) (S)	2B	increased		normal	normal				206
M540MM	2B	• requires less risto., • normal • spontaneous		Normal	partial reduced	increased			217 208; 212; 218
R543L	2B	spontaneous							219

Mutation(s) and Type		RIPA	vWF:RCo	Botrocetin aggregatie	Botrocetin binding	SIPA	Shear adhesion	Heparin binding	Reference
R543Q	2B	• spontaneous • reduced • requires less risto	reduced in plasma	spontaan, normal			normal	normal	208; 213; 220-222
R543W	2B	• Requires less ristocetin • spontaneous		• spontaneous • increased			reduced	normal	201; 208; 213; 220; 222-227
R543C	2B 2A								208
R545P	2B	• spontaneous • increased • requires less risto		normal				normal	208; 213; 220
R545C	2B	Requires less risto	reduced (pl), normal (rec.)	normal				• normal • reduced	228 220; 224-226; 229
R545A (S)	2B	• extra strong • spontaneous		• extra strong • requires less botro	normal				206
I546V	2B	• Requires less risto • norm	normal						208; 224; 230
I546V/G561S	2M						not active		203
S547F	2B	increased	reduced						231
K549A (S)	2B	• Normal • requires less risto		• normal • requires less botro	partial reduced			normal	199; 216
K549-552(2A) (Ab) (S)	2M	not active		not active					206
W550C	2B	• spontaneous • requires less rist							232
V551F	2B	• spontaneous • requires less risto.	reduced	Norm.		increased		reduced	213; 217; 225
V551D	2B								unpublished
V551L	2B	spontaan, req.less rist							225; 227
R552C	2M 2A							strong reduced	213; 233
R552A (S) (Ab)	2A								199
R552A	2A	strong reduced		reduced				reduced	216
V553M	2B	• spontaneous • requires less risto • partial reduced plasma	reduced in plasma	• normal • increased				normal	201; 208; 213; 217; 221; 224-226; 234-236
E557Q (S)	2M	reduced					• reduced • not active		203; 215
557-559-560-563 (4A) (S)		normal		normal	normal				206
D560S (S)	2M	reduced					reduced		215
H559F	2M						not active		203
D560R (S)	2M	partial reduced					not active		203; 215
G561S	2M	strong reduced		normal				normal	237 213; 238
G561A	2M	strong reduced		Norm		Strong reduced			208; 217; 239
G561S (S)	2M	Normal					not active		215; 240
I662F	2M								208
H563T (S)	2M	Norman					not active		215
Y565A (S)	2M						not active		203; 240
569KDRKR573(3A) (s)	2M	• strong reduced • reduced		normal	reduced			normal	206; 216
569-570-571-572-573 (5A)								normal	241
K569A (S)		normal		reduced	normal				199

Mutation(s)[1,2] and Type		RIPA[3,4]	vWF:RCo[3,5]	Botrocetin aggregatie[3,6]	Botrocetin binding[3,7]	SIPA[3,8]	Shear adhesion[3,9]	Heparin binding[3,10]	Reference
D570A (S)		normal		normal	normal				199
R571A (S)	2M	not active		normal	normal				199
571-578 (6A)								strong reduced	241
K572A (S)	2M	reduced		normal	normal		not active		199; 203
A572T	2M								A
R573A (S)		normal		normal	normal				199
P574L	2B	• not spontaneous • requires less risto							208; 234; 242
576-578-579 (3A) (S)	2B	increased		normal	normal				206
R578L	2B	• spontaneous • increased • requires less risto		• spontaneous • normal				normal	208; 220
R578Q	2B	• spontaneous • requires less risto, • reduced in plasma • normal • increased	reduced in plasma	Normal				normal	208; 213; 217; 220; 224-226; 235; 243
R578W	2B								233
R578P	2B								……
Q583R (S)	2M	reduced					strong reduced		215
K585E (S)	2M	reduced					strong reduced		215
K585A (S)		normal		normal	normal		normal		203; 206
Q590R	2M	partial reduced					normal		215
T594S/E596A (S)	2M	normal					not active		215
596-599 (2A) (S)	2M	not active		reduced	normal				206
E596K	2M			Norm.		Strong red.		normal	208; 213; 217
E596A (S)	2M	not active		partial reduced	normal		strong reduced		199; 203; 240
K599A (S)	2M	not active		not active	normal		not active		199; 203; 240
K599T	2M	not active							unpublished
Q604R (S)	2M	normal					not active		215
F606I	2M	reduced		normal					244
S607R (S)	2M	normal					not active		215
K608A (S)		normal		normal	reduced				199
608-610-611(3A) (Ab) (S)	2M	not active		not active	not active				206
D610A (S)	2M	normal		normal	normal				199
R611A (S) (Ab)	2M								199
R611L	2M							partial reduced	208; 213
R611H	2M /2a	reduced		reduced		reduced			208; 217
R611H	2B /2a	reduced	strong reduced					reduced	213; 245-247
R611C	2B /2a	• reduced • no effect of risto	strong reduced					reduced	213; 246; 247
		•							

Mutation(s)[1,2] and Type		RIPA[3,4]	vWF:RCo[3,5]	Botrocetin aggregatie[3,6]	Botrocetin binding[3,7]	SIPA[3,8]	Shear adhesion[3,9]	Heparin binding[3,10]	Reference
R611C	2M /2a								208
E613A (S)	2M	not active		normal	normal				199
613-616(2A) (S) (Ab)	2M	not active		not active	not active				206
R616A (S)	2M	not active		normal	reduced				199
E626A (S)	2M	not active		normal	bit reduced				199; 206
Q628R	2M	Norm. actief					strong reduced		215
629-639Δ	2M	not active		not active				not active	248
R629,632,636A (S)	2M						reduced		240
R629,632A (S) (Ab)	2M	not active		not active	not active				206
R629A (S)	2M	not active		reduced	reduced		partial reduced		199; 240
R629E (S)		reduced					normal		215
R632A (S)							normal		203; 240
R632A (S) (Ab)	2M	not active		not active	not active				206
R636A (S)		normal		strong reduced	reduced		normal		199; 206; 240
Y637F (S)	2M						reduced		240
K642A (S)	2M	not active		normal	normal				199
642-645ΔK (S)	2M	Strong reduced		normal				reduced	216
642-643-644-645 (4A) (S)	2M	not active		reduced	normal			partial reduced	206; 241
K643A (S)		normal		normal	normal				199
K643,645A (S)	2M						Reduced		240
K644A (S)		bit reduced		normal	normal		normal		199; 203; 240
K645A (S)		normal		normal	normal				199
H656A (S)		normal		normal	normal		normal		199; 203; 240
656-660 (2A) (S)		normal		normal	normal				206
H656E (S)	2M	reduced					strong reduced		215
L659R (S)	2M	reduced					reduced		215
K660A (S)		normal		reduced	reduced		normal		199; 240
K660E (S)	2M	reduced					strong reduced		215
K661A								normal	241
I662F (S)	2M	reduced		normal		strong reduced		normal	208; 213; 217; 244
R663A (S)		normal		normal	normal		normal		199; 240
663-666-667 (3A) (S)		normal		reduced	reduced				206
R663A								normal	241
E666A (S)	2M	reduced		normal	normal				199
K667A (S)		normal		reduced	reduced				199
671-673 (2A) (S)		normal		normal	normal				206
A674T	2M								unpublished
681-682-684 (3A) (S)		partial reduced		normal	normal				206

Mutation(s)[1,2] and Type		RIPA[3,4]	vWF:RCo[3,5]	Botrocetin aggregatie[3,6]	Botrocetin binding[3,7]	SIPA[3,8]	Shear adhesion[3,9]	Heparin binding[3,10]	Reference
687-688-689 (3A) (S)	2B	• extra strong • not apontaneous		increased	normal				206
L694V	2B	reduced		normal					201
C695G (S)	2B 2A	not active		not active	not active				210; 211
696-700 (2A) (S)		normal		normal	normal				206
L697V	2B	• requires less risto • increased • reduced	reduced	• normal • increased				normal	201; 208; 213; 217; 221; 249
A698V	2B	• spontaneous • requires less risto. • increased • normal	normal	partial ncreased					201; 208; 221
A698D	2B	requires less risto							unpublished
A701V	2B	• requires less risto. • increased		normal					201
P702-703-704R/D (S)		not active							94
P704S	2M	• asymptomatic in patients							unpublished
L706V	2M	reduced		normal					201
D709A (S)		normal		normal	normal				206
reduced/alkylated		• binds spontaneous to GpIb, • no effect of risto.		partial increased	not active				87; 88; 96; 250

1. (S) represents identified by scanning mutagenesis.
2. (Ab) indicates that a monoclonal Ab reacts less well with the mutant, suggesting that the mutation (partially) unfolds the domain.
3. Normal indicates an activity > 90 %, partial reduced between 75 % - 90 %, reduced between 25 % - 75 %, strong reduced indicates activity between 10 – 25 % and not active < 10 %.
4. Ristocetin induced platelet aggregation.
5. vWF ristocetin cofactor activity.
6. Botrocetin induced platelet aggregation.
7. Binding of botrocetin to vWF.
8. Shear induced platelet aggregation.
9. Adhesion of platelets to a surface in a perfusion system.
10. Binding of vWF to heparin.

Reference List

1. Owen CA. A History of Blood Coagulation. In: Anonymous. Mayo Foundation for Medical education and Research; 2001.

2. Titani K, Kumar S, Takio K, et al. Amino acid sequence of human von Willebrand Factor. Biochemistry. 1986;25:3171-3184.

3. Verweij CL, de Vries CJ, Distel B, et al. Construction of cDNA coding for human von Willebrand factor using antibody probes for colony-screening and mapping of the chromosomal gene. Nucleic Acids Res. 1985;13:4699-4717.

4. Mancuso DJ, Tuley EA, Westfield LA, et al. Structure of the gene for human von Willebrand factor. J Biol Chem. 1989;264:19514-19527.

5. Sakariassen KS, Bolhuis PA, Sixma JJ. Human blood platelet adhesion to artery subendothelium is mediated by factor VIII-von Willebrand factor bound to the subendothelium. Nature. 1979;279:636-638.

6. Kehrel B. Platelet-collagen interactions. Thromb Haemost. 1995;21:123-129.

7. Rand JH, Glanville RW, Wu XX, et al. The significance of subendothelial von Willebrand factor. Thromb Haemost. 1997;78:445-450.

8. Mazzucato M, Spessotto P, Masotti A, et al. Identification of domains responsible for von Willebrand factor type VI collagen interaction mediating platelet adhesion under high flow. J Biol Chem. 1999;274:3033-3041.

9. Sixma JJ, van Zanten GH, Huizinga EG, et al. Platelet adhesion to collagen: An update. Thromb Haemost. 1997;78:434-438.

10. Sixma JJ, Schiphorst ME, Verweij CL, Pannekoek H. Effect of deletion of the A1 domain of von Willebrand factor on its binding to heparin, collagen and platelets in the presence of ristocetin. Eur J Biochem. 1991;196:369-375.

11. Savage B, Almus-Jacobs F, Ruggeri ZM. Specific synergy of multiple substrate-receptor interactions in platelet thrombus formation under flow. Cell. 1998;94:657-666.

12. Savage B, Saldívar E, Ruggeri ZM. Initiation of platelet adhesion by arrest onto fibrinogen or translocation on von Willebrand factor. Cell. 1996;84:289-297.

13. Miura S, Li CQ, Cao Z, Wang H, Wardell MR, Sadler JE. Interaction of von Willebrand Factor domain A1 with platelet glycoprotein Ibα-(1-289). Slow intrinsic binding kinetics mediate rapid platelet adhesion. J Biol Chem. 2000;275:7539-7546.

14. Brakebusch C, Bergmeier W, Schulte V, et al. Glycoprotein VI but not alpha2beta1 integrin is essential for platelet interaction with collagen. EMBO J. 2001;20:2120-2130.

15. Goto S, Ikeda Y, Saldívar E, Ruggeri ZM. Distinct mechanisms of platelet aggregation as a consequence of different shearing flow conditions. J Clin Invest. 1998;101:479-486.

16. Mancuso DJ, Tuley EA, Westfield L.A., et al. Human von Willebrand Factor gene and pseudogene: structural analysis and differentiation by polymerase chain reaction. Biochemistry. 1991;30:253-269.

17. Nachman R, Levine R, Jaffe EA. Synthesis of factor VIII antigen by cultured guinea pig megakaryocytes. J Clin Invest. 1977;60:914-921.

18. Jaffe EA, Nachman RL, Becker CG, Minick CR. Culture of human endothelial cells derived from umbilical veins. Identification by morphologic and immunologic criteria. J Clin Invest. 1973;52:2745-2756.

19. Yamamoto K, De Waard V, Fearns C, Loskutoff DJ. Tissue distribution and regulation of murine von Willebrand factor gene expression in vivo. Blood. 1998;92:2791-2801.

20. Sadler JE. Biochemistry and genetics of von Willebrand factor. Annu Rev Biochem. 1998;67:395-424.

21. Marti T, Rosselet SJ, Titani K, Walsh KA. Identification of disulfide-bridged substructures within human von Willebrand factor. Biochemistry. 1987;26:8099-8109.

22. Vischer UM, Wagner DD. von Willebrand factor proteolytic processing and multimerization precede the formation of Weibel-Palade bodies. Blood. 1994;83:3536-3544.

23. Haberichter SL, Montgomery RR. von Willebrand factor storage and multimerization: 2 independent intracellular processes. Blood. 2000;96:1808-1815.

24. Verweij CL, Hart M, Pannekoek H. Expression of variant von Willebrand factor (vWF) cDNA in heterologous cells: requirement of the pro-polypeptide in vWF multimer formation. EMBO J. 1987;6:2885-2890.

25. Wise RJ, Pittman DD, Handin RI, Kaufman RJ, Orkin SH. The propeptide of von Willebrand factor independently mediates the assembly of von Willebrand multimers. Cell 1988; 52, 229-236.

26. Preininger A, Schlokat U, Mohr G, et al. Strategies for recombinant Furin employment in a biotechnological process: complete target protein precursor cleavage. Cytotechnology. 1999;30:1-15.

27. Turecek PL, Pichler L, Auer W, et al. Evidence for extracellular processing of pro-von Willebrand factor after infusion in animals with and without severe von Willebrand disease. Blood. 1999;94:1637-1647.

28. Sadler JE. von Willebrand factor. J Biol Chem. 1991;266:22777-22780.

29. Wagner DD. Cell biology of von Willebrand factor. Annu Rev Cell Biol. 1990;6:217-46.:217-246.

30. Wagner DD, Olmsted JB, Marder VJ. Immunolocalization of von Willebrand protein in Weibel-Palade bodies of human endothelial cells. J Cell Biol. 1982;95:355-360.

31. Chen CI, Federici AB, Cramer EM, et al. Studies of multimerin in patients with von Willebrand disease and platelet von Willebrand factor deficiency. Br J Haematol. 1998;103:20-28.

32. Haberichter SL, Montgomery RR. Identification of amino acids in the von Willebrand Factor propeptide critical for storage of vWF [abstract]. Thrombosis and Haemostasis, Supplement. 2001.

33. Van Mourik JA, Boertjes RC, Huisveld IA, et al. von Willebrand factor propeptide in vascular disorders: a tool to distinguish between acute and chronic endothelian cell pertuberation. Blood. 1999;94:179-185.

34. Romeuf C, Mazurier C. Comparison between von Willebrand Factor (vWF) and vWF antigen II in normal individuals and patients with von Willebrand disease. Thromb Haemost. 1998;80:37-41.

35. Sodetz JM, Paulson JC, Mc Kee PA. Carbohydrate composition and identification of blood group A, B and H oligosaccharide structures on human factor VIII/von Willebrand factor. J Biol Chem. 1979;254:10154-10160.

36. De Romeuf C, Samor B, Mazurier C. Characterisation of von Willebrand factor antigen II in a therapeutic von Willebrand Factor concentrate [abstract]. Br J Haematol. 1996;93.

37. Mannucci PM, Ruggeri ZM, Pareti FI, Capitanio A. 1-Deamino-8-d-arginine vasopressin: a new pharmacological approach to the management of haemophilia and von Willebrands' diseases. Lancet. 1977;1:869-872.

38. Verweij CL, Diergaarde PJ, Hart M, Pannekoek H. Full-length von Willebrand factor (vWF) cDNA encodes a highly repetitive protein considerably larger than the mature vWF subunit. EMBO J. 1986;5:1839-1847.

39. Voorberg J, Fontijn R, Van Mourik JA, Pannekoek H. Domains involved in multimer assembly of von willebrand factor (vWF): multimerization is independent of dimerization. EMBO J. 1990;9:797-803.

40. Dong Z, Thoma RS, Crimmins DL, McCourt DW, Tuley EA, Sadler JE. Disulfide bonds required to assemble functional von Willebrand factor multimers. J Biol Chem. 1994;269:6753-6758.

41. Fujimura Y, Titani K, Holland LZ, et al. von Willebrand Factor: A reduced and alkylated 52/48-kDa fragment beginning at amino acid residue 449 contains the domain interacting with platelet glycoprotein Ib. J Biol Chem. 1986;261:381-385.

42. Katsumi A, Tuley EA, Sadler JE, Sadler JE. localisation of disulfide bonds in the cysteine knot domain of human von Willebrand factor. J Biol Chem. 2000;275:25585-25594.

43. Kaufman RJ, Dorner AJ, Fass DN. von Willebrand factor elevates plasma factor VIII without induction of factor VIII messenger RNA in the liver. Blood. 1999;93:193-197.

44. Foster PA, Fulcher CA, Marti T, Titani K, Zimmerman TS. A major factor VIII binding domain resides within the amino-terminal 272 amino acid residues of von Willebrand factor. J Biol Chem. 1987;262:8443-8446.

45. Takahashi Y, Kalafatis M, Girma JP, Sewerin K, Anderson LO, Meyer D. Localisation of a factor VIII binding domain on a 34 kilodalton fragment of the N-terminal portion of von Willebrand Factor. Blood. 1987;70:1679-1682.

46. Koedam JA, Hamer RJ, Beeser-Visser NH, Bouma BN, Sixma JJ. The effect of von Willebrand factor on activation of factor VIII by factor Xa. Eur J Biochem. 1990;189:229-234.

47. Bendetowicz AV, Wise RJ, Gilbert GE. Collagen-bound von Willebrand factor has reduced affinity for factor VIII. J Biol Chem. 1999;274:12300-12307.

48. Roth GJ, Titani K, Hoyer LW, Hickey MJ. Localization of binding sites within human von Willebrand factor for monomeric type III collagen. Biochemistry. 1986;25:8357-8361.

49. Hoylaerts MF, Yamamoto H, Nuyts K, Vreys I, Deckmyn H, Vermylen J. von Willebrand factor binds to native collagen VI primarily via its A1 domain. Biochem J. 1997;324:185-191.

50. Fujimura Y, Titani K, Holland LZ, et al. A heparin-binding domain of human von Willebrand factor. J Biol Chem. 1987;262:1734-1739.

51. Christophe O, Obert B, Meyer D, Girma J-P. The binding domain of von Willebrand factor to sulfatides is distinct from those interacting with glycoprotein Ib, heparin, and collagen and resides between amino acid residues Leu 512 and Lys 673. Blood. 1991;78:2310-2317.

52. Data RE, Williams SB, Roberts DD, Gralnick HR. Platelets adhere to sulfatides by von willebrand factor dependent and independent mechanisms. Thromb Haemost. 1991;65:581-587.

53. Koivunen E, Ranta TM, Annila A, et al. Inhibition of beta(2) integrin-mediated leukocyte cell adhesion by leucine-leucine-glycine motif-containing peptides. J Cell Biol. 2001;153:905-916.

54. Zheng X, Chung D, Takayama TK, Majerus EM, Sadler JE, Fujikawa K. Structure of von Willebrand factor-cleaving protease (ADAMTS13), a metalloprotease involved in thrombotic thrombocytopenic purpura. J Biol Chem. 2001;276:41059-41063.

55. Lankhof H, van Hoeij M, Schiphorst ME, et al. A3 domain is essential for interaction of von Willebrand factor with collagen type III. Thromb Haemost. 1996;75:950-958.

56. Plow EF, Haas TA, Zhang L, Loftus J, Smith JW. Ligand binding to integrins. J Biol Chem. 2000;275:21785-21788.

57. Fischer BE, Kramer G, Mitterer A, et al. Effect of multimerization of human and recombinant von Willebrand factor on platelet aggregation, binding to collagen and binding of coagulation factor VIII. Thromb Res. 1996;84:55-66.

58. De Romeuf C, Mazurier C. Heparin binding assay of von willebrand factor (vWF) in plasma milieu - evidence of the importance of the mulktimerisation degree of vWF. Thromb Haemost. 1993;69:436-440.

59. Van der Plas RM, Gomes L, Marquart JA, et al. Binding of von Willebrand Factor to Collagen type III: Role of specific amino acids in the collagen binding domain of vWF and effects of neighbouring domains. Thromb Haemost. 2000;84:1005-1011.

60. Cruz MA, Yuan H, Lee JR, Wise RJ, Handin RI. Interaction of the von Willebrand Factor (vWF) with collagen. J Biol Chem. 1995;270:10822-10827.

61. Colombatti A, Bonaldo P, Doliana R. Type A Modules: Interacting domains found in several non-fibrillar collagens and in other extracellular matrix proteins. Matrix. 1993;13:297-306.

62. van Zanten GH, Saelman EUM, Schut-Hese KM, et al. Platelet adhesion to collagen type IV under flow conditions. Blood. 1996;88:3862-3871.

63. Mohri H, Yoshioka A, Zimmerman TS, Ruggeri ZM. Isolation of the von Willebrand factor domain interacting with platelet glycoprotein Ib, heparin, and collagen and characterization of its three distinct functional sites. J Biol Chem. 1989;264:17361-17367.

64. Hoylaerts MF, Yamamoto H, Nuyts K, Vreys I, Deckmyn H, Vermylen J. von Willebrand factor binds to native collagen VI primarily via its A1 domain. Biochem J. 1997;324:185-191.

65. Fujimura Y, Holland LZ, Ruggeri ZM, Zimmerman TS. The von willebrand factor domain-mediating botrocetin-induced binding to glycoprotein IB lies between Val449 and Lys728. Blood. 1987;70:985-988.

66. Hoylaerts MF, Nuyts K, Peerlinck K, Deckmyn H, Vermylen J. Promotion of binding of von Willebrand factor to platelet glycoprotein Ib by dimers of ristocetin. Biochem J. 1995;306:453-463.

67. Verkleij MW, Morton LF, Knight CG, de-Groot PG, Barnes MJ, Sixma JJ. Simple collagen-like peptides support platelet adhesion under static but not under flow conditions: Interaction via $\alpha\beta1$ and von Willebrand factor with specific sequences in native collagen is a requirement to resist shear forces. Blood. 1998;91:3808-3816.

68. Levy GG, Nichols WC, Lian EC, et al. Mutations in a member of the ADAMTS gene family cause thrombotic thrombocytopenic purpura. Nature. 2001;413:488-494.

69. Obert B, Houllier A, Meyer D, Girma JP. Conformational changes in the A3 domain of von Willebrand factor modulate the interaction of the A1 domain with platelet glycoprotein Ib. Blood. 1999;93:1959-1968.

70. Rich RL, Deivanayagam CCS, Owens RT, et al. Trench-shaped binding sites promote multiple classes of interactions between collagen and the adherence receptors, $\alpha_1\beta_1$ integrin and *Staphylococcus aureus* Cna MSCRAMM. J Biol Chem. 1999;274:24906-24913.

71. Kamata T, Liddington RC, Takada Y. Interaction between collagen and the α_2 I-domain of integrin $\alpha_2\beta_1$ - Critical role of conserved residues in the metal ion-dependent adhesion site (MIDAS) region. J Biol Chem. 1999;274:32108-32111.

72. Estavillo D, Ritchie A, Diacovo TG, Cruz MA. Functional analysis of a recombinant glycoprotein Ia/IIa (integrin a2b1) I domain that inhibits platelet adhesion to collagen and endothelial matrix under flow conditions. J Biol Chem. 1999;274:35921-35926.

73. Ivaska J, Kapyla J, Pentikäinen O, et al. A peptide inhibiting the collagen binding function of integrin $\alpha2$ I domain. J Biol Chem. 1999;274:3513-3521.

74. Smith C, Estavillo D, Emsley J, Bankston LA, Liddington RC, Cruz MA. Mapping the collagen-binding site in the I domain of the glycoprotein Ia/IIa (integrin $\alpha_2\beta_1$). J Biol Chem. 2000;275:4205-4209.

75. Emsley J, King SL, Bergelson JM, Liddington RC. Crystal structure of the I domain from integrin $\alpha2\beta1$. J Biol Chem. 1997;272:28512-28517.

76. Camper L, Hellman U, Lundgren-Åkerlund E. Isolation, cloning and sequence analysis of the integrin subunit alpha10, a beta1-associated collagen binding integrin expressed on chondrocytes. J Biol Chem. 1998;273:20383-20389.

77. Velling T, Kusche-Gullberg M, Sejersen T, Gullberg D. cDNA cloning and chromosomal localization of human α_{11} integrin - A collagen-binding, I domain-containing, β_1-associated integrin α-chain present in muscle tissues. J Biol Chem. 1999;274:25735-25742.

78. Vieren van der M, Crowe DT, Hoekstra D, et al. The leukocyte integrin alpha D beta 2 binds VCAM-1: evidence for a binding interface between I domain and VCAM-1. J Immunol. 1999;163:1984-1990.

79. Qu A, Leahy DJ. Crystal structure of the I-domain from the CD11a/CD18 (LFA-1,$\alpha_L\beta 2$ integrin. Proc Natl Acad Sci U S A. 1995;92:10277-10281.

80. AnonymousCharacteristics of cation binding to the I domains of LFA-1 and MAC-1. J Biol Chem. 1998;273:22113-22119.

81. Anonymousa novel divalent cation-binding site in the A domain of the $\beta 2$ integrin CR3 (CD11b/CD18) is essential for ligand binding. Cell. 1993;72:857-867.

82. Lee JO, Rieu P, Arnaout MA, Liddington RC. Crystal structure of the A domain from the α subunit of integrin CR3 (CD11/CD18). Cell. 1995;80:631-638.

83. Celikel R, Varughese KI, Madhusudan, Yoshioka A, Ware J, Ruggeri ZM. Crystal structure of the von Willebrand factor A1 domain in complex with the function blocking NMC-4 Fab. Nature Struct Biol. 1998;5:189-194.

84. Emsley J, Cruz M, Handin R, Liddington RC. Crystal structure of the von Willebrand factor A1 domain and implications for the binding of platelet glycoprotein Ib. J Biol Chem. 1998;273:10396-10401.

85. Matsui T, Hamako J, Matsushita T, Nakayama T, Fujimura Y, Titani K. Binding site on human von Willebrand factor of bitiscetin, a snake venom-derived platelet aggregation inducer. Biochemistry. 2002;41:7939-7946.

86. Baruch D, Ajzenberg N, Denis C, Legendre P, Lormeau JC, Meyer D. Binding of heparins fractions to von Willebrand Factor: Effect of molecular weight and affinity for antithrombin III. Thromb Haemost. 1994;71:141-146.

87. Miura S, Fujimura Y, Sugimoto M, et al. Structural elements influencing von Willebrand factor (vWF) binding affinity for platelet glycoprotein Ib within a dispase- digested vWF fragment. Blood. 1994;84:1553-1558.

88. Azuma H, Hayashi T, Dent JA, Ruggeri ZM, Ware J. Disulfide bond requirements for assembly of the platelet glycoprotein Ib-binding domain of von Willebrand factor. J Biol Chem. 1993;268:2821-2827.

89. Cruz MA, Handin RI, Wise RJ. The interaction of the von Willebrand factor-A1 domain with platelet glycoprotein Ib/IX. The role of glycosylation and disulfide bonding in a monomeric recombinant A1 domain protein. J Biol Chem. 1993;268:21238-21245.

90. Miyata S, Ruggeri ZM. Distinct structural attributes regulating von Willebrand factor A1 domain interaction with platelet glycoprotein Ibα under flow. J Biol Chem. 1999;274:6586-6593.

91. Nakayama T, Matsushita T, Dong Z, et al. Identification of the regulatory elements of human von Willebrand factor for binding to platelet GPIb. Importance of structural integrity of the regions flanked by CYS509-CYS695 disulfide bond. J Biol Chem. 2002.

92. Carew JA, Quinn SM, Stoddart JH, Lynch DC. O-Linked carbohydrate of recombinant von Willebrand factor influences ristocetin-induced binding to platelet Glycoprotein Ib. J Clin Invest. 1992;90:2258-2267.

93. De Marco L, Girolami A, Russell S, Ruggeri ZM. Interaction of asialo-von Willebrand factor with glycoprotein Ib induces fibrinogen binding to the glycoprotein IIb/IIIa complex and mediates platelet aggregation. J Clin Invest. 1985;75:1198-1203.

94. Azuma H, Sugimoto M, Ruggeri ZM, Ware J. A role for von Willebrand factor proline residues 702-704 in ristocetin-mediated binding to platelet glycoprotein Ib. Thromb Haemost. 1993;69:192-196.

95. Azuma H, Dent JA, Sugimoto M, Ruggeri ZM, Ware J. Independent assembly and secretion of a dimeric adhesive domain of von Willebrand factor containing the glycoprotein Ib-binding site. J Biol Chem. 1991;266:12342-12347.

96. Sugimoto M, Dent J, McClintock R, Ware J, Ruggeri ZM. Analysis of structure-function relationships in the platelet membrane glycoprotein Ib-binding domain of von Willebrand's factor by expression of deletion mutants. J Biol Chem. 1993;268:12185-12192.

97. Gerritsen HE, Robles R, Lammle B, Furlan M. Partial amino acid sequence of purified von Willebrand factor-cleaving protease. Blood. 2001;98:1654-1661.

98. Cal S, Obaya AJ, Llamazares M, Garabaya C, Quesada V, Lopez-Otin C. Cloning, expression analysis, and structural characterization of seven novel human ADAMTSs, a family of metalloproteinases with disintegrin and thrombospondin-1 domains. Gene. 2002;283:49-62.

99. Furlan M, Robles R, Lämmle B. Partial purification and characterization of a protease from human plasma cleaving von Willebrand factor to fragments produced by in vivo proteolysis. Blood. 1996;87:4223-4234.

100. Tsai HM. Physiologic cleavage of von Willebrand factor by a plasma protease is dependent on its conformation and requires calcium ion. Blood. 1996;87:4235-4244.

101. Sadler JE. a revised classification of von willebrand desease. Thromb Haemost. 1994;71:520-525.

102. Tsai HM, Sussman II, Nagel RL. Shear stress enhances the proteolysis of von Willebrand factor in normal plasma. Blood. 1994;83:2171-2179.

103. Chow TW, Turner NA, Chintagumpala M, et al. Increased von Willebrand factor binding to platelets in single episode and recurrent types of thrombotic thrombocytopenic purpura. Am J Hematol. 1998;57:293-302.

104. Cruz MA, Yuan H, Lee JR, Wise RJ, Handin RI. Interaction of the von Willebrand factor (vWF) with collagen. Localization of the primary collagen-binding site by analysis of recombinant vWF a domain polypeptides [published erratum appears in J Biol Chem 1995 Aug 18;270(33):19668]. J Biol Chem. 1995;270:10822-10827.

105. Huizinga EG, Van der Plas RM, Kroon J, Sixma JJ, Gros P. Crystal structure of the A3 domain of human von Willebrand factor: implications for collagen binding. Structure. 1997;5:1147-1156.

106. Bienkowska J, Cruz MA, Atiemo A, Handin RI, Liddington R. The von Willebrand Factor A3 domain does not contain a metal ion-dependent adhesion site motif. J Biol Chem. 1997;272:25162-25167.

107. Lee JO, Bankston LA, Arnout MA, Liddington RC. Two conformations of the integrin A domain (I domain): A pathway for activation? Structure. 1995;3:1333-1340.

108. Dickeson SK, Walsh JJ, Santoro SA. contributions of the I and EF hand domains to the divalent cation-dependent collagen binding activity of the $\alpha 2\beta 1$ integrin. J Biol Chem. 1997;227:7661-7668.

109. Tuckwell DS, Calderwood DA, Green LJ, Humphries MJ. Integrin $\alpha 2$ I-domain is a binding site for collagens. J Cell Sci. 1995;108:1629-1637.

110. Tulla M, Pentikainen OT, Viitasalo T, et al. Selective binding of collagen subtypes by integrin alpha 1I, alpha 2I, and alpha 10I domains. J Biol Chem. 2001;276:48206-48212.

111. Pietu G, Fressinaud E, Girma JP, Nieuwenhuis HK, Rothschild C, Meyer D. Binding of human von Willebrand factor to collagen and to collagen- stimulated platelets. J Lab Clin Med. 1987;109:637-646.

112. Emsley J, Knight CG, Farndale RW, Barnes MJ, Liddington RC. Structural basis of collagen recognition by integrin $\alpha 2\beta 1$. Cell. 2000;100:47-56.

113. Dickeson SK, Mathis NL, Rahman M, Bergelson JM, Santoro SA. Determinants of ligand binding specificity of the $\alpha_1\beta_1$ and $\alpha_2\beta_1$ integrins. J Biol Chem. 1999;274:32182-32191.

114. Cruz MA, Bienkowska J, Mato A., Liddington R, Handin RI. Identification of the collagen binding site in the vWF-A3 domain by molecular structure and site specific mutagenesis [abstract]. Blood. 1997;Supplement I:23a.

115. Verkleij MW, IJsseldijk MJW, Heijnen-Snyder GJ, et al. Adhesive domains in the collagen III fragment α1(III)CB4 that support α2β1-and von Willebrand factor-mediated platelet adhesion under flow conditions. Thromb Haemost. 1999;82:1137-1144.

116. Beumer S, Heijnen HFG, IJsseldijk MJW, Orlando E, de Groot PG, Sixma JJ. Platelet adhesion to fibronectin in flow: The importance of von Willebrand factor and glycoprotein Ib. Blood. 1995;86:3452-3460.

117. Ware J. Molecular analyses of the platelet glycoprotein Ib-IX-V receptor. Thromb Haemost. 1998;79:466-478.

118. Berndt MC, Shen Y, Dopheide SM, Gardiner EE, Andrews RK. The vascular biology of the glycoprotein Ib-IX-V complex. Thromb Haemost. 2001;86:178-188.

119. Kenny D, Morateck PA, Montgomery RR. The cysteine knot of platelet glycoprotein Ibbeta (GPIbbeta) is critical for the interaction of GPIbbeta with GPIX. Blood. 2002;99:4428-4433.

120. Munday AD, Berndt MC, Mitchell CA. Phosphoinositide 3-kinase forms a complex with platelet membrane glycoprotein Ib-IX-V complex and 14-3-3zeta. Blood. 2000;96:577-584.

121. Andrews RK, Berndt MC. Adhesion-dependent signalling and the initiation of haemostasis and thrombosis. Histol Histopathol. 1998;13:837-844.

122. Kovacsovics TJ, Bachelot C, Toker A, et al. Phosphoinositide 3-kinase inhibition spares actin assembly in activating platelets but reverses platelet aggregation. J Biol Chem. 1995;270:11358-11366.

123. Lopez JA, Leung B, Reynolds CC, Li CQ, Fox JE. Efficient plasma membrane expression of a functional platelet glycoprotein Ib-IX complex requires the presence of its three subunits. J Biol Chem. 1992;267:12851-12859.

124. Poujol C, Ware J, Nurden AT, Nurden P. Absence of GPIbalpha is responsible for aberrant membrane development during megakaryocyte maturation. Ultrastructural study using a transgenic model. Exp Hematol. 2002;30:352-360.

125. Fredrickson BJ, Dong JF, McIntire LV, López JA. Shear-dependent rolling on von Willebrand factor of mammalian cells expressing the platelet glycoprotein Ib-IX-V complex. Blood. 1998;92:3684-3693.

126. Moog S, Mangin P, Lenain N, et al. Platelet glycoprotein V binds to collagen and participates in platelet adhesion and aggregation. Blood. 2001;98:1038-1046.

127. Shen Y, Romo GM, Dong JF, et al. Requirement of leucine-rich repeats of glycoprotein (GP) Ibα for shear-dependent and static binding of von Willebrand factor to the platelet membrane GP Ib-IX-V complex. Blood. 2000;95:903-910.

128. Kobe B, Kajava AV. The leucine-rich repeat as a protein recognition motif. Curr Opin Struct Biol. 2001;11:725-732.

129. Whisstock JC, Shen Y, Lopez JA, Andrews RK, Berndt MC. Molecular modeling of the seven tandem leucine-rich repeats within the ligand-binding region of platelet glycoprotein Ibα. Thromb Haemost. 2002;87:329-333.

130. Shen Y, Dong JF, Romo G, et al. Functional analysis of the C-terminal flanking sequence of platelet glycoprotein Ibα using canine-human chimers. Blood. 2002;99:145-150.

131. Tait AS, Dong JF, Lopez JA, Dawes IW, Chong BH. Site-directed mutagenesis of platelet glycoprotein Ibalpha demonstrating residues involved in the sulfation of tyrosines 276, 278, and 279. Blood. 2002;99:4422-4427.

132. Marchese P, Murata M, Mazzucato M, et al. Identification of three tyrosine residues of glycoprotein Ibα with distinct roles in von Willebrand factor and α-thrombin binding. J Biol Chem. 1995;270:9571-9578.

133. Dong J, Ye P, Schade AJ, et al. Tyrosine sulfation of glycoprotein I(b)alpha. Role of electrostatic interactions in von Willebrand factor binding. J Biol Chem. 2001;276:16690-16694.

134. Murata M, Ware J, Ruggeri ZM. Site-directed mutagenesis of a soluble recombinant fragment of platelet glycoprotein Ibα demonstrating negatively charged residues involved in von Willebrand factor binding. J Biol Chem. 1991;266:15474-15480.

135. Li C, Pasquale DN, Roth GJ. Bernard-Soulier syndrome with severe bleeding: absent platelet glycoprotein Ib alpha due to a homozygous one-base deletion. Thromb Haemost. 1996;76:670-674.

136. Afshar-Kharghan V, Craig FE, Lopez JA. Bernard-Soulier syndrome in a patient doubly heterozygous for two frameshift mutations in the glycoprotein ib alpha gene. Br J Haematol. 2000;110:919-924.

137. Miller JL, Lyle VA, Cunningham D. Mutation of leucine-57 to phenylalanine in a platelet glycoprotein Ib alpha leucine tandem repeat occurring in patients with an autosomal dominant variant of Bernard-Soulier disease. Blood. 1992;79:439-446.

138. Kenny D, Jonsson OG, Morateck PA, Montgomery RR. Naturally occurring mutations in glycoprotein Ibalpha that result in defective ligand binding and synthesis of a truncated protein. Blood. 1998;92:175-183.

139. Simsek S, Admiraal LG, Modderman PW, van der Schoot CE, dem Borne AE. Identification of a homozygous single base pair deletion in the gene coding for the human platelet glycoprotein Ib alpha causing Bernard- Soulier syndrome. Thromb Haemost. 1994;72:444-449.

140. Kenny D, Morateck PA, Gill JC, Montgomery RR. The critical interaction of glycoprotein (GP) 1bβ with GPIX - A genetic cause of Bernard-Soulier syndrome. Blood. 1999;93:2968-2975.

141. Li C, Martin SE, Roth GJ. The genetic defect in two well-studied cases of Bernard-Soulier syndrome: a point mutation in the fifth leucine-rich repeat of platelet glycoprotein Ib alpha. Blood. 1995;86:3805-3814.

142. Ware J, Russell SR, Marchese P, et al. Point mutation in a leucine-rich repeat of platelet glycoprotein Ibα resulting in the Bernard-Soulier syndrome. J Clin Invest. 1993;92:1213-1220.

143. de la Salle C, Baas MJ, Lanza F, et al. A three-base deletion removing a leucine residue in a leucine- rich repeat of platelet glycoprotein Ib alpha associated with a variant of Bernard-Soulier syndrome (Nancy I). Br J Haematol. 1995;89:386-396.

144. Simsek S, Noris P, Lozano M, et al. Cys209 Ser mutation in the platelet membrane glycoprotein Ib alpha gene is associated with Bernard-Soulier syndrome. Br J Haematol. 1994;88:839-844.

145. Dong J, Schade AJ, Romo GM, et al. Novel gain-of-function mutations of platelet glycoprotein IBalpha by valine mutagenesis in the Cys209-Cys248 disulfide loop. Functional analysis under statis and dynamic conditions. J Biol Chem. 2000;275:27663-27670.

146. Kanaji T, Okamura T, Kuroiwa M, et al. Molecular and genetic analysis of two patients with Bernard- Soulier syndrome - Identification of new mutations in glycoprotein Ibα gene. Thromb Haemost. 1997;77:1055-1061.

147. Ware J, Russell SR, Vicente V, et al. Nonsense mutation in the glycoprotein Ibα coding sequence associated with Bernard-Soulier syndrome. Proc Natl Acad Sci USA. 1990;87:2026-2030.

148. Kunishima S, Miura H, Fukutani H, et al. Bernard-Soulier syndrome Kagoshima: Ser 444-->stop mutation of glycoprotein (GP) Ib alpha resulting in circulating truncated GPIb alpha and surface expression of GPIb beta and GPIX. Blood. 1994;84:3356-3362.

149. Noda M, Fujimura K, Takafuta T, et al. Heterogeneous expression of glycoprotein Ib, IX and V in platelets from two patients with Bernard-Soulier syndrome caused by different genetic abnormalities. Thromb Haemost. 1995;74:1411-1415.

150. Kenny D, Newman PJ, Morateck PA, Montgomery RR. A dinucleotide deletion results in defective membrane anchoring and circulating soluble glycoprotein Ibα in a novel form of Bernard-Soulier syndrome. Blood. 1997;90:2626-2633.

151. Afshar-Kharghan V, López JA. Bernard-Soulier syndrome caused by a dinucleotide deletion and reading frameshift in the region encoding the glycoprotein Ibα transmembrane domain. Blood. 1997;90:2634-2643.

152. Holmberg L, Karpman D, Nilsson I, Olofsson T. Bernard-Soulier syndrome Karlstad: Trp 498-->Stop mutation resulting in a truncated glycoprotein Ibα that contains part of the transmembramous domain. Br J Haematol. 1997;98:57-63.

153. Ludlow LB, Schick BP, Budarf ML, et al. Identification of a mutation in a GATA binding site of the platelet glycoprotein Ibβ promoter resulting in the Bernard- Soulier Syndrome. J Biol Chem. 1996;271:22076-22080.

154. Budarf ML, Konkle BA, Ludlow LB, et al. Identification of a patient with Bernard-Soulier syndrome and a deletion in the DiGeorge/velo-cardio-facial chromosomal region in 22q11.2. Hum Mol Genet. 1995;4:763-766.

155. Ludlow LB, Schick BP, Budarf ML, et al. Identification of a mutation in a GATA binding site of the platelet glycoprotein Ibbeta promoter resulting in the Bernard-Soulier syndrome. J Biol Chem. 1996;271:22076-22080.

156. Kunishima S, Naoe T, Kamiya T, Saito H. Novel heterozygous missense mutation in the platelet glycoprotein Ib beta gene associated with isolated giant platelet disorder. Am J Hematol. 2001;68:249-255.

157. Kunishima S, Tomiyama Y, Honda S, et al. Homozygous Pro74-->Arg mutation in the platelet glycoprotein Ibbeta gene associated with Bernard-Soulier syndrome. Thromb Haemost. 2000;84:112-117.

158. Kunishima S, Lopez JA, Kobayashi S, et al. Missense mutations of the glycoprotein (GP) Ibβ gene impairing the GPIb α/β disulfide linkage in a family with giant platelet disorder. Blood. 1997;89:2404-2412.

159. Kurokawa Y, Ishida F, Kamijo T, et al. A missense mutation (tyr88 to cys) in the platelet membrane glycoprotein Ibbeta gene affects GPIb/IX complex expression--Bernard- Soulier syndrome in the homozygous form and giant platelets in the heterozygous form. Thromb Haemost. 2001;86:1249-1256.

160. Rivera CE, Villagra J, Riordan M, Williams S, Lindstrom KJ, Rick ME. Identification of a new mutation in platelet glycoprotein IX (GPIX) in a patient with Bernard-Soulier syndrome. Br J Haematol. 2001;112:105-108.

161. Wright SD, Michaelides K, Johnson DJ, West NC, Tuddenham EG. Double heterozygosity for mutations in the platelet glycoprotein IX gene in three siblings with Bernard-Soulier syndrome. Blood. 1993;81:2339-2347.

162. Sae-Tung G, Dong JF, Lopez JA. Biosynthetic defect in platelet glycoprotein IX mutants associated with Bernard-Soulier syndrome. Blood. 1996;87:1361-1367.

163. Dinesen B, Feddersen C. An enzyme immunoassay (ELISA) for the quantitation of human factor VIII coagulant antigen (VIII:CAg). Thromb Res. 1983;31:707-718.

164. Noris P, Arbustini E, Spedini P, Belletti S, Balduini CL. A new variant of Bernard-Soulier syndrome characterized by dysfunctional glycoprotein (GP) Ib and severely reduced amounts of GPIX and GPV. Br J Haematol. 1998;103:1004-1013.

165. Vanhoorelbeke K, Schlammadinger A, Delville JP, et al. Occurrence of the Asn45Ser mutation in the GPIX gene in a Belgian patient with Bernard Soulier syndrome. Platelets. 2001;12:114-120.

166. Noris P, Simsek S, Stibbe J, dem Borne AE. A phenylalanine-55 to serine amino-acid substitution in the human glycoprotein IX leucine-rich repeat is associated with Bernard-Soulier syndrome. Br J Haematol. 1997;97:312-320.

167. Noda M, Fujimura K, Takafuta T, et al. A point mutation in glycoprotein IX coding sequence (Cys^{73}(TGT) to Tyr(TAT)) causes impaired surface expression of GPIb/IX/V complex in two families with Bernard-Soulier syndrome. Thromb Haemost. 1996;76:874-878.

168. Wang Z, Shi J, Han Y. [A novel point mutation in the transmembrane domain of platelet glycoprotein IX gene identified in a Bernard-Soulier syndrome patient]. Zhonghua Xue Ye Xue Za Zhi. 2001;22:464-466.

169. Murata M, Russell SR, Ruggeri ZM, Ware J. Expression of the phenotypic abnormality of platelet-type von Willebrand disease in a recombinant glycoprotein Ib alpha fragment. J Clin Invest. 1993;91:2133-2137.

170. Miller JL, Cunningham D, Lyle VA, Finch CN. Mutation in the gene encoding the alpha chain of platelet glycoprotein Ib in platelet-type von Willebrand disease. Proc Natl Acad Sci U S A. 1991;88:4761-4765.

171. Tait AS, Cranmer SL, Jackson SP, Dawes IW, Chong BH. Phenotype changes resulting in high-affinity binding of von Willebrand factor to recombinant glycoprotein Ib-IX: analysis of the platelet-type von Willebrand disease mutations. Blood. 2001;98:1812-1818.

172. Russell SD, Roth GJ. Pseudo-von Willebrand disease: a mutation in the platelet glycoprotein Ib alpha gene associated with a hyperactive surface receptor. Blood. 1993;81:1787-1791.

173. Moriki T, Murata M, Kitaguchi T, et al. Expression and functional characterization of an abnormal platelet membrane glycoprotein Ibα (Met^{239}-->Val) reported in patients with platelet-type von Willebrand disease. Blood. 1997;90:698-705.

174. Scott JP, Montgomery RR, Retzinger GS. Dimeric ristocetin flocculates proteins, binds to platelets, and mediates von Willebrand factor-dependent agglutination of platelets. J Biol Chem. 1991;266:8149-8155.

175. Bardsley B, Williams D.H., Baglin TP. Cleavage of rhamnose from ristocetin A removes its ability to induce platelet aggregation. Blood Coagul Fibrinolysis. 1998;9:241-244.

176. Girma JP, Takahashi Y, Yoshioka A, Diaz J, Meyer D. Ristocetin and botrocetin involve two distinct domains of von Willebrand factor for binding to platelet membrane glycoprotein Ib. Thromb Haemost. 1990;64:326-332.

177. Andrews RK, Booth WJ, Gorman JJ, Castaldi PA, Berndt MC. Purification of botrocetin from *Bothrops jararaca* venom. Analysis of the botrocetin-mediated interaction between von Willebrand factor and the human platelet membrane glycoprotein Ib- IX complex. Biochemistry. 1989;28:8317-8326.

178. Fujimura Y, Titani K, Usami Y, et al. Isolation and chemical characterization of two structurally and functionally distinct forms of botrocetin, the platelet coagglutinin isolated from the venom of Bothrops jararaca. Biochemistry. 1991;30:1957-1964.

179. Usami Y, Fujimura Y, Suzuki M, et al. Primary structure of two-chain botrocetin, a von Willebrand factor modulator purified from the venom of *Bothrops jararaca*. PNAS. 1993;90:928-932.

180. De Luca M, Ward CM, Ohmori K, Andrews RK, Berndt MC. Jararhagin and jaracetin: novel snake venom inhibitors of the integrin collagen receptor, alpha 2 beta 1. Biochem Biophys Res Commun. 1995;206:570-576.

181. Hamako J, Matsui T, Suzuki M, et al. Purification and characterization of bitiscetin, a novel von Willebrand factor modulator protein from *Bitis arietans* snake venom. Biochem Biophys Res Commun. 1996;226:273-279.

182. Hirotsu S, Mizuno H, Fukuda K, et al. Crystal structure of bitiscetin, a von Willebrand factor-dependent platelet aggregation inducer. Biochemistry. 2001;40:13592-13597.

183. Nurden P, Chretien F, Poujol C, Winckler J, Borel-Derlon A, Nurden A. Platelet ultrastructural abnormalities in three patients with type 2B von Willebrand disease. Br J Haematol. 2000;110:704-714.

184. Sobel M, McNeill PM, Carlson PL, et al. Heparin inhibition of von Willebrand factor-dependent platelet function in vitro and in vivo. J Clin Invest. 1991;87:1787-1793.

185. Shin Y, Okuyama I, Hasegawa J, Morita T. Molecular cloning of glycoprotein Ib-binding protein, flavocetin-A, which inhibits platelet aggregation. Thromb Res. 2000;99:239-247.

186. Fukuda K, Mizuno H, Atoda H, Morita T. Crystal structure of flavocetin-A, a platelet glycoprotein Ib-binding protein, reveals a novel cyclic tetramer of C-type lectin-like heterodimers. Biochemistry. 2000;39:1915-1923.

187. Taniuchi Y, Kawasaki T, Fujimura Y, et al. Flavocetin-A and -B, two high molecular mass glycoprotein Ib binding proteins with high affinity purified from Trimeresurus flavoviridis venom, inhibit platelet aggregation at high shear stress. Biochim Biophys Acta. 1995;1244:331-338.

188. Peng M, Lu W, Kirby EP. Characterization of three alboaggregins purified from *Trimeresurus albolabris* venom. Thromb Haemost. 1992;67:702-707.

189. Sakurai Y, Fujimura Y, Kokubo T, et al. The cDNA cloning and molecular characterization of a snake venom platelet gpycoprotein Ib-binding protein, mamushgin, from *Agkistrodon halys blomhoffii* venom. Thromb Haemost. 1998;79:1199-1207.

190. Yeh CH, Wang WC, Hsieh TTHTF. Agkistin, a snake venom-derived glycoprotein Ib antagonist, disrupts von Willebrand factor-endothelial cell interaction and inhibits angiogenesis. J Biol Chem. 2000;275:18615-18618.

191. Polgar J, Magnenat EM, Peitsch MC, Wells TN, Saqi MS, Clemetson KJ. Amino acid sequence of the alpha subunit and computer modelling of the alpha and beta subunits of echicetin from the venom of Echis carinatus (saw-scaled viper). Biochem J. 1997;323 (Pt 2):533-537.

192. Peng M, Holt JC, Niewiarowski S. Isolation, characterization and amino acid sequence of echicetin beta subunit, a specific inhibitor of von Willebrand factor and thrombin interaction with glycoprotein Ib. Biochem Biophys Res Commun. 1994;205:68-72.

193. Peng M, Lu W, Beviglia L, Niewiarowski S, Kirby EP. Echicetin: a snake venom protein that inhibits binding of von Willebrand factor and alboaggregins to platelet glycoprotein Ib. Blood. 1993;81:2321-2328.

194. Kawasaki T, Fujimura Y, Usami Y, et al. Complete amino acid sequence and identification of the platelet glycoprotein Ib-binding site of jararaca GPIb-BP, a snake venom protein isolated from Bothrops jararaca. J Biol Chem. 1996;271:10635-10639.

195. Fujimura Y, Ikeda Y, Miura S, et al. Isolation and characterization of jararaca GPIb-BP, a snake venom antagonist specific to platelet glycoprotein Ib. Thromb Haemost. 1995;74:743-750.

196. Kawasaki T, Taniuchi Y, Hisamichi N, et al. Tokaracetin, a new platelet antagonist that binds to platelet glycoprotein ib and inhibits von Willebrand factor-dependent shear- induced platelet aggregation. Biochem J. 1995;308 (Pt 3):947-953.

197. Girma JP, Fressinaud E, Christophe O, et al. Aurin tricarboxylic acid inhibits platelet adhesion to collagen by binding to the 509-695 disulphide loop of von Willebrand factor and competing with glycoprotein Ib. Thromb Haemost. 1992;68:707-713.

198. Sen U, Vasudevan S, Subbarao G, et al. Crystal Structure of the von Willebrand Factor Modulator Botrocetin. Biochemistry. 2001;40:345-352.

199. Matsushita T, Meyer D, Sadler JE. Localization of von willebrand factor-binding sites for platelet glycoprotein Ib and botrocetin by charged-to-alanine scanning mutagenesis. J Biol Chem. 2000;275:11044-11049.

200. Huizinga EG, Schouten A, Romijn RAP, et al. Crystal strucures of snake venom botrocetin and its complex with the von willebrand Factor A1 domain [abstract]. Thromb Haemost. 2001.

201. Hilbert L, Gaucher C, Mazurier C. Effects of different amino-acid substitutions in the leucine694-proline708 segment of recombinant von Willebrand factor. Br J Haematol. 1995;91:983-990.

202. Dong JF, Berndt MC, Schade A, McIntire LV, Andrews RK, Lopez JA. Ristocetin-dependent, but not botrocetin-dependent, binding of von willebrand factor to the platelet glycoprotein Ib-IX-V complex correlates with shear-dependent interactions. Blood. 2001;97:162-168.

203. Celikel R, Ruggeri ZM, Varughese KI. Von Willebrand Factor conformation and adhesive function is modulated by an internalized water molecule. Nature Struct Biol. 2000;7:881-884.

204. Miller JL. Platelet-type von Willebrand disease. Thromb Haemost. 1996;75:865-869.

205. Nurden AT, Didry D, Rosa JP. Molecular defects of platelets in Bernard-Soulier syndrome. Blood Cells. 1983;9:333-358.

206. Matsushita T, Sadler JE. Identification of amino acid residues essential for von Willebrand factor binding to platelet glycoprotein Ib. Charged-to-alanine scanning mutagenesis of the A1 domain of human von Willebrand factor. J Biol Chem. 1995;270:13406-13414.

207. Holmberg L, Dent JA, Schneppenheim R, Budde U, Ware J, Ruggeri ZM. von Willebrand factor mutation enhancing interaction with platelets in patients with normal multimeric structure. J Clin Invest. 1993;91:2169-2177.

208. Meyer D, Fressinaud E, Gaucher C, et al. Gene defects in 150 unrelated French cases with type 2 von Willebrand disease: from the patient to the gene. INSERM Network on Molecular Abnormalities in von Willebrand Disease. Thromb Haemost. 1997;78:451-456.

209. Rabinowitz I, Rand JH, Shindler KS, Tuley EA, Rustagi PK, Sadler JE. Type IIB mutation His-505-Asp implicates a nwew segment in the control of von Willebrand factor binding to platelet glycoprotein Ib. J Biol Chem. 1993;268:20497-20501.

210. Siguret V, Ribba AS, Christophe O, et al. Characterization of recombinant von Willebrand factors mutated on cysteine 509 or 695. Thromb Haemost. 1996;76:453-459.

211. Girma JP, Ribba AS, Meyer D. Structure-function relationship of the A1 domain of von Willebrand factor. Thromb Haemost. 1995;74:156-160.

212. Christophe O, Ribba AS, Baruch D, et al. Influence of mutations and size of multimers in type II von Willebrand disease upon the function of von Willebrand factor. Blood. 1994;83:3553-3561.

213. Rastegar-Lari G, Ajzenberg N, Ribba AS, et al. Defect of heparin binding in plasma and recombinant von Willebrand factor with type 2 von Willebrand disease mutations. Thromb Haemost. 2001;86:1459-1465.

214. AnonymousIdentification of type 2M von Willebrand Disease of 5 new candidate mutations in the N-terminal part of the A1 loop of von Willebrand Factor [abstract]. Thrombosis and Haemostasis, Supplement. 1999;x:283-284.

215. Cruz MA, Diacovo TG, Emsley J, Liddington R, Handin RI. Mapping the glycoprotein Ib-binding site in the von willebrand factor A1 domain. J Biol Chem 2000 Jun 23 ;275 (25):19098 -105.275:19098-19105.

216. Kroner PA, Frey AB. Analysis of the structure and function of the von Willebrand factor A1 domain using targeted deletions and alanine-scanning mutagenesis. Biochemistry. 1996;35:13460-13468.

217. Ajzenberg N, Ribba AS, Rastegar-Lari G, Meyer D, Baruch D. effect of recombinant von Willebrand factor reproducing type 2B or type 2M mutations on shear-induced platelet aggregation. Blood. 2000;95:3796-3803.

218. Ribba AS, Lavergne JM, Bahnak BR, Derlon A, Pietu G, Meyer D. Duplication of a methionine within the glycoprotein Ib binding domain of von Willebrand factor detected by denaturing gradient gel electrophoresis in a patient with type IIB von Willebrand disease. Blood. 1991;78:1738-1743.

219. Facey DA, Favaloro EJ, Koutts J, Berndt MC, Hertzberg MS. Identification and characterization of a novel mutation in von Willebrand factor causing type 2B von Willebrand's disease. Br J Haematol. 1999;105:538-541.

220. Hilbert L. Identification of "new" type 2B von Willebrand disease mutations:R543Q, R545P and R578L [abstract]. Br J Haematol. 1996;93:310.

221. De Romeuf C, Hilbert L, Mazurier C. Platelet activation and aggregation induced by recombinant von Willebrand factors reproducing four type 2B von Willebrand disease missense mutations. Thromb Haemost. 1998;79:211-216.

222. Lankhof H, Damas C, Schiphorst ME, et al. Functional studies on platelet adhesion with recombinant von Willebrand factor type 2B mutants R543Q and R543W under conditions of flow. Blood. 1997;89:2766-2772.

223. Facey DA, Favaloro EJ, Maxwell E, Baker R, Hertzberg MS. Type 2B von Willebrand's disease in thirteen individuals from five unrelated Australian families: phenotype and genotype correlations. Am J Hematol 2000; 63 (4):197 -9.63:197-199.

224. Federici AB, Mannucci PM, Stabile F, et al. A type 2b von Willebrand disease mutation (Ile546-->Val) associated with an unusual phenotype. Thromb Haemost. 1997;78:1132-1137.

225. Cooney KA, Ginsburg D. Comparative analysis of type 2B von Willebrand Disease mutations: implications for the mechanism of von Willebrand Factor binding to platelets. Blood. 1996;87:2322-2328.

226. Rand JH, Jorieux S, Tuley EA, Mazurier C, Sadler JE. Recombinant von Willebrand factor Arg578-Gln. J Biol Chem. 1992;267:21187-21192.

227. Donner M, Kristoffersson AC, Lenk H, et al. Type IIB von Willebrand's disease: gene mutations and clinical presentation in nine fanilies fram Denmark, Germany and Sweden. Br J Haematol. 1992;82:58-65.

228. Donner M, Kristoffersson AC, Andersson AM, Nilsson AC, Dahlback B, Holmberg L. An Arg545Cys substitution mutation of the von Willebrand factor in type IIb von Willebrand's disease. Eur J Haematol. 1991;47:342-345.

229. Gurevitz O, Goldfarb A, Hod H, et al. Recombinant von Willebrand factor fragment AR545C inhibits platelet aggregation and enhances thrombolysis with rtPA in a rabbit thrombosis model. Arterioscler Thromb Vasc Biol. 1998;18:200-207.

230. Miyata S, Goto S, Federici AB, Ware J, Ruggeri ZM. Conformational changes in the A1 domain of von Willebrand factor modulating the interaction with platelet glycoprotein Ibα. J Biol Chem. 1996;271:9046-9053.

231. Wood N, Standen GR, Bowen DJ, et al. UHG-based mutation screening in type 2B von Willebrand's disease: detection of a candidate mutation Ser547Phe. Thromb Haemost. 1996;75:363-367.

232. Ware J, Dent JA, Azuma H, et al. Identification of a point mutation in type IIB von Willebrand disease illustrating the regulation of von Willebrand factor affinity for the platelet membrane glycoprotein Ib-IX receptor. Proc Natl Acad Sci USA. 1991;88:2946-2950.

233. Casana P, Martinez F, Espinos C, Haya S, Lorenzo JI, Aznar JA. Search for mutations in a segment of the exon 28 of the human von Willebrand factor gene: new mutations, R1315C and R1341W, associated with type 2M and 2B variants. Am J Hematol. 1998;59:57-63.

234. Dent JA, Galbusera M, Ruggeri ZM. Heterogeneity of plasma von Willebrand factor multimers resulting from proteolysis of the constituent subunit. J Clin Invest. 1991;88:774-782.

235. Randi AM, Jorieux S, Tuley EA, Mazurier C, Sadler JE. Recombinant von Willebrand factor Arg578-->Gln. A type IIB von Willebrand disease mutation affects binding to glycoprotein Ib but not to collagen or heparin. J Biol Chem. 1992;267:21187-21192.

236. Murray E, Giles AR, Lillicrap D. Germ-line mosaicism for a Valine-to-Methionine substitutionn at residue 553 in the glycoprotein Ib-binding domain of von Willebrand factor, causing type IIB von Willebrand disease. Am J Hum Genet. 1992;50:199-207.

237. Rabinowitz I, Tuley EA, Mancuso DJ, et al. von Willebrand disease type B: a missense mutation selectively abolishes ristocetin-induced von Willebrand factor binding to platelet glycoprotein Ib. Proc Natl Acad Sci U S A. 1992;89:9846-9849.

238. Hilbert L, Gaucher C, Fressinaud E, Meyer D, Mazurier C. a new type 2M ("type B") vWD mutation (G1324A) also at position 561 of the mature vWF subunit [abstract]. Thrombosis and Haemostasis, Supplement. 1997;77:654.

239. Hilbert L, Fressinaud E, Ribba AS, Meyer D, Mazurier C. Identification of a new type 2M von Willebrand disease mutation also at position 1324 of von Willebrand factor. Thromb Haemost. 2002;87:635-640.

240. Vasudevan S, Roberts JR, McClintock RA, et al. Modeling and functional analysis of the interaction between von Willebrand factor A1 domain and glycoprotein Ibalpha. J Biol Chem 2000 Apr 28 ;275 (17):12763 -8.275:12763-12768.

241. Rastegar-Lari G, Legendre P, Ribba AS, Meyer D, Baruch D. A cluster of six charged residues within the main heparin-binding site of von Willebrand Factor is essential for heparin binding [abstract]. Thrombosis and Haemostasis, Supplement. 2001.

242. Kroner PA, Kluessendorf ML, Scott JP, Montgomery RR. A Pro574>leu substitution in von Willebrand Factor enhances the binding of expressed protein to platelets and is linked to type IIB von Willebrand disease [abstract]. Thrombosis and Haemostasis, Supplement. 1991;65:763.

243. Song KS, Kang SH, Kang MS, et al. von Willebrand disease with G4022A mutation (vWd Sungnam): a case report. J Korean Med Sci. 1999;14:93-96.

244. Hillery CA, Mancuso DJ, Sadler JE, et al. Type 2M von Willebrand disease: F606I and I662F mutations in the glycoprotein Ib binding domain selectively impair ristocetin - but not botrocetin-mediated binding of von Willebrand factor to platelets. Blood. 1998;91:1572-1581.

245. Castaman G, Eikenboom JC, Rodeghiero F, Briet E, Reitsma PH. A novel candidate mutation (Arg611-->His) in type I 'platelet discordant' von Willebrand's disease with desmopressin-induced thrombocytopenia. Br J Haematol. 1995;89:656-658.

246. Hilbert L, Gaucher C, Mazurier C. Identification of two mutations (Arg611Cys and Arg611His) in the A1 loop of von Willebrand factor (vWF) responsible for type 2 von Willebrand disease with decreased platelet-dependent function of vWF. Blood. 1995;86:1010-1018.

247. Nishikubo T, Christophe O, Lavergne JM, et al. Abnormal proteolytic processing of von Willebrand Factor Arg611Cys and Arg611His. Thromb Haemost. 1997;77:174-182.

248. Mancuso DJ, Kroner PA, Christopherson PA, Vokac EA, Gill JC, Montgomery RR. Type 2M:Milwaukee-1 von Willebrand disease: an in-frame deletion in the Cys509-Cys695 loop of the von Willebrand factor A1 domain causes deficient binding of von Willebrand factor to platelets. Blood. 1996;88:2559-2568.

249. Hilbert L, Gaucher C, Romeuf C, Horellou MH, Vink T, Mazurier C. Leu 697-Val mutation in mature von Willebrand factor in responcible for type 2B Willebrand disease. Blood. 1994;83:1542-1550.

250. Sugimoto M, Mohri H, McClintock RA, Ruggeri ZM. Identification of discontinuous von Willebrand factor sequences involved in complex formation with botrocetin. A model for the regulation of von Willebrand factor binding to platelet glycoprotein Ib. J Biol Chem. 1991;266:18172-18178.

Chapter 2

Identification of the collagen-binding site of the von Willebrand Factor A3-domain

Roland A.P. Romijn[¶†], Barend Bouma[¶‡], Winnifred Wuyster[†], Piet Gros[‡], Jan Kroon[‡], Jan J. Sixma[†] and Eric G. Huizinga[†‡]

[†] Thrombosis and Haemostasis Laboratory, Department of Haematology, University Medical Center and Institute of Biomembranes, HP G03.647, PO box 85500, 3508 GA Utrecht, The Netherlands and

[‡] Bijvoet Center for Biomolecular Research, Department of Crystal and Structural Chemistry, Utrecht University, Padualaan 8, 3584 CH Utrecht, The Netherlands.

[§] These authors contributed equally

Published in the Journal of Biological Chemistry, 276 (13), 9985-9991, 2001

Summary

Von Willebrand factor (vWF) is a multimeric glycoprotein that mediates platelet adhesion and thrombus formation at sites of vascular injury. VWF functions as a molecular bridge between collagen and platelet receptor glycoprotein Ib. The major collagen-binding site of vWF is contained within the A3 domain, but its precise location is unknown. To localize the collagen-binding site, we determined the crystal structure of A3 in complex with a Fab fragment of antibody RU5 that inhibits collagen binding. The structure shows that RU5 recognizes a non-linear epitope consisting of residues 962-966, 981-997 and 1022-1026. Alanine-mutants were constructed of residues Arg963, Glu987, His990, Arg1016 and His1023, located in or close to the epitope. Mutants were expressed as fully processed multimeric vWF. Mutation of His1023 abolished collagen binding, while mutation of Arg963 and Arg1016 reduced collagen binding by 25 – 35%. These residues are part of loops $\alpha 3\beta 4$ and $\alpha 1\beta 2$ and α-helix 3, respectively, and lie near the bottom face of the domain. His1023 and flanking residues display multiple conformations in available A3-crystal structures suggesting that binding of A3 to collagen involves an induced-fit mechanism. The collagen-binding site of A3 is located distant from the top face of the domain where collagen-binding sites are found in homologous integrin I-domains.

Introduction

Platelet adhesion to damaged vessel walls is the first step in the formation of an occluding platelet plug, which leads to the arrest of bleeding during normal hemostasis. Platelet adhesion can also cause thrombotic complications such as the occlusion of aetherosclerotic arteries [1]. The multimeric glycoprotein von Willebrand factor (vWF)[1] plays an essential role in platelet adhesion under conditions of high shear stress [2; 3]. In this process vWF serves as a molecular bridge that links collagen exposed by the damaged vessel wall to glycoprotein Ib located on the platelet surface. Collagens that act as binding sites for vWF include types I and III in perivascular connective tissue and type VI in the sub-endothelial matrix [3; 4].

Mature vWF consists of a 2,050 residue monomer that contains multiple copies of so called A, B, C and D-type domains and one CK (cystine knot) domain arranged in the order D'-D3-A1-A2-A3-D4-B1-B2-B3-C1-C2-CK [1; 3]. Disulfide-bond formation between N-terminal D3 domains and between C-terminal CK domains generates vWF multimers that consist of up to 80 monomers. The A1 domain contains the binding site for glycoprotein Ib [5]. The A3 domain (residues 920-1111) contains the major binding site for collagen types I and III [6]. The multimeric structure of vWF is essential for high-affinity collagen binding [7]. Multimeric vWF binds collagen with an apparent K_d of 1-7 nM [8], while a recombinant A3 domain has a much higher K_d of 2 μM [9]. Deletion of the A2 and D4 domains, that flank the A3 domain, or deletion of the A1 domain does not decrease collagen binding of multimeric vWF [6; 8]. These data show that a monomeric A3 domain contains a fully active collagen-binding site, the only requirement for tight binding to collagen being the presence of multiple A3 domains within one vWF multimer.

Integrin I-type domains are homologous to vWF A-type domains [10; 11]. I-domains of integrin α-chains α1, α2, α10 and α11 all possess collagen-binding sites. A crystal structure of the α_2 I-domain reveals binding of a collagen-like peptide to a groove in the surface of the 'top' face of the domain [12]. This groove contains a so-called metal ion-dependent adhesion site (MIDAS) [13; 14] which engages a glutamate residue of collagen.

The location of the collagen-binding site in the vWF-A3 domain is not known. Crystal structures of A3 do not display a collagen-binding groove in the top face, instead, the surface of A3 is rather smooth [15; 16]. Although the MIDAS motif is partly conserved, binding of A3 to collagen does not require a metal ion [17; 18] and no metal ion is observed in crystal structures of A3. Moreover, point mutations in the MIDAS motif of A3 do not disrupt collagen binding [8; 16] showing that the motif is not involved in collagen binding, at all. Site-directed mutagenesis

studies of other residues in the top face of A3 have yielded conflicting results. Cruz *et al.* [19] reported in abstract form that amino-acid substitutions D1069R, R1074D, R1090D and E1092R resulted in a 50% reduction in binding of monomeric A3 to collagen. Van der Plas *et al.* [8], however, observed normal collagen binding of fully processed multimeric vWF containing mutations D1069R, D1069A or R1074A. In the same study, mutations V1040A/V1042A, D1046A and D1066A also displayed normal collagen binding, suggesting that the collagen-binding site of vWF-A3 is not located in its top face.

The crystallographic study presented here was conducted to provide new clues on the location of the collagen-binding site of the vWF-A3 domain. We determined the structure of the A3 domain in complex with a Fab fragment of monoclonal antibody RU5, which inhibits binding of vWF to collagen. Site-directed-mutagenesis of residues located in the epitope-region show that the collagen-binding site is located distant from the top face of A3.

Experimental procedures

Purification of vWF-A3 and RU5

Recombinant seleno-methionine (Se-Met) A3, comprising residues 920 to 1111 of human vWF, was expressed and purified as described before [15]. For production of monoclonal antibody RU5 ($IgG_{2a,\ \kappa}$) hybridoma cells were injected in mice and ascites fluid was collected (Eurogentec, Seraing, Belgium). IgG was purified on a protein G-Sepharose column and Fab fragments were generated using an ImmunoPure Fab Kit (Pierce, Rockford IL, USA). RU5-Fab was further purified with A3-affinity chromatography. For that end, 10 mg of A3 was irreversibly bound via its N-terminal histidine tag to cobalt(III)-iminodiacetate chelating Sepharose (Pharmacia Biotech, Uppsala, Sweden), according to a procedure described by Hale [20]. RU5 Fab fragment was loaded onto the A3-affinity column, washed with PBS and subsequently eluted with 50 mM tri-ethylamine solution (pH 10.0). Some aggregates were removed on a Superdex 75 HR 10/30 gel-filtration column (Pharmacia, Uppsala, Sweden). Running buffer was 10 mM Tris-HCl pH 8.0, 25 mM NaCl. Next, RU5-Fab was mixed with a twofold molar excess of (Se-Met) A3. The A3-RU5 complex was separated from excess A3 by gel-filtration chromatography. Dynamic-light scattering measurements on a Dynapro-801 DLS Instrument (Protein Solutions, Charlottesville VA, USA) indicated the presence of 69-kDa particles in agreement with an expected molecular weight of about 72 kDa of the complex between A3 and RU5.

Determination of RU5 Variable Domain Sequences

The amino-acid sequence of the variable domain of the heavy chain (V_H) of RU5 was deduced from a cDNA nucleotide sequence. Cloning and sequencing was carried out using established procedures. Total RNA was extracted from $4*10^6$ RU5 hybridoma cells with RNAzol using the RNA-isolation protocol of the supplier (Campro Scientific, Veenendaal, The Netherlands). First-strand cDNA was synthesized using Superscript II reverse transcriptase (Gibco, Rockville MD, USA) in the presence of 3.2 U/µl of RNase-inhibitor RNaseOUT (Gibco, Rockville MD, USA). cDNA encoding the V_H domain was amplified by polymerase chain reaction (PCR) with Pwo DNA polymerase (Boehringer, Mannheim, Germany). A backward variable-region consensus primer (B4: CCA GGG GCC AGT GGA TAG ACA AGC TTG GGT GTC GTT TT) was used together with a forward primer (B3c: CGG ATG GCC AGG T[C/G][A/C] AGC TGC AG[C/G] AGT C[A/T]G G) that hybridizes with a consensus sequence in the J_H region [21]. The PCR product was extended with a 3'-A overhang using Taq DNA polymerase (Promega, Madison WI, USA) and cloned into the pCR2.1-TOPO vector according to the manufacturer's protocol (Invitrogen, Leek, The Netherlands). Nucleotide sequences of three clones were determined[2] (figure 1A).

For determination of the sequence of the variable domain (V_L) of the RU5 κ-light chain, the same procedure was used as for the V_H domain. For cloning of the V_L gene, one backward variable-region consensus primer (PD1: GAT ATT GTG ATG ACC CAG TCT [C/G]T) and two forward variable-region consensus primers (PD3: CAG GAA ACA GCT ATG ACC GAG CTC GTG ATC ACC CAG TCT CC; PD4: TGT AAA ACG ACG GCC AGT TCT AGA TGG TGG GAA GAT GGA) were used. However, determination of the sequence was hampered by the abundance of mRNA encoding the light chain of the non-producing myeloma-fusion partner of the RU5 hybridoma cell, a known drawback of myeloma-cell line P363Ag8.653 [22].

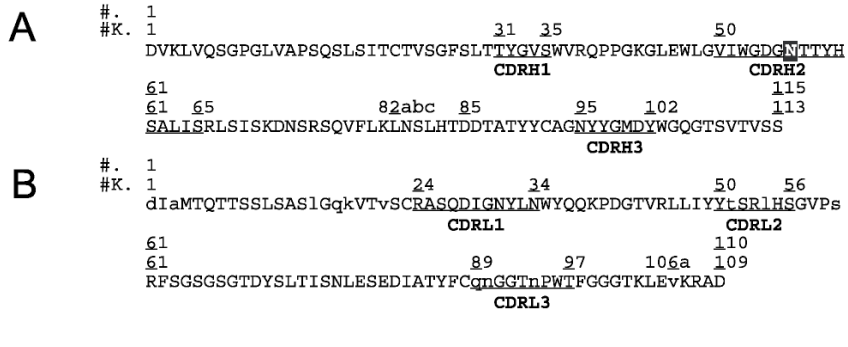

Figure 1: Amino acid sequences of RU5 V_L and V_H domains. CDRs (underlined) were defined according to Kabat *et al.* [23]. Strict sequential numbering (#) is used throughout the text. Numbering according to the convention of Kabat *et al.* [23] (#K) is also shown. *A*. The amino acid sequence of V_H was deduced from cDNA. Residues 1 to 7 could not be deduced precisely due to the use of a primer complementary to the 5' coding region. Asn56 in CDR_{H2} (shaded) is N-glycosylated. The nucleotide sequence of V_H has been deposited in the GeneBank database under Accession Number AF286587. *B*. The amino acid sequence of the V_L domain was deduced from the electron density of the A3-RU5 complex and an alignment of 110 Fab V_L chains. Side chains of thirteen amino acid residues that could not be determined unambiguously from the electron density and the consensus sequence are shown as lower case characters.

Crystallization and Data Collection

Crystals of the (Se-Met) A3-RU5 complex were grown by hanging-drop vapor-diffusion at 4° C using a protein concentration of 15 mg/ml and a precipitant solution consisting of 13% (v/v) iso-propanol, 22% (v/v) 2-methyl-2,4-pentanediol (MPD) and 100 mM cacodylic acid pH 5.3. The crystal used for structure determination had a size of 0.1x0.1x0.2 mm^3 and was equilibrated in a cryo-protectant solution consisting of 8% iso-propanol, 30% MPD, 100 mM cacodylic acid pH 5.3. X-ray diffraction data were collected on beam line BW7B of the synchrotron-radiation facility of the EMBL outstation (Hamburg, Germany) with a Mar345 imaging plate (Mar, Evanston IL, USA). Data reduction, merging and scaling were performed with DENZO and SCALEPACK [23]. Diffraction-data statistics can be found in Table I. Diffraction of the A3-RU5 crystal was anisotropic. For structure determination, anisotropic B-factors were applied with SCALEIT and SFTOOLS [24] to correct for the observed anisotropy.

Table I

Diffraction-data and refinement statistics

Diffraction data	
Wavelength (Å)	0.8469
Resolution (Å)	29.9-2.56/2.03[a]
Space group	C2
a, *b*, *c* (Å)	121.80, 183.55, 131.84
α, β, γ (°)	90.0, 116.21, 90.0
Mosaicity (°)	0.22
Redundancy	4.2
No. of unique reflections	143,255
$\langle I \rangle / \langle \sigma(I) \rangle$	20.4 (2.4)[b]
Completeness (%)	85.9 (51.5)[a]
R_{merge} (%)[c]	6.1 (40.4)
Refinement	
Resolution (Å)	29.9 - 2.03
R-factor	0.227
R_{free}	0.264
r.m.s.d. bond distances (Å)	0.007
r.m.s.d. angles (°)	1.41
Average overall B-factor ($Å^2$)	38
No. of protein atoms[d]	13,889
No. of carbohydrate atoms	100
No. of cacodylate ions	1
No. of solvent molecules	878

[a] Data completeness is 100% between 29.9-2.56 Å resolution and drops to 51.5% between 2.56-2.03 Å resolution, due to anisotropic diffraction.

[b] Numbers in parentheses indicate statistics for highest resolution shells.

[c] $R_{merge} = \sum_h \sum_i |I_{hi} - \langle I_h \rangle| / \sum_h \sum_i |I_{hi}|$

[d] An asymmetric unit contains three A3-RU5 complexes.

Structure Determination and Refinement

A self-rotation function calculated with POLARRFN [24] and the unit-cell volume suggested the presence of three A3-RU5 complexes in the asymmetric unit (a.u.) with a V_M of 3.3 Å^3/Da and a solvent content of 63%. Initial attempts to solve the structure by molecular replacement failed. Therefore, a rather weak anomalous signal ($<\Delta F_{ano}/\sigma(F)> = 1.18$) arising from the presence of Se-Met in A3 was used to locate Se sites from an anomalous Patterson map. Six Se sites could be assigned to Met947, Met998 and Met1097 of two A3 molecules on the basis of inter-atomic distances and the observed two-fold non-crystallographic symmetry (n.c.s). The positioning of two A3 molecules in the a.u. allowed further molecular replacement to proceed in a straightforward manner. A Fab-fragment of protein data bank entry 2MPA [25; 26] was oriented using the program AmoRe [27] followed by Patterson correlation refinement using CNS [28; 29]. Cross translation functions calculated with CNS identified the position of three Fab-fragments. A third A3 molecule was placed on the basis of n.c.s. The a.u. finally contained three A3-RU5 complexes with an R-factor of 42.6% after rigid body refinement.

For model building, sequences of the constant domain of the light chain (C_L) and of the constant domain of the heavy chain (C_{H1}) of RU5 were taken from $IgG_{2a,\kappa}$ monoclonal antibody 4-4-20 [30; 31]. The sequence of residues 1 to 110 of the V_L domain of RU5 (Fig. 1B) was derived from the electron density aided by a consensus sequence based on an alignment of 110 Fab sequences. For model refinement, cycles of rebuilding using O [32] and positional and B-factor refinement using CNS were performed until convergence. Cross validation was used throughout refinement using a 5% test set of reflections. Refinement used the maximum-likelihood algorithm [33]. Bulk-solvent correction and anisotropic scaling of diffraction data was applied. During the first cycles of refinement n.c.s. restraints were used. Based on the behavior of the free R-factor, n.c.s. restraints were omitted in later stages of refinement. Water molecules were placed in difference electron-density peaks with a peak height of at least 2.8 σ, a distance of 2.5-3.4 Å to a hydrogen-bond donor or acceptor and a B-factor smaller than 65 Å^2.

Construction of vWF Point Mutants

Point mutations were introduced in the vWF-A3 domain using the Quikchange method (Stratagene, La Jolla CA, USA) and specific primers (Amersham Pharmacia Biotech, Roosendaal, The Netherlands). First, a 518 base pair NheI-Csp45I fragment corresponding to amino acid residues 940 to 1113 of mature vWF was subcloned into pBluescript SKII (Stratagene, La Jolla CA, USA). To this end a unique Csp45I restriction site was introduced at position 5628 of

expression vector pNUT-vWFcas [8] in the following way. The BamHI - EcoRV fragment of pNUT-vWFcas was ligated into pBluescript SKII. The Csp45I site was introduced using Quickchange and confirmed by sequencing. The NheI – EcoRV fragment containing the new Csp45I site was ligated into pNUT-vWFcas generating pNUT-vWFcas2. Next, the NheI - Csp45I fragment of pNUT-vWFcas2 was made blunt by filling in of 5' overhangs using Pwo DNA polymerase. Ligation of this fragment into EcoRI - AccI digested and Pwo treated pBluescript SKII, produced mutagenesis plasmid pBSvWF-NC. This plasmid retains the NheI and Csp45I restriction sites. Point mutations R963A, E987A, H990A, R1016A and H1023A were introduced in pBSvWF-NC. Mutation H1023A causes the disappearance of a NsiI restriction site. The NheI - Csp45I fragment of this mutant was ligated directly into pNUT-vWFcas2 and confirmed by restriction analysis. The NheI – Csp45I fragment of the other point mutants were ligated into pNUT-vWFcas2-H1023A, with reappearance of the NsiI site.

Expression, Purification and Characterization of vWF

vWF was stably expressed in fur-BHK cells, a baby hamster kidney cell line overexpressing furin necessary for proper removal of vWF propeptide [6; 34]. VWF was purified by immuno-affinity chromatography using monoclonal antibody RU8, which is directed against the D4 domain [6]. VWF-containing fractions were pooled and stored in aliquots at –20 °C until use.

The concentration of vWF was determined by a sandwich ELISA using polyclonal α-vWF and horseradish peroxidase (HRP) conjugated polyclonal α-vWF (DAKO, Glostrup, Denmark) for immobilization and detection, respectively [6]. Normal pooled plasma from 40 healthy donors was used as a reference.

The multimeric structure of vWF was analyzed by agarose gel electrophoresis followed by Western blotting as described by Lawrie *et al.* [35].

Binding of vWF to monoclonal antibody RU5 was analyzed as follows. Microtiter-plate wells (Costar, Cambridge MA, USA) were coated with 2.5 µg/ml polyclonal α-D'D3 [8] in 50 mM carbonate buffer pH 9.6 (3 h, 20 °C). Wells were washed with PBS/0.1% Tween-20 (PBS/T) and blocked with 3 % BSA in PBS/T (1 h, 37 °C). Wells were incubated with 100 ng/ml vWF in PBS/T including 3% BSA (1 h, 37 °C). After washing, 5 µg/ml RU5 was added (1 h, 37 °C). Wells were washed and incubated with HRP conjugated swine-anti-rabbit antibody (DAKO, Glostrup, Denmark) diluted 1:2500 in PBS/T containing 3% BSA (1 h, 37 °C). O-phenylenediamine was used as substrate for detection.

Collagen-Binding Assay

vWF binding to fibrillar human placenta collagen type I (Sigma, St. Louis MO, USA, cat. No. C-7774) and collagen type III (Sigma, cat. No. C-4407) was studied in a solid-state binding assay according to Van der Plas *et al.* [8]. Collagen was coated at 50 μg/ml instead of 100 μg/ml as used previously [8]. A vWF concentration of 2.5 μg/ml was used in the binding experiments.

Results

A3-RU5 Structure Determination and Refinement

The structure of the vWF (Se-Met) A3-domain in complex with a Fab-fragment of RU5 was solved to 2.0 Å resolution. The structure was determined using the anomalous signal from selenium atoms in (Se-Met) A3 to position two A3 molecules and was completed by molecular replacement. The a.u. contains three A3-Fab complexes. The structure has been refined to an R-factor of 22.7% and a free R-factor of 26.4% (Table I).

The sequence of the RU5 V_L domain could not be determined from cDNA and was therefore deduced from electron density aided by an alignment of 110 Fab V_L sequences. The identity of thirteen amino acid residues could not be determined uniquely (see Fig. 1). The structure displays good model geometry with 88.8% of the residues in the most favored region of the Ramachandran plot and 10.8% in the additionally allowed region. Residue Thr51 of RU5 V_L domains occurs in the disallowed region of the Ramachandran plot, but its electron density is convincing.

The a.u. consists of three A3-RU5 complexes that are denoted *A*, *B* and *C*. The overall structure of the (Se-Met) A3 molecule is the same as the structure of native A3 [15; 16]. It consists of a central six-stranded β-sheet on both sides flanked by α-helices. The final model comprises amino-acid residues 921-1110 of A3 molecules in complexes *A* and *B* and residues 920-1110 of the A3 molecule in complex *C*. Positions of the N- and C-termini of A3, including disulfide bond Cys923-Cys1109 that connects these termini, are poorly defined. The model of RU5 consists of residues 1-211 of the light chains and residues 1-129 and 136-216 of the heavy chains. Residues 130-135 of the heavy chains display very weak electron density and are excluded from the model. Disorder of this loop is a commonly observed feature in Fab structures [36]. Asn56 of the V_H domain is N-glycosylated. Electron density near Asn56 accounted for a GlcNAc(-Fuc)-GlcNAc

moiety in complexes *A* and *B* and only a GlcNAc-Fuc moiety in complex *C*. The model contains one cacodylate ion from the crystallization solution.

Crystal Packing and Differences between Complexes

In the a.u. A3-RU5 complexes *B* and *C* form a tightly interacting anti-parallel dimer and are related by two-fold n.c.s. A3-RU5 complex *A* forms a similar anti-parallel dimer with a crystallographically related complex *A'*. Complexes within dimers *B*-*C* and *A*-*A'* have large contact areas of 932 Å^2 and 1,454 Å^2, respectively (GRASP [37]). These large interaction-surface areas suggest that the dimer of A3-RU5 complexes may also be stable in solution. DLS measurements, however, clearly indicated that the A3-RU5 complex does not form dimers in solution. Therefore, dimers observed in the crystal are a result of crystal packing.

Superposition of C_α-atoms of the three A3-RU5 complexes gives large root-mean-square (r.m.s.) coordinate differences ranging from 0.7 to 0.9 Å. When superpositions are limited to A3 molecules with bound V_H and V_L domains r.m.s. coordinate differences of 0.5-0.6 Å are obtained. Visual inspection of these superpositions (figure 2) shows that the A3-RU5 interaction region is well conserved, whereas regions of A3 and the variable domains located further away from the interaction region superimpose less well. A more detailed inspection of the A3-RU5 binding region reveals that all side-chain conformations are very similar (data not shown). In conclusion, the A3-RU5 interaction region is well conserved among the three complexes in the a.u.

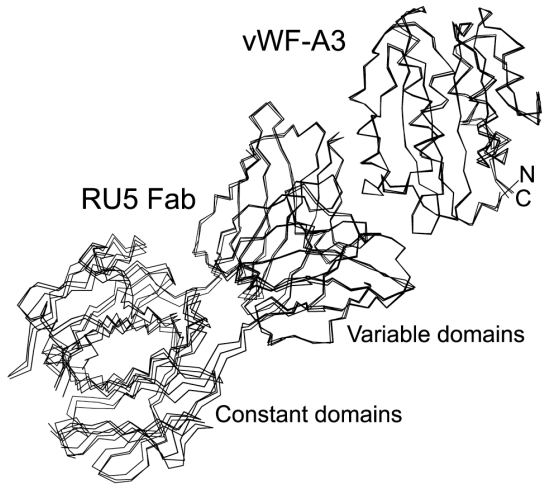

Figure 2: Structural overlay of C_α-traces of the three A3-RU5 Fab complexes in the asymmetric unit. For calculation of the best superposition C_α-atoms of A3 and variable domains of RU5-Fab were used. The A3-RU5 interaction region is well conserved amongst the three complexes, while relatively large differences are shown in orientations of the RU5 constant domains with respect to its variable domains and A3. The diagram was generated with MOLSCRIPT [38].

The Epitope of RU5

A3 interacts with RU5 through a non-linear epitope comprising residues in loop α1β2, loop β3α2 followed by helix α2, and loop α3β4 (Table II). All three loops that contribute to the epitope are

located in the bottom face of A3 (figure 3). The N- and C-termini of A3 that are also located in the bottom face do not interact with RU5. This observation is in agreement with the fact that RU5 was raised against complete vWF in which the termini connect A3 to flanking A2 and D4 domains. Residues of RU5 that interact with loops α1β2 and α3β4 are located in CDR_{L1} and CDR_{L2} (figure 1). All six CDRs interact with residues in the contiguous segment formed by loop β3α2 and helix α2. The A3-RU5 interactions involve five hydrogen bonds and one salt bridge. The buried surface area of A3 molecules in the complex is approximately 1,200 $Å^2$, which is about 7% of the total surface area of A3. Interestingly, the fucose moiety attached to residue Asn56 in CDR_{H2} of complex *A* interacts with Lys988-Ala989 of A3. The carbohydrate moieties attached to Asn56 in complexes *B* and *C* do not interact with A3.

Conformational Changes in A3

To analyze whether binding of RU5 causes conformational changes in A3 we compared models of A3 in the A3-RU5 complex with two structures of free A3[4 15; 16]. The two structures of free A3 were determined from different crystal forms with unrelated crystal-packing interactions. In both crystal forms two molecules are present in the a.u. Since the A3-RU5 complex was obtained with (Se-Met) A3 we also included the structure of free (Se-Met) A3 in the comparison to detect possible structural differences caused by Se-Met (E.G. Huizinga, unpublished results). R.m.s. coordinate differences after pair-wise superimposing C_α-atoms of all eight models range from 0.24 to 0.81 Å. Large differences are restricted to three loops located within the RU5-binding site and to two loops that are located distant from the epitope (figure 3, Table II).

The three conformational diverse loops located in the RU5-epitope are α1β2, β3α2 and α3β4 (figure 4A). Loop α1β2 has a unique conformation in the A3-RU5 complex, indicating that this conformation is induced by RU5. Loops β3α2 and α3β4 have considerable conformational freedom. Conformations observed in the A3-RU5 complex are, however, not systematically different from the conformations observed in free A3, indicating that the conformations observed in the complex are not induced by RU5.

Distant from the RU5 epitope conformational variation is observed for loops β1α1 and α5β6. Loop β1α1 is located in the top face of the domain and contains part of the vestigial MIDAS motif. Multiple conformations are observed for residues Ser938-Phe-Pro940 (figure 4B). Phe939 is solvent exposed in A3-RU5 complex *C* and all models of free A3. In complexes *A* and *B* Phe939 is buried in the hydrophobic core of A3. The buried conformation is likely caused by

crystal packing interactions involving A3 residues 940-942. These packing interactions would not allow for the position of Pro940 observed in models of A3 that have an exposed conformation of Phe939. Since both the exposed and buried conformations of Phe939 are observed in the three A3-RU5 complexes the conformation of this loop is certainly not determined by binding of RU5.

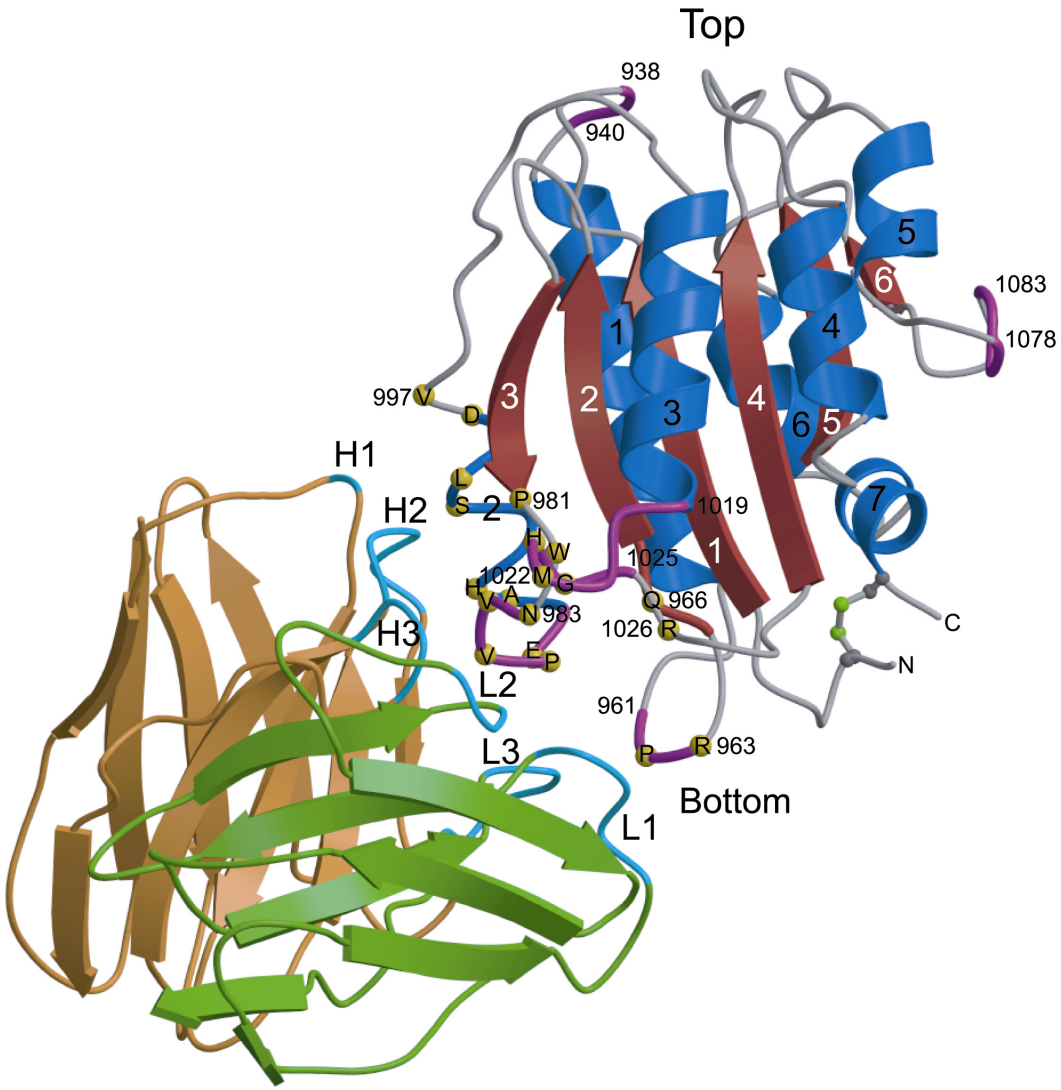

Figure 3: Ribbon diagram of A3 and RU5 variable domains. Residues of A3 that are part of the epitope of RU5 are indicated by yellow spheres. Regions of RU5 CDRs that interact with A3 are color-coded in light blue. Regions of A3 that show different conformations among four crystal structures are shown in purple trace. Disulfide bond Cys923-Cys1109 is shown in green ball-and-stick. The α-helices and β-strands of A3 are depicted in blue and red, respectively. For clarity, α-helix 2 is not shown by a ribbon, but in 'coil' representation. The V_H domain of RU5 is in brown, the V_L domain is in green. The diagram was generated with MOLSCRIPT [38] and RASTER3D [39].

click on this link for rotating image

Table II
The epitope of RU5 and loops of A3 that show conformational variation among eight models of A3 from four different crystal structures

Residues in the RU5 epitope[a]	
Structural element	Residues
Loop α1β2	Pro962-Arg963 Gln966
Loop β3α2	Pro981-Trp-Asn-Val-Val-Pro-Glu987
Helix α2	Lys988-Ala-His990 Ser993-Leu994 Asp996-Val997
Loop α3β4	Met1022-His-Gly1024 Arg1026
Residues with variable conformations[b]	
Structural element	Residues
Loop β1α1	Ser938-Phe-Pro940
Loop α1β2	Gly961-Pro-Arg963
Loop β3α2	Asn983-Val-Val-Pro-Glu987
Loop α3β4	Thr1019-Ser-Glu-Met-His-Gly-Ala1025
Loop α5β6	Gly1078-Pro-Ala-Gly-Asp-Ser1083

[a] Residues listed are positioned within 4.0 Å distance from RU5.
[b] Residues that are also part of the epitope of RU5 are underlined.

Loop α5β6 located in a side face of A3 has an aberrant conformation in A3 domain *B* of the structure of Bienkowska *et al.* [16] (figure 4C). This aberrant conformation coincides with crystal contacts unique to molecule *B*. No crystal contacts are present in the other structures. The conformations observed in the A3-RU5 complex are not systematically different from the conformations observed in free A3. Thus, binding of RU5 does not cause conformational changes in regions of A3 that are distant from the epitope.

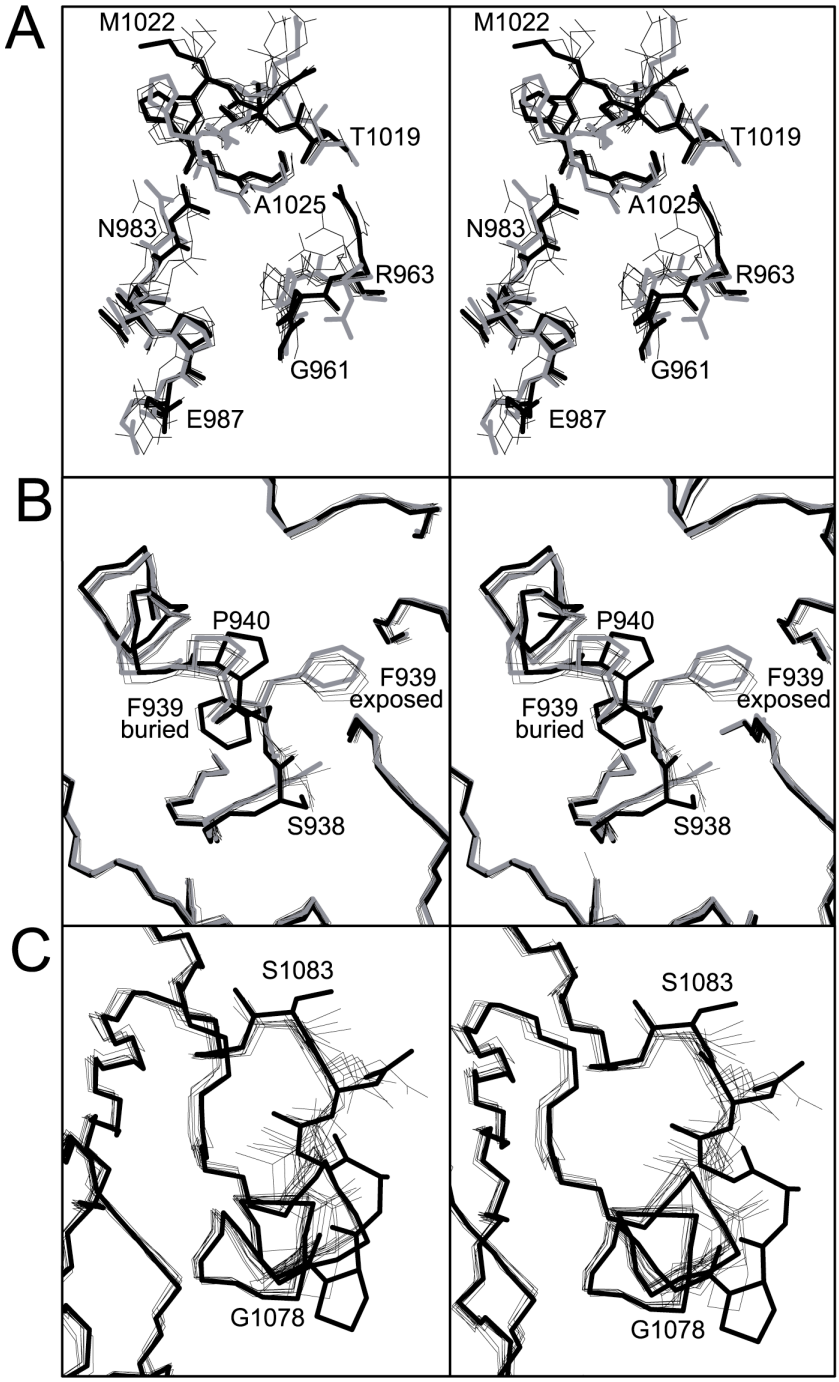

Figure 4: The conformation of five loops varies among different crystal structures of A3. Models compared include free A3[4], free (Se-Met) A3 and A3 from the A3-RU5 complex. *A.* Stereo picture of loops α1β2 (residues 961-963), β3α2 (983-987) and α3β4 (1019-1025). Residues of A3 in A3-RU5 complex *A* are shown in thick line. A3 domain *A* from the structure of Huizinga *et al.* [15] is shown in gray. *B.* Stereo diagram of residues Ser938-Phe-Pro940 in the top face of A3. Buried and exposed conformations of Phe939 are labeled. *C.* Stereo diagram of loop α5β6 (residues 1078-1083). The aberrant A3 domain *B* from the structure of Bienkowska *et al.* [16] is shown in thick line. The diagram was generated with MOLSCRIPT [38].

Selection and Characterization of vWF Mutants

To confirm the location of the collagen-binding site indicated by the A3-RU5 complex we constructed charged-to-alanine mutations of five residues. These residues are located within 5 Å of the RU5 Fab fragment and are solvent exposed in free A3. Residues selected were Arg963 located in loop α1β2, Glu987 (β3α2), His990 (α2), Arg1016 (α3), and His1023 (α3β4). Mutants were produced as multimeric vWF in stable baby hamster kidney cell lines. The multimer distribution of vWF mutants and wild-type vWF, as analyzed by agarose gel electrophoresis, were

indistinguishable (data not shown). RU5 binding to purified point mutants was not significantly different from RU5 binding to wild-type vWF (figure 5).

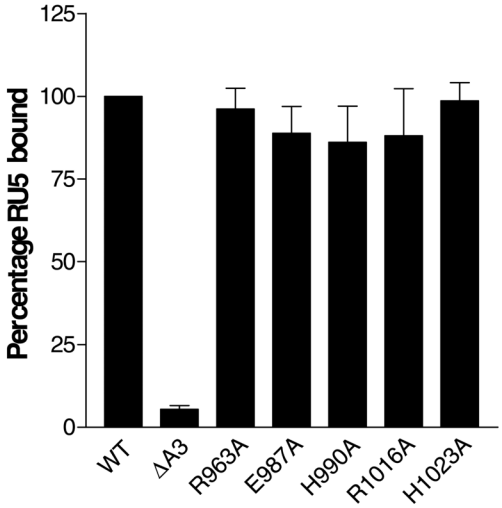

Figure 5: Binding of monoclonal antibody RU5 to vWF mutants. VWF immobilized in microtiter-plate wells via polyclonal αD'D3 was incubated with 5 µg/ml RU5. Bound RU5 was detected by horse radish peroxidase conjugated swine-anti-rabbit antibody as described under "Experimental Procedures". Wild-type vWF and ΔA3-vWF, which lacks the A3 domain [6], were used as positive and negative controls, respectively. Binding of RU5 to vWF mutants was percentualized against wt-vWF. Each data point represents the mean ± SD of two measurements in duplicate.

Collagen Binding of vWF Mutants

The effect of point mutations on vWF binding to collagen types I and III was investigated by ELISA (figure 6). Similar results were obtained for both types of collagen. Mutation H1023A almost completely abolished collagen binding. The level of residual binding observed for this mutant was similar to binding observed for ΔA3-vWF, a deletion mutant that lacks the entire A3 domain [6]. Collagen binding of mutants R963A and R1016A was reduced by 25 - 35%, whereas collagen binding of mutants E987A and H990A was normal.

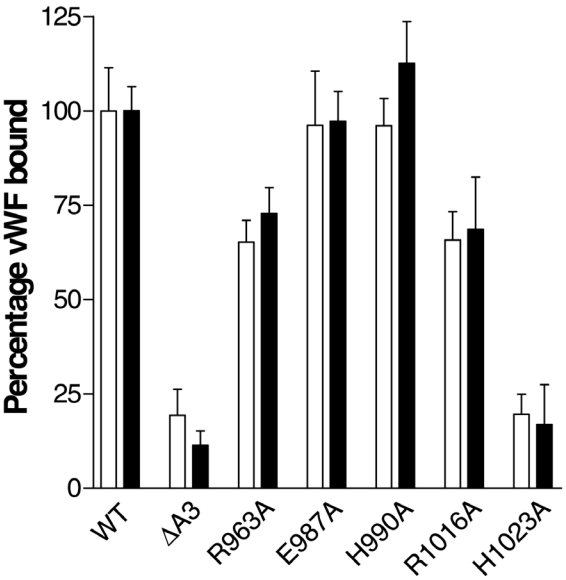

Figure 6: Binding of vWF point mutants to collagen types I and III. Collagen type I (white bar) or III (black bar) was coated in microtiter-plate wells. Wells were incubated with vWF at a concentration of 2.5 µg/ml and bound vWF was detected as described under "Experimental Procedures". ΔA3-vWF was used as a negative control. Bound vWF mutant was percentualized against wt-vWF. Each data point represents the mean ± SD of three independent experiments performed in duplicate.

Discussion

The current study was aimed at locating the collagen-binding site of the vWF-A3 domain. For this purpose we solved the crystal structure of A3 in complex with a Fab fragment of RU5 that inhibits collagen binding. The structure of the complex shows that RU5 binds to residues within A3 sequences 962-966, 981-997 and 1022-1026. These residues are located in α-helix 2 and in loops α1β2, β3α2 and α3β4 at the bottom of one of the side faces of the A3 domain (see figure 3). Comparison of structures of A3 shows that RU5 binding does not induce long range conformational changes. This excludes a mechanism in which RU5 induced conformational changes inhibit collagen binding. It seems likely, therefore, that RU5 inhibits collagen binding by steric hindrance, which implies that the collagen-binding site is located at or close to the RU5 epitope.

To confirm the location of the collagen-binding site we constructed five charged-to-alanine mutations of residues located in or close to the RU5 epitope. The multimer distribution of these mutants was similar to that of wild-type vWF. Therefore, observed differences in collagen binding are not caused by the known dependence of collagen binding on vWF multimer-size [7]. All five mutants bound normally to RU5, which shows that none of the mutated residues plays a dominant role in the A3-RU5 interaction and, more importantly, that the conformation of A3 in the neighbourhood of the epitope and the collagen-binding site is not disturbed.

Mutation H1023A abolished collagen binding almost completely, residual-binding being similar to that observed for ΔA3-vWF, a deletion mutant that lacks the entire A3 domain. Therefore, His1023 plays a central role in A3-mediated collagen binding. His1023 is located in loop α3β4 and lies at the edge between the 'front' face of the domain, formed by helices α2 and α3 and strand β3, and the bottom face, which is composed of several loops and contains the N- and C-termini (see figure 7). A small reduction of collagen binding was observed for mutants R963A and R1016A located in the bottom and front face of the domain, respectively.

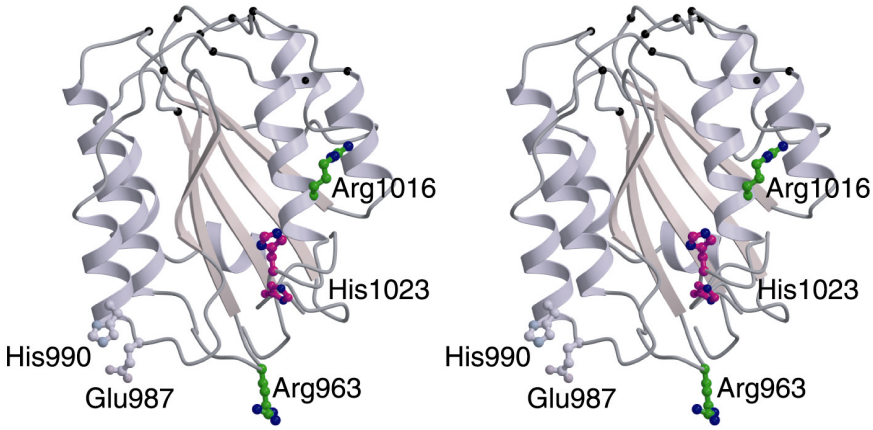

Figure 7: Residues of vWF-A3 involved in collagen binding. Stereographic representation of the vWF-A3 domain showing amino-acid residues that have been mutated to alanine in ball-and-stick. Mutation of His1023 (magenta) abolishes collagen binding almost completely. Mutation of Arg963 and Arg1016 (green) reduces collagen binding by 25-35%. Mutation of Glu987 and His990 (gray) does not have an effect on collagen binding. To illustrate the range of conformations of His1023 observed in different crystal forms of A3, two conformations of this residue and the back-bone trace of flanking residues are shown. Residues that have been mutated in previous studies [8; 16; 19] are located in the top face of A3 and are indicated by black spheres. The diagram was generated with MOLSCRIPT [38] and RASTER3D [39].

Interestingly, His1023 and flanking residues display a large variety of conformations among eight models of A3 (figures 4 and 7). In some A3 structures His1023 protrudes prominently from the surface of the domain which may be a favorable position for interaction with collagen. Multiple conformations are also observed for loop β3α2. Like His1023, loop β3α2 is located at the edge between the front and bottom faces of A3. Since we did not mutate residues in loop β3α2 its involvement in collagen binding remains to be established. The observed flexibility of His1023 suggests that collagen binding may involve an induced-fit mechanism in which significant conformational changes occur in loop α3β4 upon binding of A3 to collagen.

The amino-acid sequence of collagen that is recognized by vWF-A3 has not yet been identified. We hypothesized previously that negatively charged residues in A3 could interact with basic residues on collagen [15]. Residues now implicated in collagen binding are positively charged. Therefore, interaction of A3 with negatively charged residues on collagen appears more likely.

In contrast to binding sites of other collagen binding domains, like the α_1, α_2 I-domains and the A-domain of *S. aureus* adhesin [12; 40], the collagen-binding region of A3 does not have a groove or trench that could accommodate a collagen triple-helix. The front face of the domain, harboring Arg1016, is rather flat. The bottom face, which contains Arg963 is less smooth, but no groove is present. Docking of a collagen triple-helix on the A3 domain is not straightforward. In particular, it is not obvious how His1023, Arg963 and Arg1016 could simultaneously contact a

triple-helix in an extended conformation. To define the collagen-binding site more precisely, characterization of additional mutants will be necessary.

Previously, the collagen-binding site of A3 was proposed to be located at its top face [15; 19] similar to the homologous I-domains of integrins $\alpha_1\beta_1$ and $\alpha_2\beta_1$ [12; 41-43]. Point mutations introduced in the top face of an A3 monomer [19] and in multimeric vWF [8] gave conflicting results. Our results now show conclusively that the collagen-binding site is located close to the bottom face and not in the top face of A3.

While our results rule out a role for the top face of the A3 domain in collagen binding, this side of the molecule may still be engaged in other interactions, such as binding of the A1 domain. Interaction between A1 and A3 has been suggested to play a role in activation of the A1 domain for binding to platelet receptor glycoprotein Ib [44]. Interesting in this respect are the buried and solvent exposed conformation observed for residue Phe939, which is located close to the vestigial MIDAS motif in the top face of the domain (figure 4B). Solvent exposure of Phe939 has been proposed to stabilize the buried Asp934 of the vestigial MIDAS motif in the absence of a bound metal ion [16]. Our observation of a buried conformation shows that exposure of Phe939 is not critical for structural stability. The two conformations of Phe939 may, however, be relevant for the putative interaction between A1 and A3, since the shape and hydrophobicity of the upper surface of A3 differs significantly between the solvent exposed and buried conformation.

In conclusion, the collagen-binding site of vWF-A3 is distinctly different from collagen-binding sites of I-domains of integrins $\alpha_1\beta_1$ and $\alpha_2\beta_1$. VWF-A3 residues involved in collagen binding are located close to the bottom face of the domain. His1023 is essential for collagen binding, while Arg963 and Arg1016 play ancillary roles. Multiple conformations observed for His1023 and adjacent residues suggest that binding of A3 to collagen involves an induced-fit mechanism.

Acknowledgements

We thank the staff of the EMBL Outstation DESY (Hamburg, Germany) for assistance in X-ray data collection and the European Union for support of the work at EMBL (Hamburg, Germany) through the HCMP Access to Large Installations Project, contract number CHGE-CT-0040.

Reference List

1. Vischer UM, De Moerloose P. von Willebrand factor: from cell biology to the clinical management of von Willebrand's disease. Crit Rev Oncol Hematol. 1999;30:93-109.

2. Ruggeri ZM, Ware J. von Willebrand factor. FASEB J. 1993;7:308-316.

3. Sadler JE. Biochemistry and genetics of von Willebrand factor. Annu Rev Biochem. 1998;67:395-424.

4. Ruggeri ZM. Structure and function of von Willebrand factor. Thromb Haemost. 1999;82:576-584.

5. Mohri H, Yoshioka A, Zimmerman TS, Ruggeri ZM. Isolation of the von Willebrand factor domain interacting with platelet glycoprotein Ib, heparin, and collagen and characterization of its three distinct functional sites. J Biol Chem. 1989;264:17361-17367.

6. Lankhof H, van Hoeij M, Schiphorst ME, et al. A3 domain is essential for interaction of von Willebrand factor with collagen type III. Thromb Haemost. 1996;75:950-958.

7. Fischer BE, Kramer G, Mitterer A, et al. Effect of multimerization of human and recombinant von Willebrand factor on platelet aggregation, binding to collagen and binding of coagulation factor VIII. Thromb Res. 1996;84:55-66.

8. Van der Plas RM, Gomes L, Marquart JA, et al. Binding of von Willebrand Factor to Collagen type III: Role of specific amino acids in the collagen binding domain of vWF and effects of neighbouring domains. Thromb Haemost. 84, 1005-1011. 2000.

9. Cruz MA, Yuan H, Lee JR, Wise RJ, Handin RI. Interaction of the von Willebrand Factor (vWF) with collagen. J Biol Chem. 1995;270:10822-10827.

10. Colombatti A, Bonaldo P. The superfamily of proteins with von Willebrand factor type A-like domains: one theme common to components of extracellular matrix, hemostasis, cellular adhesion, and defense mechanisms. Blood. 1991;77:2305-2315.

11. Perkins SJ, Smith KF, Williams SC, Haris PI, Chapman D, Sim RB. the secondary structure of the von Willebrand Factor type A domain in factor B of human complement by Fourier transform infrared spectroscopy. Its occurence in collagen types VI, VII, XII and XIV, the integrins and other proteins by avaraged structure predictions. J Biol Chem. 1994;238:104-119.

12. Emsley J, Knight CG, Farndale RW, Barnes MJ, Liddington RC. Structural basis of collagen recognition by integrin $\alpha 2\beta 1$. Cell. 2000;100:47-56.

13. Lee JO, Rieu P, Arnaout MA, Liddington RC. Crystal structure of the A domain from the α subunit of integrin CR3 (CD11/CD18). Cell. 1995;80:631-638.

14. Michishita M, Videm V, Arnaout MA. A novel divalent cation-binding site in the A domain of the beta 2 integrin CR3 (CD11b/CD18) is essential for ligand binding. Cell. 1993;72:857-867.

15. Huizinga EG, Van der Plas RM, Kroon J, Sixma JJ, Gros P. Crystal structure of the A3 domain of human von Willebrand factor: implications for collagen binding. Structure. 1997;5:1147-1156.

16. Bienkowska J, Cruz MA, Atiemo A, Handin RI, Liddington R. The von Willebrand Factor A3 domain does not contain a metal ion-dependent adhesion site motif. J Biol Chem. 1997;272:25162-25167.

17. Pietu G, Fressinaud E, Girma JP, Nieuwenhuis HK, Rothschild C, Meyer D. Binding of human von Willebrand factor to collagen and to collagen- stimulated platelets. J Lab Clin Med. 1987;109:637-646.

18. Bockenstedt PL, McDonagh j, Handin RI. binding and covalent cross-linking of purified von Willebrand factor to native monomeric collagen. J Clin Invest. 1986;78:551-556.

19. Cruz MA, Bienkowska J, Mato A., Liddington R, Handin RI. Identification of the collagen binding site in the vWF-A3 domain by molecular structure and site specific mutagenesis [abstract]. Blood. 1997;Supplement I:23a.

20. Hale JE. Irreversible, oriented immobilisation of antibodies to Cobalt iminodiacetate resin for ue as immunoaffinity media. Anal Biochem. 1995;231:46-49.

21. Dübel S, Breitling F, Fuchs P, et al. Isolation of IgG antibody Fv-DNA from various mouse and rat hybridoma cell lines using the polymerase chain reaction with a simple set of primers. J Immunol Methods. 1994;175:89-95.

22. Carrol WL, Mendel E, Levy S. Hybridoma fusion cel lines containing an aberrant kappa transcript. Mol Immunol. 1988;25:991-995.

23. Otwinowski Z, Minor O. Processing of X-ray diffraction data collected in oscillation mode. Methods Enzymol. 1996;276:307-326.

24. Collaborative Computational Project No 4. The CCP4 suite: programs for protein crystallography. Acta Crystallogr D. 1994;50:760-763.

25. Berman HM, Westbrook J, Feng Z, et al. The protein databank. Nucleic Acids Res. 2000;28:235-242.

26. Van den Elsen JM, Herron JN, Hoogerhout P, et al. Bacterial antibody recognition for a PorA epitope of Neisseria meningitidid: acrystal structure of a Fab fragment in complex with a fluorescein-confugated peptide. Proteins. 1997;29:113-125.

27. Navazza J. AMoRe: an automated package for molecular replacement. Acta Crystallogr A. 1994;50:157-163.

28. Brünger AT. Extention of molecular replacement: a new search strategy based on Patterson correlation refinement. Acta Crystallogr A. 1990;46:46-57.

29. Brünger AT, Adams PD, Clore GM, et al. Crystallography and NMR system: A new software suite for macromolecular structure determination. Acta Crystallogr D. 1998;54:905-921.

30. Bedzyk WD, Johnson LJ, Riordan GS, Voss Jr. EW. Comparison of variable region primary structures within an anti-fluorescein idiotype family. J Biol Chem. 1989;265:18615-18620.

31. Herron JN, He X-M, Mason ML, Voss Jr. EW, Edmundson AB. Three dimentional structure of a fluorescein-Fab complex crystallized in 2-methyl-2,4-pentanediol. Proteins. 1989;5:271-280.

32. Jones TA, Zou JY, Cowan SW, Kjeldgaard M. Improved methods for the building of protein models in electron density maps and the location of error in these models. Acta Crystallogr A. 1991;47:110-119.

33. Pannu NS, Read RJ. Improved structure refinement through Maximim Likelihood. Acta Crystallogr A. 1996;52:659-668.

34. Graham F, van der Eb A. A new technique for the assay of infectivity of human adenovirus 5 DNA. Virology. 1973;52:456.

35. Lawrie AS, Horser MJ, Savidge GF. Phast assessment of vWF:Ag multimeric distribution. Thromb Haemost. 1990;59:369.

36. Stanfield RI, Fieser TM, Lerner RA, Wilson IA. Crystal structure of an antibody to a peptide and its complex with peptide antigen at 2.8 Angstroms. Science. 1990;248:712-719.

37. Nicholls A, Sharp KA, Honig B. GRASP: Graphical representation and analysis of surface properties. Biophys J. 1993;64:166-170.

38. Kraulis P. Molscript: a program to produce both detailed and schematic plots of protein structures. J Appl Crystallogr. 1991;25:649-950.

39. Merritt EA, Bacon DJ. Raster3D: photorealistic molecular graphics. Methods Enzymol. 1997;277:505-524.

40. Rich RL, Deivanayagam CCS, Owens RT, et al. Trench-shaped binding sites promote multiple classes of interactions between collagen and the adherence receptors, $\alpha_1\beta_1$ integrin and *Staphylococcus aureus* Cna MSCRAMM. J Biol Chem. 1999;274:24906-24913.

41. Kamata T, Puzon W, Takada Y. Identification of putative ligand binding sites within I domain of integrin alpha 2 beta 1 (VLA-2, CD49b/CD29). J Biol Chem. 1994;269:9659-9663.

42. Kamata T, Takada Y. Direct binding of collagen to the I-domain of integrin $\alpha2\beta1$ (Vla-2, CD49b/CD29)

in a divalent cation-independent manner. J Biol Chem. 1994;269:26006-26010.

43. Smith C, Estavillo D, Emsley J, Bankston LA, Liddington RC, Cruz MA. Mapping the collagen-binding site in the I domain of the glycoprotein Ia/IIa (integrin $\alpha_2\beta_1$). J Biol Chem. 2000;275:4205-4209.

44. Obert B, Houllier A, Meyer D, Girma JP. Conformational changes in the A3 domain of von Willebrand factor modulate the interaction of the A1 domain with platelet glycoprotein Ib. Blood. 1999;93:1959-1968.

Chapter 3

Mapping the collagen-binding site in the von Willebrand Factor A3-domain

Roland A.P. Romijn[†], Erik Westein[†], Barend Bouma[‡], Marion Schiphorst[†], Jan J. Sixma[†], Peter J. Lenting[†] and Eric G. Huizinga[†‡]

[†] Thrombosis and Haemostasis Laboratory, Department of Haematology, University Medical Center and Institute of Biomembranes, HP G03.647, PO box 85500, 3508 GA Utrecht, The Netherlands

[‡] Bijvoet Center for Biomolecular Research, Department of Crystal and Structural Chemistry, Utrecht University, Padualaan 8, 3584 CH Utrecht, The Netherlands.

Summary

Von Willebrand factor (vWF) is a multimeric plasma glycoprotein that mediates platelet adhesion to collagen at sites of vascular damage. VWF binds to collagen via its A3 domain. Recently we identified the approximate location of the collagen-binding site in the vWF-A3 domain *(JBC, 276, 2001, 9985-9991)*. In this paper we have studied 22 point mutants to map the collagen-binding site in detail. Our results map the collagen-binding site at strand β3, helix α3 and loops β2β3, α2α3 and α3β4 at the "front" face of the domain. Residues Asp^{979}, Ser^{1020} and His^{1023} in the lower half of the collagen-binding site are essential for collagen binding, whereas Ile^{975}, Thr^{977}, Val^{997}, Glu^{1001} and Arg^{1016} in the upper part play an additional role. These residues define a rather flat collagen-binding site. Most likely, multiple collagen sequences bind to A3. Surface properties of the collagen-binding site indicate that collagen sequences containing hydrophobic and positively charged residues binds to A3.

Introduction

Human vessel wall has a high content of collagen sub-types I, III, IV, V, VI, VIII, XII, XIII and XIV [1-3] that determine the thrombogenicity of the vessel wall. Blood is separated from these components by a thin layer of endothelial cells. Upon disruption of the endothelial cell layer blood is exposed to collagens in the vessel wall.

Collagen subtypes I, III, IV and VI are strong activators of platelet adhesion and aggregation (see for reviews [3-6]). At low shear force platelets interact directly with collagen via integrin $\alpha_2\beta_1$ and glycoprotein (Gp) VI [5]. At high shear force platelet adhesion to collagen is a von Willebrand factor (vWF) dependent process [6; 7]. In this process, vWF functions as a molecular bridge between collagen and platelet receptor GpIb-IX-V complex. Human fibrillar collagen type I and III from perivascular connective tissue are the main collagen subtypes that interact with the vWF-A3 domain [8; 9]. Collagen type VI from subendothelial cell matrix also interacts with vWF, but the binding site for collagen type VI appears to be located in the A1 domain [10; 11].

Mature monomeric vWF contains 2050 amino-acid residues and is composed of twelve domains in the order D'-D3-A1-A2-A3-D4-B1-B2-B3-C1-C2-CK [6; 12]. VWF dimerises at the CK domains [13] and multimerises at the D3 domains [14]. VWF with a reduced multimeric size has a decreased affinity for collagen [15].

VWF-mediated platelet adhesion to collagen subtypes I and III involves first the binding of the A3 domain to collagen and subsequently the binding of the A1 domain to platelet receptor GpIbα *in vitro* [16-18]. Recently, Wu *et al.* showed for the first time in an *in vivo* model that the vWF-A1 and A3 domains are essential in thrombus formation [19; 20]. A-type domains and homologous integrin I-domains adopt a so-called di-nucleotide-binding fold, or Rossman fold composed of a central β-sheet surrounded by six or seven α-helices [21-24]. Binding of the I-domain of integrins α_1, α_2, α_{10} and α_{11} to collagen involves a divalent cation [25; 26] bound to the metal ion dependent adhesion site (MIDAS) motif and amino-acid residues at the "top" face of the domain [27; 28]. The A3 domain does not contain a functional MIDAS motif and binding of A3 to collagen is cation independent [29; 30]. Recently we have identified His^{1023}, Arg^{963} and Arg^{1016} located at the front- and bottom face of A3 to be involved in collagen binding [31]. Mutation H1023A completely

abolished collagen binding, whereas mutations R963A and R1016A reduced collagen binding by 20 – 30 %.

This study was aimed at identifying the collagen-binding site in the vWF-A3 domain in detail by means of site-directed mutagenesis. We did so by constructing nineteen alanine mutants and three histidine mutants that were expressed as multimeric vWF. Collagen-binding was evaluated.

Experimental procedures

Selection and construction of vWF Point Mutants

Selection of amino-acid residues for mutagenesis was based on the approximate location of the collagen binding site as identified in our previous study [31] and the crystal structure of the vWF-A3 domain [21; 22]. Selected residues are solvent exposed in the isolated A3 domain. Residues Gln^{966}, Ser^{974}, Ile^{975}, Thr^{977}, Asp^{979}, Val^{980}, Pro^{981}, Asn^{983}, Val^{984}, Val^{985}, Ser^{993}, Val^{997}, Gln^{999}, Glu^{1001}, Gln^{1006}, Asp^{1009}, Ser^{1020}, Glu^{1021} and Met^{1022} were mutated to alanine. In addition, Pro^{962}, Pro^{981} and Pro^{1027} were mutated to histidine to inhibit collagen binding by steric hindrance. Backbone conformations of these proline residues suggested that the histidine side chain would protrude from the protein surface.

Point mutations were introduced in the vWF-A3 domain using the Quikchange method (Stratagene, La Jolla CA, USA) as described previously [31].

Expression, Purification and Characterization of vWF

VWF was stably expressed in baby hamster kidney cells overexpressing furin required for proper removal of vWF propeptide [17; 32]. Cells were cultured in serum-free medium. VWF was purified by immuno-affinity chromatography using monoclonal antibody RU8, which is directed against the D4 domain [17] and stored in 50 mM Hepes, 100 mM NaCl pH 7.4 at –20 °C.

VWF concentration was determined by a sandwich ELISA using polyclonal α-vWF and horseradish peroxidase (HRP) conjugated polyclonal α-vWF (DAKO, Glostrup, Denmark) for immobilization and detection, respectively [17]. Normal pooled plasma from 40 healthy donors was used as a reference.

The multimeric structure of vWF was analyzed by agarose gel electrophoresis followed by Western blotting as described by Lawrie *et al.* [33].

Binding of monoclonal antibody RU5 [34] to vWF was analysed as described before [31] with some modifications. Microtiter-plate wells (Costar, Cambridge MA, USA) were coated with a polyclonal antibody directed against the D' and D3 domains of vWF [34] diluted to 2.5 μg/ml with 50 mM carbonate buffer pH 9.6. Coating was carried out for 3 h at 37 ^{o}C. Wells were washed with PBS containing 0.1% Tween-20 (PBS-T) and blocked with 3 % BSA in PBS-T for 1 h at 37 ^{o}C. Expression medium containing (mutant) vWF was diluted with mock medium to a final concentration of 1 μg/ml vWF. Wells were incubated with diluted medium for 1 h at 37 ^{o}C. After washing, 2 μg/ml RU5 in PBS-T containing 3% BSA was added for 1 h at 37 ^{o}C. Wells were washed again and incubated for 1 h at 37 ^{o}C with HRP-conjugated rabbit-anti-mouse antibodies (DAKO, Glostrup, Denmark) diluted 1:2500 in PBS-T containing 3% BSA. O-phenylenediamine was used as substrate for detection.

Static Collagen-Binding Assay

Binding of vWF in expression medium to fibrillar human placenta collagen type III (Sigma Chemical Co., St. Louis MO, USA, cat. No. C-4407) was studied in a solid-state binding assay at a vWF concentration of 0.1 μg/ml as described before [31].

Surface Plasmon Resonance Collagen-binding Assay

Surface Plasmon Resonance (SPR) binding studies were performed using a Biacore2000 system (Biacore AB, Uppsala, Sweden). Human placenta collagen type III was dissolved in 50 mM acetic acid at a final concentration of 1 mg/ml (16h, 4 ^{o}C) and immobilized on a CM5-biosensor chip using the amine-coupling kit as instructed by the supplier. Approximately 3000 RU, corresponding with ~33 fmol/mm^2, collagen type III was immobilized. A reference channel was coated with human placenta collagen type IV (3000 RU; Sigma, cat. No. C-7521) that does not interact with vWF [5]. Analysis was performed in Biacore standard buffer 25 mM Hepes, 125 mM NaCl, 2.5 mM $CaCl_2$, 0.005% (v/v) Tween-20, pH 7.4 at 25 ^{o}C at a flow rate of 10 μl/min. Binding of vWF to the collagen type III-coated channel was corrected for binding to the collagen type IV-coated channel. Binding isotherms were determined by injecting increasing concentrations of vWF. Each injection was continued for 30 minutes, facilitating accurate

determination of the steady state (Req) by fitting the binding curve with a 1:1 Langmuir interaction model (Biaeveluation software version 3.0.1), which gave the best fit with the experimental data. The delay between two subsequent injections was seven minutes in which the biosensor chip was flushed with biacore-standard buffer without regeneration. After measuring all concentrations of a vWF-variant, the biosensor chip was regenerated by injection of 1 mM EDTA, 1 M NaCl, 0.1 M sodium citrate, pH 5.0 (1 min, 10 µl/min) and 10 mM taurodeoxycholic acid, 100 mM Tris, pH 9.0 (1 min, 10 µl/min) and 0.1 M H_3PO_4 (1 min, 10 µl/min).

Binding isotherms were constructed using the computer program GraphPad Prism 3.0 [35]. The response units at equilibrium (Req) were plotted against the injected vWF concentration and the data points were fitted with a 1:1 interaction model $R_{eq}=R_{eq,max}*[vWF]/(K_D + [vWF])$, where $R_{eq,max}$ is the response at infinite vWF concentration and K_D is the dissociation constant. Since the interactions between vWF and collagen are multivalent and we used a 1:1 interaction model, the calculated dissociation constants must be regarded as apparent values.

Results

Characterization of vWF Mutants

The conformation of the A3 domain and the multimeric size of vWF determine its reactivity towards collagen. Multimer distributions of vWF mutants and recombinant wt-vWF were indistinguishable (data not shown). The conformation of the A3 domain was evaluated with conformation dependent monoclonal antibody RU5. Binding of RU5 to 18 of the 22 point mutants was similar as the binding of RU5 to wt-vWF. As expected, RU5 did not bind to vWF lacking the A3 domain, ΔA3-vWF [17] (figure 1A). Four of the point mutants, P962H, P981A, V984A and V985A, had a significantly reduced RU5 binding, ranging from 60 to 80 % compared to wt-vWF. However, collagen binding of these mutants was normal (see below). Reduced RU5-binding can be explained by direct interactions of these residues with RU5, as observed in the crystal structure of the A3•RU5 complex [31]. Overall, these data suggest that the A3 domain of all vWF-variants is correctly folded.

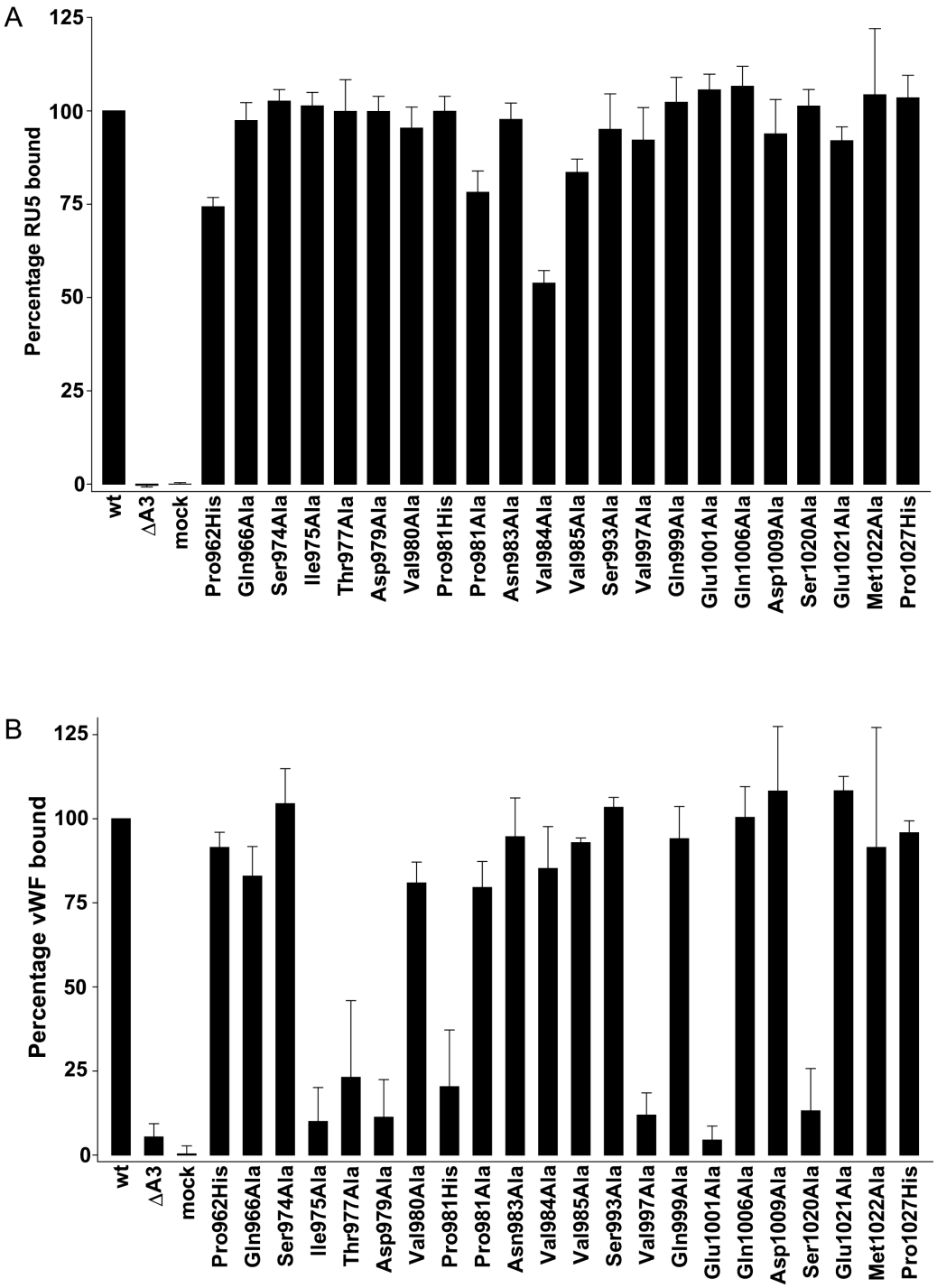

Figure 1: Characterisation of vWF-A3 mutants. A: Binding of conformation dependent monoclonal antibody RU5. VWF was immobilized in microtiter-plate wells via polyclonal antibody αD'D3. Immobilized vWF was incubated with RU5 and bound RU5 was detected as described under "Experimental Procedures". Wild-type vWF and ΔA3-vWF, which lacks the A3 domain [17], were used as a positive and negative control, respectively. Binding of RU5 to vWF mutants is expressed as a percentage of wt-vWF binding. Each data-point represents the mean ± SD of three experiments performed in duplicate. B: Binding of vWF point mutants to fibrillar collagen type III in a solid-state collagen-binding assay. Human placenta collagen type III was coated in microtiter-plate wells. Wells were incubated with vWF at a concentration of 0.1 µg/ml. Bound vWF was detected as described under "Experimental Procedures". ΔA3-vWF [17] was used as a negative control. Bound vWF is expressed as a percentage of wt-vWF binding. Each data point represents the mean ± SD of three independent experiments performed in duplicate.

Collagen Binding Affinity of vWF Mutants

In a first screen the effect of the mutations in collagen type III binding was assessed by a solid-state collagen-binding assay (figure 1B). Immobilized collagen was incubated with expression medium at a vWF concentration of 0.1 µg/ml. Binding of ΔA3-vWF to collagen was only 8 % compared to wt-vWF. Mutations I975A, T977A, D979A, P981H, V997A, E1001A and S1020A strongly reduced collagen binding, showing a residual binding of less than 25 %. To further investigate the effect of the seven mutations, these mutants, and mutant H1023A from our previous study [31], were purified by immuno-affinity chromatography. Collagen binding of the purified mutants was analysed by surface plasmon resonance (SPR). In addition to wt-vWF, mutants P981A and E1021A that bound normally to collagen in the solid-state collagen-binding assay were selected as positive controls.

Binding isotherms of purified vWF-variants were determined. Human placenta collagen type III was coated at a density of 3000 RU. Wild-type vWF bound dose dependent and saturable to collagen type III, with an apparent K_D of 3.6 ± 0.4 nM and a maximum binding at equilibrium, $R_{eq,max}$, of 521 ± 14 RU (figure 2, Table I).

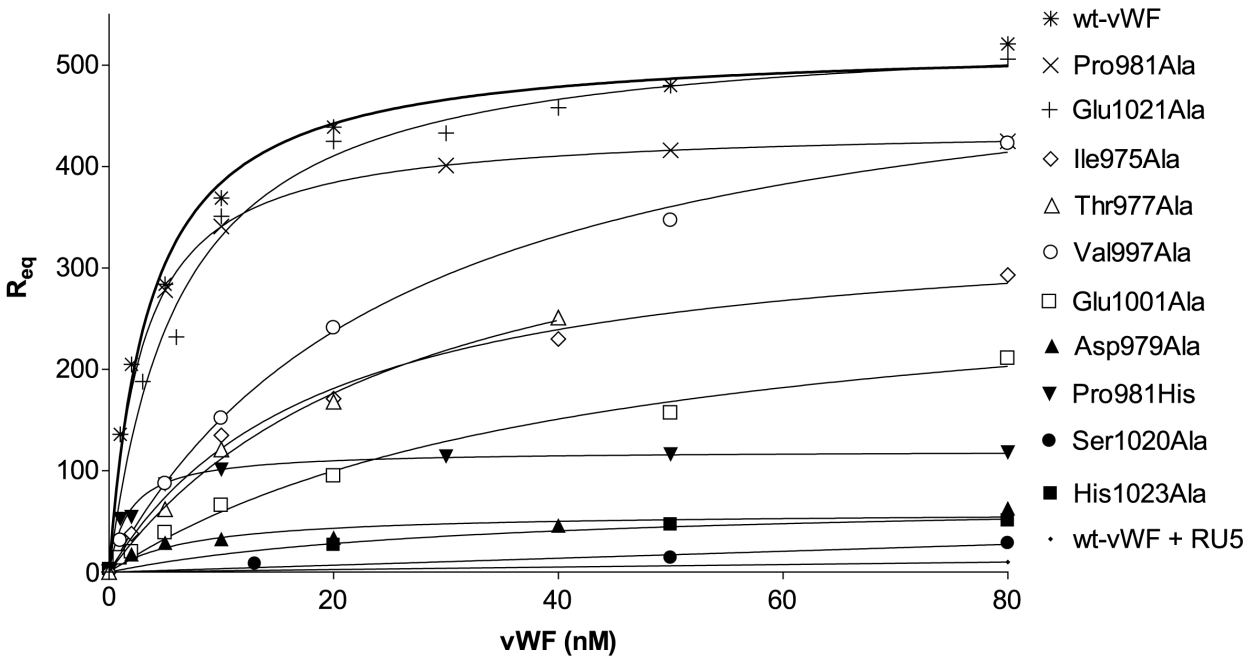

Figure 2: Binding-isotherms of vWF mutants to collagen type III in an SPR-based assay. Human placenta collagen types III and IV were immobilized on a CM5 biosensor chip for a detection and reference channel, respectively. Wild-type vWF and wt-vWF pre-incubated with a five-fold molar excess of RU5 Fab-fragment were used as a positive and negative control, respectively. Sequentially, increasing concentrations of vWF variants were injected and equilibrium binding was determined.

Table I

Dissociation- and maximum binding at equilibrium for the vWF – collagen interaction

vWF variant	K_D[1] (± SD) (nM)	$R_{eq,max}$[1] (± SD) (RU)
wt-vWF	3.6 (0.4)	521 (14)
P981A	2.9 (0.0059)	440 (0.14)
E1021A	6.3 (0.69)	540 (14)
I975A	19 (3.0)	352 (20)
T977A	27 (4.7)	419 (38)
V997A	26 (2.7)	551 (23)
E1001A	42 (8.8)	310 (31)
D979A[2]		50
P981H	1.8 (0.26)	120 (3.4)
S1020A[2]		30
H1023A[2]		50

[1] Since vWF and collagen are multivalent and we used a 1:1 interaction model to fit the experimental data these values must be regarded as apparent.
[2] Collagen-binding of these variants was to low to calculate reliable dissociation constants.

Addition of the RU5 Fab fragment to wt-vWF almost completely inhibited collagen binding, confirming that the A3 domain contains the binding site for collagen type III. Mutants P981A and E1021A that bound normally to collagen in the solid-state collagen-binding assay also had similar binding affinities and number of binding sites as wt-vWF for collagen in the SPR-based assay. Mutants that exhibited strongly reduced collagen-binding in the solid-state assay divided in two populations in the SPR collagen-binding assay. Mutations I975A, T977A, V997A and E1001A reduced the affinity of vWF for collagen five to ten fold, whereas at saturation the number of binding sites was at least 60 % compared to wt-vWF (Table I). Mutants D979A, P981H, S1020A and H1023A had a residual binding at saturation of less than 20 % compared to wt-vWF. The affinity could be calculated only for mutant P981H and it was similar to wt-vWF.

As shown in figure 3A, mutations that reduce collagen binding are located at the front face of the domain and define a rather flat collagen-binding site. Mutations at the bottom face did not have an effect. Interestingly, mutations that strongly inhibit collagen binding cluster at the lower part of the collagen-binding site, whereas mutations that partially inhibit collagen binding cluster at the upper part.

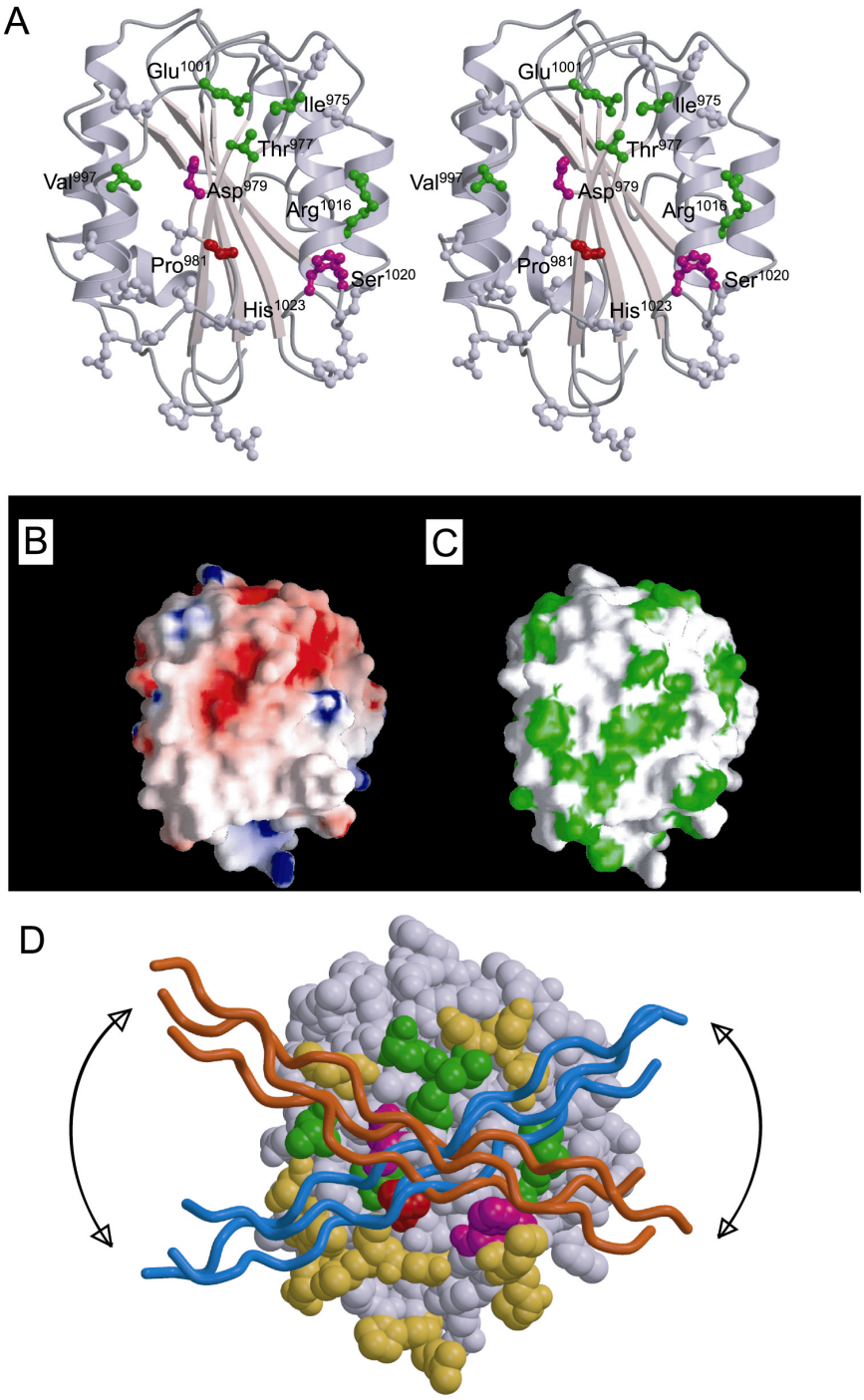

Figure 3: Characteristics of the collagen-binding site on the vWF-A3 domain. The front-face of the A3 domain is shown. A: Representation of the A3 domain that shows the effect of mutations in collagen-binding by colour. Residues in *magenta* display strongly reduced collagen binding. Residues in *green* display a partially reduced collagen binding, whereas collagen binding of residues in *grey* is comparable to recombinant wt-vWF. Pro^{981} is shown in *red*. The effect of five mutations investigated in our previous study [31], R963A, E987A, H990A, R1016A and H1023A, are included in the figure.
B: Solvent accessible surface with electrostatic potential contoured from *red* (-10kT/e) to blue (+1- kT/e). C: Solvent accessible surface with hydrophobic- and hydrophilic regions in *green* and *white*, respectively. D: CPK-representation of the A3 domain with two collagen triple helices that indicate the putative range of orientations for the A3-collagen interaction. Residues of A3 are color-coded as in figure 3A, except that residues that show no effect in collagen binding are colored in *yellow* and residues of which no data are available are shown in *grey*.

Surface properties of the collagen binding site are shown in figures 3B and 3C. The upper part of the collagen binding site contains a small negatively charged patch. In addition, the collagen binding site contains one large and two smaller hydrophobic patches.

Docking of a Collagen Triple Helix on A3

Identification of residues involved in collagen binding allows us to dock a collagen triple helix on A3. Attempts using an automated procedure [36] were not successful. Possibly this was caused by the use of a triple helix consisting of glycine-proline-hydroxyproline repeats, because specific collagen sequences that interact with A3 have not been identified. Therefore, we manually docked a collagen triple helix on A3 using the computer program O [37] and the following constraints: (i) the diameter of a collagen triple helix is approximately 17 Å, (ii) all residues shown to be involved in collagen binding should contact the triple helix, and (iii) since RU5 blocks collagen binding to A3, the position of the triple helix should overlap the position of the RU5 Fab fragment [31]. A broad range of orientations of a collagen triple helix on A3 fulfil these constraints (figure 3D). Six to eight consecutive collagen residues interact with the A3 domain.

Discussion

Von Willebrand Factor A-type domains are found in many proteins including collagens, complement proteins and integrins where they are named I-domains. These proteins are involved in several biological functions like cell-cell interaction and ligand-receptor binding. In integrins, these interactions are mediated by a divalent cation present in the MIDAS motif at the top of the domain.

vWF contains three A-type domains, of which the A3 domain binds to collagen. The vWF-A3 domain does not contain a functional MIDAS motif and collagen binding is cation independent [21; 29]. Previously, we have identified the approximate location of the collagen binding site [31]. Based on these results we constructed a panel of twenty-two point mutants in which solvent exposed residues were mutated to either alanine or histidine. These mutations were introduced into multimeric vWF, and collagen-binding was evaluated.

Collagen binding of the point mutants was screened in a solid-state collagen-binding assay. Seven of the twenty-two mutants, I975A, T977A, D979A, P981H, V997A, E1001A and S1020A, displayed reduced collagen binding. Because the solid-state collagen-binding assay is a static assay that reveals collagen-binding under non-equilibrium conditions, we further characterised these seven mutants and mutant H1023A, which also binds strongly reduced to collagen [31], by SPR under equilibrium conditions. The apparent dissociation constant of wt-vWF for collagen was 3.6 nM, which is similar to values determined by van der Plas *et al.* and Saenko *et al.* [34; 38]. Addition of a five-fold molar excess of the RU5 Fab fragment to wt-vWF completely abolished collagen binding. Interestingly, at equilibrium conditions the mutants that were qualified as "strongly reduced" in the solid-state assay now separated in two groups. Collagen binding of mutants D979A, S1020A and H1023A, was 80 – 90 % inhibited and therefore these residues are essential for collagen binding. Mutants I975A, T977A, V997A and E1001A, were characterised by a 5 – 10 fold reduced affinity, but had a normal number of binding sites suggesting that these residues are involved in collagen binding, but are not essential. Mutation P981H strongly reduced collagen binding but the apparent affinity is similar to wt-vWF. Interestingly, mutation P981A did not reduce collagen binding. This indicates that Pro^{981} is spatially very close, but does not interact with the collagen triple helix. Most likely, mutation P981H inhibits via sterical hindrance the binding of collagen sequences that contain large residues, but does not affect the binding of other collagen sequences.

Mutated residues that displayed reduced collagen binding define the collagen-binding site at the front face of A3. Residues that are essential in collagen binding, residues Asp^{979}, Ser^{1020} and His^{1023}, cluster at the lower part of the collagen-binding site and are located in strand β3 and loop α3β4. Residues that bind to collagen, but are not essential, residues Ile^{975}, The^{977}, Val^{997}, Glu^{1001} and Arg^{1016}, cluster at the upper part of the collagen-binding site and are located in loops β2β3, α2α3, helix α3 and strand β3. Previously we hypothesised the possible involvement of loop β3α2 in collagen binding [31], but mutations in this loop did not inhibit collagen binding excluding its involvement. None of the mutations at the bottom-face of A3 reduced collagen binding and therefore we excluded the A3 bottom face to be involved in collagen binding.

High affinity sites within collagen to which vWF binds are still unknown. Based on the surface characteristics of the collagen-binding site, we suggest that a collagen triple helix containing positively charged and hydrophobic residues binds A3. Since mutation P981H

strongly reduces the number of collagen binding sites with retaining normal affinity, whereas mutation P981A does not affect collagen-binding at all, it suggests that the collagen triple helix is spatially close to Pro^{981} and may contain a large residue. In addition to this it is likely that A3 recognizes multiple collagen sequences. Also for the I-domain of α_1 integrin it has been observed that it recognizes multiple collagen sequences [39].

Manual docking of a collagen triple helix on the front face of the A3 domain suggested a broad range of engagements of a collagen triple helix on the A3 domain (figure 3D). Therefore the models must be regarded as a crude approximation. This model predicts that at most eight consecutive residues in a collagen molecule interacts with A3.

The vWF-A3 collagen-binding site is located at the front face of the domain, whereas the collagen-binding site of homologous integrin I-domains is located at the top and requires a functional MIDAS motif [27; 40]. The collagen-binding site of I-domains contain a protruding helix that determines the specificity towards collagen [24; 41]. The collagen-binding site of A3 does not contain such a protruding helix and it is rather flat. This suggests a low specificity of A3 for collagen sequences.

Recently, four mutations (S968T, Q971H, I978T, Q999R) in the A3 domain have been identified in patients that have either no or mild bleeding problems [42; 43]. This questions the relevance of the A3 domain for immobilisation of vWF to the vascular matrix [42]. However, Wu *et al.* [20] characterised a monoclonal antibody that binds to A3 and inhibits platelet adhesion *in vivo*, confirming the relevance of the A3 domain in the vWF – collagen interaction. In addition, these four residues are located in the region of the collagen-binding site that contains residues that are involved but not essential in collagen binding. Such mutations may therefore not give bleeding symptoms. In contrast, mutations in the region that contains residues that are essential in collagen binding may be associated with bleeding symptoms.

In summary, we mapped the collagen-binding site at the front face of the domain. Residues in the lower half of the collagen-binding site are essential for collagen binding, whereas residues in the upper half are involved but not essential. We suggest that a collagen triple helix that interacts with A3 contains hydrophobic and positively charged residues. Further understanding of the vWF-collagen interaction requires the identification of specific collagen sequences involved in vWF binding.

Reference List

1. Bornstein P, Sage H. Structurally distinct collagen types. Annu Rev Biochem. 1980;49:957-1003.

2. Prockop DJ, Kivirikko KI. Collagens: molecular biology, disease, and potentials for therapy. Annu Rev Biochem. 1995;64:403-434.

3. Kehrel B. Platelet-collagen interactions. Thromb Haemost. 1995;21:123-129.

4. Moroi M, Jung SM. Platelet receptors for collagen. Thromb Haemost. 1997;78:439-444.

5. Sixma JJ, van Zanten GH, Huizinga EG, et al. Platelet adhesion to collagen: An update. Thromb Haemost. 1997;78:434-438.

6. Sadler JE. Biochemistry and genetics of von Willebrand factor. Annu Rev Biochem. 1998;67:395-424.

7. Ruggeri ZM, Ware J. von Willebrand factor. FASEB J. 1993;7:308-316.

8. Ruggeri ZM. Structure and function of von Willebrand factor. Thromb Haemost. 1999;82:576-584.

9. Houdijk WPM, Sakariassen KS, Nievelstein PFEM, Sixma JJ. Role of Factor VIII-von Willebrand factor and Fibronectin in the interaction of platelets in flowing blood with monomeric and fibrillar human collagen types I and III. J C I. 1985;75:1-10.

10. Hoylaerts MF, Yamamoto H, Nuyts K, Vreys I, Deckmyn H, Vermylen J. von Willebrand factor binds to native collagen VI primarily via its A1 domain. Biochem J. 1997;324:185-191.

11. Denis C, Baruch D, Kielty CM, Ajzenberg N, Christophe O, Meyer D. Localization of von Willebrand factor binding domains to endothelial extracellular matrix and to type VI collagen. Arterioscler Thromb. 1993;13:398-406.

12. Vischer UM, De Moerloose P. von Willebrand factor: from cell biology to the clinical management of von Willebrand's disease. Crit Rev Oncol Hematol. 1999;30:93-109.

13. Dong Z, Thoma RS, Crimmins DL, McCourt DW, Tuley EA, Sadler JE. Disulfide bonds required to assemble functional von Willebrand factor multimers. J Biol Chem. 1994;269:6753-6758.

14. Vischer UM, Wagner DD. von Willebrand factor proteolytic processing and multimerization precede the formation of Weibel-Palade bodies. Blood. 1994;83:3536-3544.

15. Fischer BE, Kramer G, Mitterer A, et al. Effect of multimerization of human and recombinant von Willebrand factor on platelet aggregation, binding to collagen and binding of coagulation factor VIII. Thromb Res. 1996;84:55-66.

16. Mohri H, Yoshioka A, Zimmerman TS, Ruggeri ZM. Isolation of the von Willebrand factor domain interacting with platelet glycoprotein Ib, heparin, and collagen and characterization of its three distinct functional sites. J Biol Chem. 1989;264:17361-17367.

17. Lankhof H, van Hoeij M, Schiphorst ME, et al. A3 domain is essential for interaction of von Willebrand factor with collagen type III. Thromb Haemost. 1996;75:950-958.

18. Cruz MA, Yuan H, Lee JR, Wise RJ, Handin RI. Interaction of the von Willebrand Factor (vWF) with collagen. J Biol Chem. 1995;270:10822-10827.

19. Wu D, Meiring M, Kotze HF, Deckmyn H, Cauwenberghs N. Inhibition of platelet glycoprotein Ib, glycoprotein IIb/IIIa, or both by monoclonal antibodies prevents arterial thrombosis in baboons. Arterioscler Thromb Vasc Biol. 2002;22:323-328.

20. Wu D, Vanhoorelbeke K, Cauwenberghs N, et al. Inhibition of the von Willebrand (VWF)-collagen interaction by an antihuman VWF monoclonal antibody results in abolition of in vivo arterial platelet thrombus formation in baboons. Blood. 2002;99:3623-3628.

21. Huizinga EG, Van der Plas RM, Kroon J, Sixma JJ, Gros P. Crystal structure of the A3 domain of human von Willebrand factor: implications for collagen binding. Structure. 1997;5:1147-1156.

22. Bienkowska J, Cruz MA, Atiemo A, Handin RI, Liddington R. The von Willebrand Factor A3 domain does not contain a metal ion-dependent adhesion site motif. J Biol Chem. 1997;272:25162-25167.

23. Colombatti A, Bonaldo P, Doliana R. Type A Modules: Interacting domains found in several non-fibrillar collagens and in other extracellular matrix proteins. Matrix. 1993;13:297-306.

24. Emsley J, King SL, Bergelson JM, Liddington RC. Crystal structure of the I domain from integrin $\alpha 2\beta 1$. J Biol Chem. 1997;272:28512-28517.

25. Tuckwell DS, Calderwood DA, Green LJ, Humphries MJ. Integrin $\alpha 2$ I-domain is a binding site for collagens. J Cell Sci. 1995;108:1629-1637.

26. Dickeson SK, Walsh JJ, Santoro SA. contributions of the I and EF hand domains to the divalent cation-dependent collagen binding activity of the $\alpha 2\beta 1$ integrin. J Biol Chem. 1997;227:7661-7668.

27. Emsley J, Knight CG, Farndale RW, Barnes MJ, Liddington RC. Structural basis of collagen recognition by integrin $\alpha 2\beta 1$. Cell. 2000;100:47-56.

28. Tulla M, Pentikainen OT, Viitasalo T, et al. Selective binding of collagen subtypes by integrin alpha 1I, alpha 2I, and alpha 10I domains. J Biol Chem. 2001;276:48206-48212.

29. Pietu G, Fressinaud E, Girma JP, Nieuwenhuis HK, Rothschild C, Meyer D. Binding of human von Willebrand factor to collagen and to collagen- stimulated platelets. J Lab Clin Med. 1987;109:637-646.

30. Bockenstedt PL, McDonagh j, Handin RI. binding and covalent cross-linking of purified von Willebrand factor to native monomeric collagen. J Clin Invest. 1986;78:551-556.

31. Romijn RA, Bouma B, Wuyster W, et al. Identification of the Collagen-binding Site of the von Willebrand Factor A3-domain. J Biol Chem. 2001;276:9985-9991.

32. Graham F, van der Eb A. A new technique for the assay of infectivity of human adenovirus 5 DNA. Virology. 1973;52:456.

33. Lawrie AS, Horser MJ, Savidge GF. Phast assessment of vWF:Ag multimeric distribution. Thromb Haemost. 1990;59:369.

34. Van der Plas RM, Gomes L, Marquart JA, et al. Binding of von Willebrand Factor to Collagen type III: Role of specific amino acids in the collagen binding domain of vWF and effects of neighbouring domains. Thromb Haemost. 2000;84:1005-1011.

35. Motulsky HJ. GraphPad Prism 3.0. 1999.

36. Gabb HA, Jackson RM, Sternberg MJE. Modelling protein docking using shape complementarity, electrostatics, and biochemical information. Journal of Molecular Biology 1997; 272, 106-120.

37. Jones TA, Zou JY, Cowan SW, Kjeldgaard M. Improved methods for the building of protein models in electron density maps and the location of error in these models. Acta Crystallogr A. 1991;47:110-119.

38. Saenko E, Kannicht C, Loster K, et al. Development and applications of surface plasmon resonance-based von Willebrand factor-- collagen binding assay. Anal Biochem. 2002;302:252-262.

39. Rich RL, Deivanayagam CCS, Owens RT, et al. Trench-shaped binding sites promote multiple classes of interactions between collagen and the adherence receptors, $\alpha_1\beta_1$ integrin and *Staphylococcus aureus* Cna MSCRAMM. J Biol Chem. 1999;274:24906-24913.

40. Smith C, Estavillo D, Emsley J, Bankston LA, Liddington RC, Cruz MA. Mapping the collagen-binding site in the I domain of the glycoprotein Ia/IIa (integrin $\alpha_2\beta_1$). J Biol Chem. 2000;275:4205-4209.

41. Dickeson SK, Mathis NL, Rahman M, Bergelson JM, Santoro SA. Determinants of ligand binding specificity of the $\alpha_1\beta_1$ and $\alpha_2\beta_1$ integrins. J Biol Chem. 1999;274:32182-32191.

42. Schneppenheim R, Obser T, Drewke E, et al. Isolated Molecular Defects of Von Willebrand Factor Binding to Collagen Do Not Correlate with Bleeding Symptoms [abstract]. Blood. 2001.

43. Ribba AS, Loisel I, Lavergne JM, et al. Ser968Thr mutation within the A3 domain of von Willebrand factor (VWF) in two related patients leads to a defective binding of VWF to collagen. Thromb Haemost. 2001;86:848-854.

Chapter 4

Mutation Ser968Thr in the von Willebrand Factor A3 domain reduces the collagen binding affinity without conformational changes

Roland A.P. Romijn[†], Piet Gros[‡], Jan J. Sixma[†] and Eric G. Huizinga[†‡]

[†] Thrombosis and Haemostasis Laboratory, Department of Haematology, University Medical Center and Institute of Biomembranes, HP G03.647, PO box 85500, 3508 GA Utrecht, The Netherlands and

[‡] Bijvoet Center for Biomolecular Research, Department of Crystal and Structural Chemistry, Utrecht University, Padualaan 8, 3584 CH Utrecht, The Netherlands.

Summary

vWF is a multimeric plasma glycoprotein that mediates platelet adhesion at sites of vascular damage. The collagen-binding site has been mapped to the front face of the vWF-A3 domain. Recently a patient has been reported with mutation Ser968Thr in the A3 domain that reduced collagen type I binding. In the present study we have evaluated binding of Ser968Thr-vWF to collagen type III. In addition platelet adhesion to collagen type III was evaluated in the presence of vWF containing this mutation. Whereas collagen binding of Ser968Thr-vWF was similar as the binding of wt-vWF to collagen, platelet adhesion in the presence of Ser968Thr-vWF was 40 % reduced.

We solved the crystal structure of Ser968Thr-A3. In the crystal structure we did not observe long- or short range conformational changes. However, since some loops at or close to the collagen binding site are flexible, we suggest that mutation Ser968Thr shifts the equilibrium between the conformations of these loops. This switches A3 from a high- to a low-affinity conformation and thereby reduces collagen binding.

Introduction

Von Willebrand factor (vWF[1]) is a large multimeric plasma glycoprotein. At sites of vascular damage it serves as a molecular bridge between collagen and the glycoprotein Ib-IX-V complex on the platelet, thereby initiating thrombus formation (reviewed in [1]). A dysfunctional vWF may lead to bleeding complications.

Mature vWF contains 2050 amino-acid residues that are arranged in domains D'-D3-A1-A2-A3-D4-B1-B2-B3-C1-C2-CK. Dimer formation involves interchain disulfide bond formation between CK domains, whereas multimers are formed by interchain disulfide bonds between D3 domains. VWF multimers contain up to 80 monomers [2]. Multimerisation is important for the function of vWF, because smaller multimers have a reduced affinity toward collagen and are less active in platelet aggregation [3]. The vWF-A3 domain is essential for platelet adhesion *in vivo* [4], since it contains the primary binding site collagen for collagen types I and III [5] that are constituents of the deeper layers of the vessel wall [6]. The collagen-binding site in A3 is located at the front face of the domain [7]. This is in contrast to homologous integrin I-domains, like the α_2-I domain, which contains the collagen-binding site at the top face [8]. Moreover, collagen binding by the vWF-A3 domain is cation independent [9], whereas integrin I-domains require the presence of a divalent cation in the metal ion dependent adhesion site motive [10; 11].

Qualitative or quantitative defects in vWF cause von Willebrand disease (vWD) [12], a very mild to severe bleeding disorder. Recently a new dysfunctional phenotype of vWF has been found with a reduced collagen binding activity, resulting in a mild bleeding tendency [13]. This was caused by mutation Ser968Thr in the vWF-A3 domain. In A3, residue Ser^{968} is not solvent exposed but it is located under the surface of the collagen binding site [7]. The mechanism by which this mutation reduces the affinity of A3 for collagen is not understood.

In this study, we investigated the platelet adhesive properties of recombinant multimeric vWF containing mutation Ser968Thr in a perfusion system. To investigate structural effects of the mutation, the crystal structure was solved of monomeric Ser968Thr-A3.

Experimental procedures

Construction, Expression, Purification and Characterization of Ser968Thr-A3

Mutation Ser968Thr was introduced in the isolated A3 domain using the Quikchange method (Stratagene, La Jolla CA, USA) and plasmid pET15b-A3 that contains vWF residues 920– 1111 [14]. The presence of the mutation was confirmed by sequencing.

Ser968Thr-A3 was expressed in *E. coli* BL21(DE3). Bacteria were cultured in LB medium containing 10 g/l peptone, 5 g/l yeast extract and 10 g/l NaC in 1 litre flasks. At a cell density of OD_{600} 1.6 induction was started by the addition of isopropyl-β-D-galactopyranoside (0.5 mM final concentration). Bacteria were cultured for an additional 3 hours, collected by centrifugation and stored at –20 ^{o}C. Ser968Thr-A3 was purified according to a procedure published by Huizinga *et al.* [14].

Construction, Expression, Purification and Characterization of Ser968Thr-vWF

Mutation Ser968Thr was introduced in multimeric vWF using the Quikchange method as described before [7]. Briefly, the mutation was introduced into mutagenesis plasmid pBSvWF-NC containing vWF residues 940 to 1113, generating pBSvWF-NC-Ser968Thr, and the presence of the mutation was confirmed by sequencing. The NheI – Csp45I fragment of pBSvWF-NC-Ser968Thr was ligated with NheI – Csp45I digested pNUTvWFcas2, generating plasmid pNUTvWFcas2-S968T.

Ser968Thr-VWF was stably expressed in baby hamster kidney cells that overexpress furin, necessary for proper removal of vWF propeptide [5; 15]. Cells were cultured in serum-free medium.

Ser968Thr-VWF was purified by immuno-affinity chromatography using monoclonal antibody RU8, which is directed against the D4 domain [5]. Ser968Thr-VWF was eluted in 50 mM Tris, 100 mM NaCl pH 7.4 and vWF-containing fractions were stored at –20 °C.

The vWF concentration was determined by a sandwich ELISA using polyclonal α-vWF and horseradish peroxidase (HRP) conjugated polyclonal α-vWF (DAKO, Glostrup, Denmark) for immobilization and detection, respectively [5]. Normal pooled plasma from 40 healthy donors was used as a reference.

The vWF multimeric structure was analyzed by agarose gel electrophoresis followed by Western blotting as described by Lawrie *et al.* [16].

Binding of monoclonal antibody (MoAb) RU5 to vWF was analyzed as described before with a few modifications [7]. Microtiter-plate wells (Costar, Cambridge MA, USA) were coated with 2.5 μg/ml polyclonal α-D'D3 [17] in 50 mM carbonate buffer pH 9.6 (3 h, 20 °C). Wells were washed with PBS/0.1% Tween-20 and blocked with 3 % BSA in PBS/0.1% Tween-20 (1 h, 37 °C). Wells were incubated with 1 μg/ml vWF in mock medium (1 h, 37 °C). After washing, 2 μg/ml RU5 in PBS/0.1% Tween-20 containing 3% BSA was added (1 h, 37 °C). Wells were washed and incubated with HRP conjugated rabbit-anti-mouse antibody (DAKO, Glostrup, Denmark) diluted 1:2500 in PBS/0.1% Tween-20 containing 3% BSA (1 h, 37 °C). O-phenylenediamine was used as substrate for detection.

Solid-State Collagen-Binding Assay

VWF binding to fibrillar human placenta collagen type III (Sigma chemical CO., St. Louis MO, USA, cat. No. C-4407) was studied in a solid-state collagen-binding assay as before [7; 17]. Collagen was coated in microtiter plate wells at a concentration of 50 μg/ml in 20 mM sodium phosphate pH 7.4 by centrifuging the mircotiter-plate 15 minutes at 1500 rpm in a table-top centrifuge. After blocking with 3% BSA in PBS/0.1% Tween-20, expression medium containing vWF was added at indicated concentrations (1 h, 37 °C). After washing with running tap water, wells were incubated with horseradish peroxidase conjugated anti-vWF antibody (DAKO, Glostrup, Denmark) in PBS/0.1% Tween-20 containing 3% BSA (1 h, 37 °C). O-phenylenediamine was used as substrate for detection. The binding-isotherms for vWF-collagen interaction were fitted with a 1:1 interaction model $Y_{eq}=Y_{eq,max}*[vWF]/(K_D + [vWF])$, in which Y represents the amount of bound vWF.

Platelet Adhesion to Ser968Thr-vWF under Flow

Human placenta collagen type III coated Thermanox® coverslips were prepared as described before [18; 19]. Citrated plasma was depleted from endogenous vWF by 3 passages over an immuno-affinity column using monoclonal antibody RU2 that is directed against the vWF-A2 domain [20; 21]. Residual endogenous vWF was less than 1% (data not shown). Reconstituted blood was prepared from vWF depleted plasma by adding recombinant vWF (8 μg/μl), washed red blood

cells (40 % (v/v) final concentration) and platelets ($2*10^5$ cells/µl) from a blood group O^+ donor [22; 23]. Perfusion, using prewarmed perfusate, was done in a miniaturized linear flow perfusion system at a wall-shear rate of 1600 s^{-1} (5 min., 37 ^oC) [19]. Coverslips were stained with May-Grünwald/Giemsa [24] and platelet adhesion was evaluated using a light microscopy at 400 fold magnification connected to an Image Analyzer (AMS 40-10, Saffron Walden, UK) and the program Optimas 6.0 (Optimas corporation, Washington, USA). Twenty fields perpendicular to the flow axis at the center of each coverslip were analysed, and platelet adhesion was expressed as a percentage of the covered surface area. As positive and negative control, washed red blood cells and platelets were added to the platelet-donors plasma or to vWF-depleted plasma, respectively. Each data point represents the mean ± SD of at least three experiments in triplicate.

Crystallization, Data Collection and Processing

Crystals of Ser968Thr-A3 were grown by the hanging-drop vapor-diffusion method at 4 ^oC using a precipitant solution consisting of 27 % (v/v) PEG 3000, 0.2 M sodium acetate pH 4.6, 0.1 M Tris/HCl pH 8.5 and a protein concentration of 6.5 mg/ml. Crystals that were obtained after 30 days. The crystals were soaked in cryoprotectant containing 30% (m/v) PEG 3000, 0.2 M sodium acetate pH 4.6, 0.1 M Tris/HCl pH 8.5, 15% (v/v) glycerol for 1 - 2 minutes and snap frozen in liquid nitrogen. Diffraction data were collected at the European Synchrotron Radiation Facility (Grenoble, France) on beam line ID14-EH3. Diffraction data were processed using the programs DENZO and Scalepack [25]. Diffraction data statistics are summarized in Table I.

Structure Determination and Refinement

The structure was solved by molecular replacement using the program CNS [26] with the structure of wt-A3 [14] as a search model. Two Ser968Thr-A3 molecules were identified in the asymmetric unit, denoted *A* and *B*. Rebuilding using O [27] and positional- and B-factor refinement using CNS were performed until convergence. Non-crystallographic symmetry restraints were applied in the initial stages of refinement. Cross validation was used throughout refinement using a 5% test set of reflections. Refinement used the maximum-likelihood algorithm [28] and bulk-solvent correction was applied. Water molecules were placed in difference electron-density peaks if the peak height was at least 3.0 σ and the distance to a hydrogen-bond donor or acceptor was 2.7-3.2 Å. Water

molecules with a B-factor above 100 $Å^2$ were rejected. The final model was analyzed with PROCHECK [29] and WHATIF [30]. Refinement statistics are summarized in Table I.

Results

Characterization of Ser968Thr-vWF

Since vWF binding to collagen is dependent on the multimer distribution and the conformation of the A3 domain, the multimeric pattern and binding of conformation specific MoAb RU5 to Ser968Thr-vWF were analyzed. The multimer distribution of Ser968Thr-vWF was similar to wt-vWF (data not shown), indicating proper post-translational processing. Binding of conformation dependent monoclonal antibody RU5 to Ser968Thr-vWF was similar to binding to wt-vWF (figure 1), suggesting that the mutation does not disrupt the overall conformation of the A3-domain.

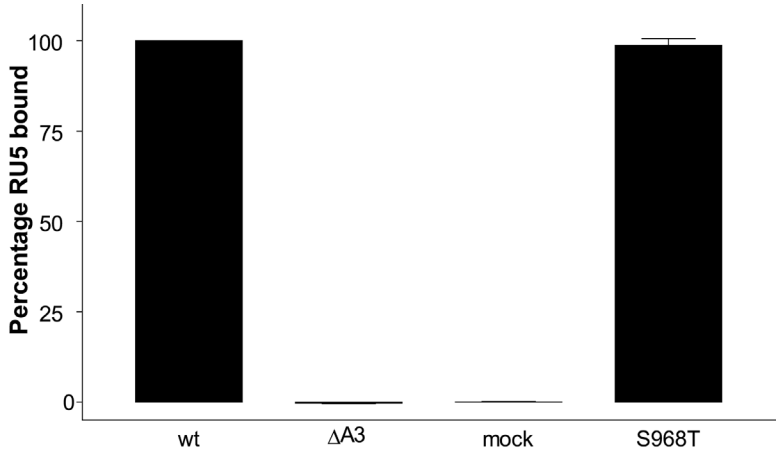

Figure 1: Binding of monoclonal antibody RU5 to Ser968Thr-vWF. VWF was immobilized in microtiter plate wells via polyclonal αD'D3 and was incubated with RU5. Bound RU5 was detected as described under "Experimental Procedures". Wild-type vWF and ΔA3-vWF, which lacks the A3 domain [5], were used as a positive and negative control, respectively. Binding of RU5 to vWF mutants is expressed as a percentage of wt-vWF. Each data-point represents the mean ± SD of two independent measurements.

Collagen binding of Ser968Thr-vWF was evaluated in a solid-state collagen-binding assay (figure 2). Wild-type vWF bound saturably and concentration dependent to collagen with a dissociation constant of 1.3 µg/ml. As expected, binding of ΔA3-vWF to collagen was markedly reduced with a maximal binding of 23 % at a concentration of 10 µg/ml. Binding of Ser968Thr-vWF to collagen was saturable and concentration dependent. At 10 µg/ml, the maximum binding Ser968Thr-vWF to collagen type III was 10 % reduced compared to wt-vWF while the dissociation constant was increased to 1.4 µg/ml. Differences between Ser968Thr-vWF and wt-vWF in binding to collagen are not significant.

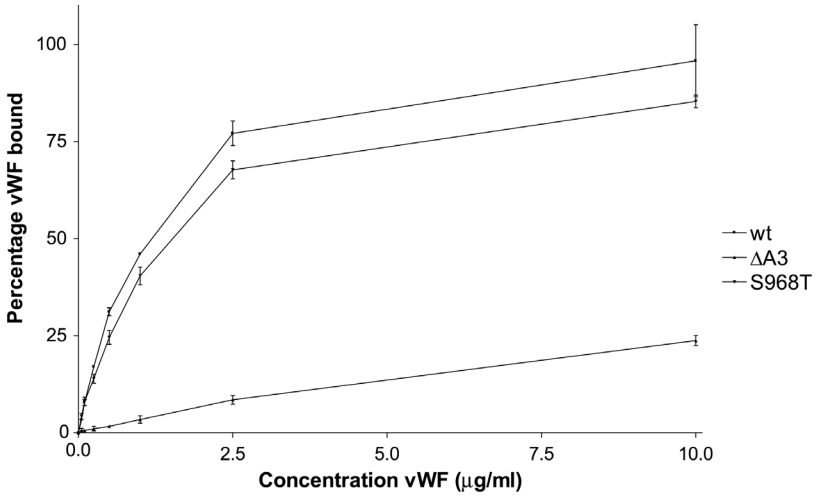

Figure 2: Binding of Ser968Thr-vWF to collagen type III in a solid-state collagen-binding assay. Fibrillar human placenta collagen type III was coated in microtiter plate wells. Wells were incubated with vWF at a concentrations indicated and bound vWF was detected as described under "Experimental Procedures". Δ-A3 vWF was used as a negative control. Bound vWF is expressed as a percentage of wt-vWF. Each data point represents the mean ± SD of three experiments performed in duplicate.

The effect of mutation Ser968Thr in platelet adhesion to a collagen type III coated surface was evaluated in a perfusion system that mimics the *in vivo* situation. To this end, either wt-vWF, ΔA3-vWF or Ser968Thr-vWF was added to vWF-depleted plasma. In each set of experiments, depleted plasma was supplemented with platelets isolated from different healthy donors, yielded a surface coverage of 9.9%, 9.3%, 30.3% and 43.4% for wt-vWF. Although the variation in platelet adhesion is rather high, donor variation has been reported before and was hypothesized to correlate with surface expression of $\alpha_2\beta_1$ on the platelet [31;32]. Platelet adhesion mediated by ΔA3-vWF and Ser968Thr-vWF was normalized against wt-vWF within each experiment. Platelet adhesion in the presence of these variants was reduced by 88 % and 49 %, respectively (figure 3).

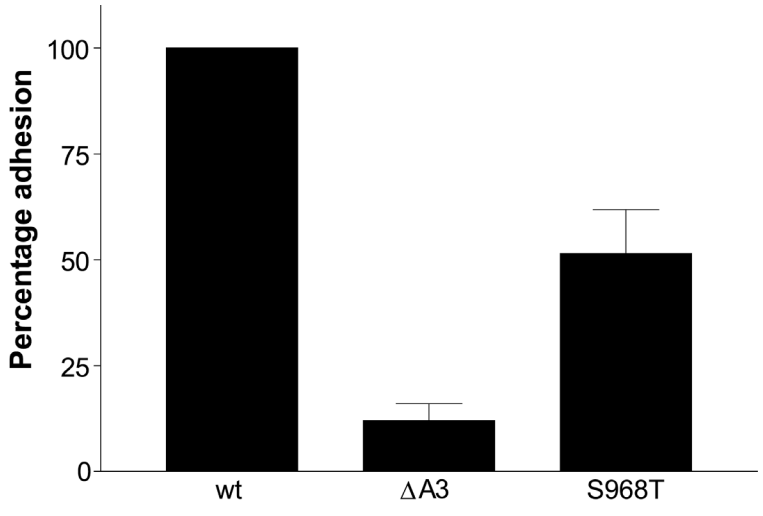

Figure 3: Platelet adhesion on collagen surface mediated by vWF variants. Human placenta collagen type III was coated on Thermanox® coverslips. VWF variants were added at a concentration of 8 µg/ml to reconstituted blood containing endogenous vWF depleted citrated plasma. Platelet coverage was evaluated after 5 minutes perfusion at a wall shear-rate of 1600 s^{-1}.

Crystal Structure of Ser968Thr-A3

Ser968Thr-A3 was purified from *E. coli* and concentrated to approximately 6.5 mg/ml. During concentration a significant fraction of the protein precipitated, suggesting that the mutation may influence the conformation of the A3 domain. Crystals of Ser968Thr-A3 were obtained by hanging-drop vapor-diffusion crystallisation at 4 ^{o}C. Crystallographic data statistics of a Ser968Thr-A3 crystal that was measured at the ESRF are summarized in Table I. Two molecules, denoted *A* and *B*, were observed in the asymmetric unit of which one is shown in figure 4A. The structure was refined to a R-factor of 18.2 % and a free R-factor of 22.8 %, contains 279 water molecules and 4 glycerol molecules. Refinement statistics are summarized in Table I. Judged from the Ramachandran plot the models were of good geometry, because 93.8 % of the residues were in the most favored region and 6.2 % in the additional allowed regions.

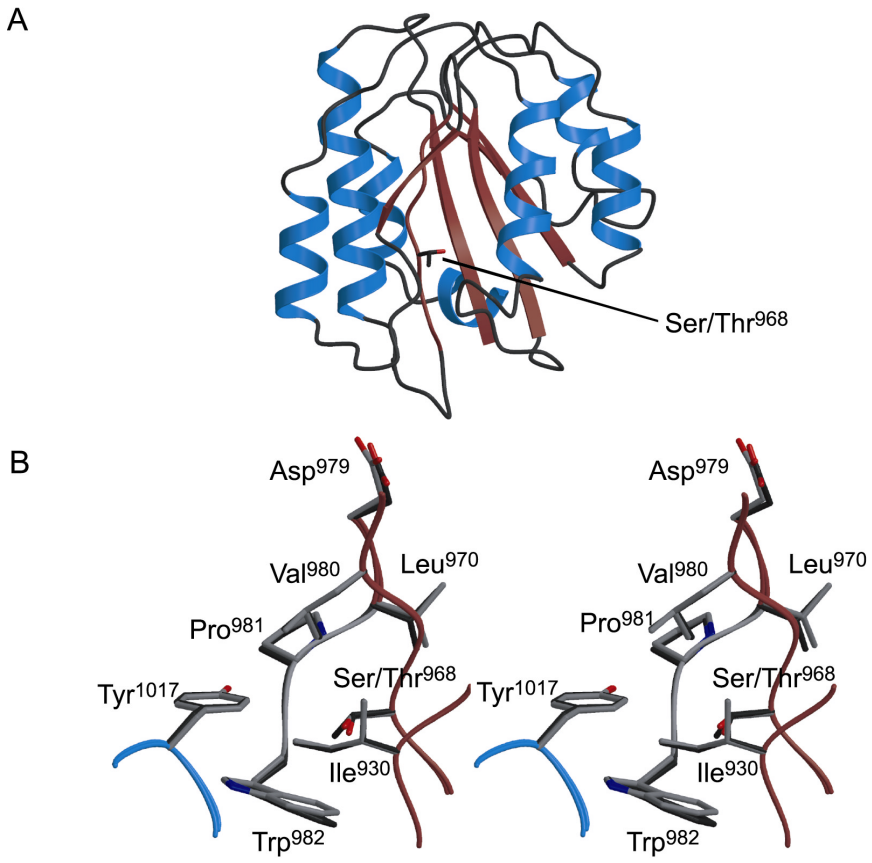

Figure 4: Crystal structure of Ser968Thr-A3. (A) Crystal structure of one of the Ser968Thr molecules is shown. Ser/Thr^{968} is shown in the structure and is buried just below the surface containing residues that are involved in collagen binding. (B) Superposition of one wt-A3 and one Ser968Thr-A3 model. Except for a small movement of the Trp^{982} side chain, the mutation does not induce local conformational changes.

Table I

Diffraction data and refinement statistics

Diffraction data	
Space group	$P2_1$
a, b, c (Å)	39.9, 61.7, 60.4
α, β, γ (^{o})	90.0, 104.1, 90.0
Mosaicity (^{o})	0.5
Redundancy	2.7
No. of unique reflections	21523
$I/\sigma(I)$,	16.1 (3.0)[a]
Completeness (%)	95.6 (90.6)[a]
R_{merge}[b] (%)	7.4 (39.5)[a]
Refinement	
Resolution (Å)	1.90 (1.97-1.90)[a]
R-factor	18.2
R_{free}	22.8
r.m.s.d. bond distances (Å)	0.0050
r.m.s.d. angles (^{o})	1.2
Average overall B-factor for protein atoms[c] (Å^2)	16.1 (21.0)
Protein residues observed	A: 925 – 1108
	B: 925 – 1099
No. of protein atoms	2696
No. of solvent molecules[d]	279 (33.7)
No. of glycerol molecules[d]	4 (35.0)

[a] Number between parentheses indicate statistics for highest resolution shell.
[b] $R_{merge} = \sum_i(I_i-<I_h>)^2 / \sum_i(I_i)^2$.
c Main chain atoms. Number between parenthesis is from side chain atoms.
[d] Average B-factor of the molecules in Å^2 is given between parenthesis.

The A3 construct contains residues 920 – 1111 of mature vWF, but the N- and C-termini are disordered in the crystal. For molecule *A* we observe residues 925 – 1108 while we see for molecule *B* residues 925 – 1099. In both molecules the Cys923-Cys1109 disulfide bridge that links the N- and C-terminal regions of the domain could not be observed. Possibly the disulfide bridge was broken by the intense X-ray beam of the synchrotron. Breaking of a disulfide bond at the surface of a protein by X-rays has been observed before in other proteins [33]. This had the most structural consequences in molecule *B* in which C-terminal residues Leu^{1100} to Ser^{1111} could not be observed.

Structural Comparison of wt-A3 and Ser968Thr-A3

Superposition of Ser968Thr-A3 molecules *A* and *B* shows variation in the conformation of loops α1β2 (residues 961 – 963), β3α2 (residues 983 – 987) and α5β6 (residues 1078 – 1084). However, a similar variation is observed within wt-A3 models [7], indicating that these loops are flexible in both wt- and mutant A3. In the proximity of Thr^{968} no variation in the backbone or side chains is observed between molecules *A* and *B*.

To investigate whether mutation Ser968Thr introduces conformational changes in the A3 domain, molecules *A* and *B* of the mutant and eight known wt-A3 models were superimposed [7; 14; 34]. The overall structure Ser968Thr-A3 and wt-A3 were indistinguishable indicating that the mutation does not induce long-range effects in A3.

In wt-A3, Ser^{968} is located just beneath the surface of the protein in close proximity of residues Ile^{975}, Thr^{977}, Asp^{979}, Val^{997}, Glu^{1001}, Arg^{1016}, Ser^{1020} and His^{1023} that are involved in collagen binding [7]. The Ser^{968} side chain adopts two conformations, indicating that there is some flexibility (figure 4B). In one conformation the hydroxyl group points to the interior of the domain, whereas in the other conformation it points to the surface and its hydroxyl group forms a hydrogen bond with the backbone carbonyl oxygen of Val^{980}. In both models of the mutant, the hydroxyl group of Thr^{968} points to the interior of the domain and occupies the same position as the inwards-oriented hydroxyl of Ser^{968} in the wild-type protein. This conformation gives some strain due to a short distance of 3.1 Å between the methyl group of the of Thr^{968} side chain and the side chain of Trp^{982}. Although the side chain of Trp^{982} moves slightly, the displacement is too small to relief the strain. No conformational changes are observed for residues at the surface of

the domain that are involved in collagen binding. Therefore, apart from the small movement of Trp^{982}, mutation Ser968Thr does not introduce local conformational changes.

Discussion

Recently, two related patients have been described who suffer from slightly increased bleeding times [13]. These patients have a mutation in the A3 domain. This mutation, Ser968Thr, is the first identified mutation in the A3 domain that reduces the affinity of vWF for collagen. In the present study we investigated the effect of the mutation multimeric vWF in platelet adhesion in a flow system. In addition, to identify conformational changes induced by the mutation we solved the structure of Ser968Thr-A3.

The multimeric structure of vWF is essential for a proper function, because vWF with a reduced multimeric size has a decreased affinity for collagen [3]. Multimeric composition of Ser968Thr-vWF was indistinguishable from wt-vWF. Moreover, binding of conformation-dependent, function-inhibiting MoAb RU5 to Ser968Thr-vWF was not reduced compared to wt-vWF. This is in agreement with Ribba *et al.* [13] who found that the binding of monoclonal antibodies 505 and B200 to Ser968Thr-vWF was normal. These results indicate that mutation Ser968Thr does not destroy the protein by means of post-translational modification or folding. Any observed effects in collagen-binding are therefore due to the (direct) involvement of Ser^{968} in collagen binding.

Collagen-binding was evaluated in a solid-state collagen-binding assay. We found that collagen-binding of Ser968Thr-vWF was not significantly reduced compared to wt-vWF, whereas Ribba *et al.* measured 50 % reduced collagen binding [13]. These authors have expressed vWF in COS-7 cells which do not cleave off the vWF propeptide. We have used vWF expressed in BHK cells that also overexpress furin that removes the vWF propeptide. However, this difference is not likely to cause the observed discrepancy. Another, more significant, difference is that in the study of Ribba *et al.* collagen binding was evaluated using human placenta collagen type I while we have used human placenta collagen type III. Apparently, mutation Ser968Thr has a different effect on different types of collagen.

Whereas mutation Ser968Thr did not significantly reduce the collagen-binding affinity in a solid-state collagen-binding assay, the mutation partially inhibited platelet adhesion to a collagen type III coated surface at high shear stress. This suggests that mutation Ser968Thr may have a different effect under shear compared to static conditions. It may be that mutation Ser968Thr does not influence the affinity under static conditions, but under conditions of shear stress it may shift the affinity to a low state.

In the crystal structure of Ser968Thr-A3 no long- or short-range conformational changes could be observed. This is in agreement with the normal reactivity of conformation dependent MoAb's 505, B200 [13] and RU5 towards Ser968Thr-vWF. However, this does not indicate that there are no conformational changes induced by the mutation. We have hypothesized before that collagen binding by the A3 domain involves an induced-fit model involving residues within loop α3β4 that is close to Ser^{968} and loop β3α2 located somewhat further away [7]. Among wild-type structures loop α3β4 is observed in two conformations, whereas in the mutant only one conformation is observed (data not shown). In the mutant similar flexibility for loop β3α2 was observed as in wt-A3. It may be that the mutation shifts the equilibrium of these loops to the low-affinity conformation, but that during the crystallization process there is preference for one of these conformations. Based on the experimental data it is not conclusive whether the high- or low-affinity conformation crystallizes.

Based on above assumptions we can not exclude that mutation Ser968Thr does not introduce long- or short range conformational changes in the A3 domain, but we are not able to observe these conformational changes in the crystal structure. Our data suggest that under shear conditions mutation Ser968Thr shifts the equilibrium between a high- and a low-affinity conformation and thereby reduces collagen binding.

Acknowledgements

We would like to thank the staff at beam line ID14-EH3 of the ESRF in Grenoble for their assistance in data collection.

Reference List

1. Sadler JE. Biochemistry and genetics of von Willebrand factor. Annu Rev Biochem. 1998;67:395-424.

2. Voorberg J, Fontijn R, Van Mourik JA, Pannekoek H. Domains involved in multimer assembly of von willebrand factor (vWF): multimerization is independent of dimerization. EMBO J. 1990;9:797-803.

3. Fischer BE, Kramer G, Mitterer A, et al. Effect of multimerization of human and recombinant von Willebrand factor on platelet aggregation, binding to collagen and binding of coagulation factor VIII. Thromb Res. 1996;84:55-66.

4. Wu D, Vanhoorelbeke K, Cauwenberghs N, et al. Inhibition of the von Willebrand (VWF)-collagen interaction by an antihuman VWF monoclonal antibody results in abolition of in vivo arterial platelet thrombus formation in baboons. Blood. 2002;99:3623-3628.

5. Lankhof H, van Hoeij M, Schiphorst ME, et al. A3 domain is essential for interaction of von Willebrand factor with collagen type III. Thromb Haemost. 1996;75:950-958.

6. Rand JH, Glanville RW, Wu XX, et al. The significance of subendothelial von Willebrand factor. Thromb Haemost. 1997;78:445-450.

7. Romijn RA, Bouma B, Wuyster W, et al. Identification of the Collagen-binding Site of the von Willebrand Factor A3-domain. J Biol Chem. 2001;276:9985-9991.

8. Emsley J, Knight CG, Farndale RW, Barnes MJ, Liddington RC. Structural basis of collagen recognition by integrin $\alpha 2\beta 1$. Cell. 2000;100:47-56.

9. Pietu G, Fressinaud E, Girma JP, Nieuwenhuis HK, Rothschild C, Meyer D. Binding of human von Willebrand factor to collagen and to collagen- stimulated platelets. J Lab Clin Med. 1987;109:637-646.

10. Dickeson SK, Mathis NL, Rahman M, Bergelson JM, Santoro SA. Determinants of ligand binding specificity of the $\alpha_1\beta_1$ and $\alpha_2\beta_1$ integrins. J Biol Chem. 1999;274:32182-32191.

11. Tuckwell DS, Calderwood DA, Green LJ, Humphries MJ. Integrin $\alpha 2$ I-domain is a binding site for collagens. J Cell Sci. 1995;108:1629-1637.

12. Sadler JE. a revised classification of von willebrand desease. Thromb Haemost. 1994;71:520-525.

13. Ribba AS, Loisel I, Lavergne JM, et al. Ser968Thr mutation within the A3 domain of von Willebrand factor (VWF) in two related patients leads to a defective binding of VWF to collagen. Thromb Haemost. 2001;86:848-854.

14. Huizinga EG, Van der Plas RM, Kroon J, Sixma JJ, Gros P. Crystal structure of the A3 domain of human von Willebrand factor: implications for collagen binding. Structure. 1997;5:1147-1156.

15. Graham F, van der Eb A. A new technique for the assay of infectivity of human adenovirus 5 DNA. Virology. 1973;52:456.

16. Lawrie AS, Horser MJ, Savidge GF. Phast assessment of vWF:Ag multimeric distribution. Thromb Haemost. 1990;59:369.

17. Van der Plas RM, Gomes L, Marquart JA, et al. Binding of von Willebrand Factor to Collagen type III: Role of specific amino acids in the collagen binding domain of vWF and effects of neighbouring domains. Thromb Haemost. 2000;84:1005-1011.

18. van Zanten GH, Saelman EUM, Schut-Hese KM, et al. Platelet adhesion to collagen type IV under flow conditions. Blood. 1996;88:3862-3871.

19. Sixma JJ, de Groot PG, Van Zanten H, IJsseldijk M. A new perfusion chamber to detect platelet adhesion using a small volume of blood. Thromb Res. 1998;92:S43-S46.

20. Perkins SJ, Smith KF, Williams SC, Haris PI, Chapman D, Sim RB. the secondary structure of the von Willebrand Factor type A domain in factor B of human complement by Fourier transform infrared spectroscopy. Its occurence in collagen types VI, VII, XII and XIV, the integrins and other proteins by avaraged structure predictions. J Biol Chem. 1994;238:104-119.

21. Houdijk WPM, Girma J-P, Van Mourik JA, Sixma JJ, Meyer D. Comparison of tryptic fragments of von Willebrand Factor involved in binding to thrombin-activated platelets with fragments involved in ristocetin-induced binding and binding to collagen. Thromb Haemost. 1986;56:391-396.

22. Lankhof H, Wu YP, Vink T, et al. Role of the glycoprotein Ib-binding A1 repeat and the RGD sequence in platelet adhesion to human recombinant von Willebrand factor. Blood. 1995;86:1035-1042.

23. Sakariassen KS, Bolhuis PA, Sixma JJ. Human blood platelet adhesion to artery subendothelium is mediated by factor VIII-von Willebrand factor bound to the subendothelium. Nature. 1979;279:636-638.

24. Sakariassen KS, Aarts PAMM, de-Groot PG, Houdijk WPM, Sixma JJ. A perfusion chamber developed to investigate platelet interaction in flowing blood with human vessel wall cells, their extracellular matrix, and purified components. J Lab Clin Med. 1983;102:522-535.

25. Otwinowski Z, Minor O. Processing of X-ray diffraction data collected in oscillation mode. Methods Enzymol. 1996;276:307-326.

26. Brünger AT, Adams PD, Clore GM, et al. Crystallography and NMR system: A new software suite for macromolecular structure determination. Acta Crystallogr D. 1998;54:905-921.

27. Jones TA, Zou JY, Cowan SW, Kjeldgaard M. Improved methods for the building of protein models in electron density maps and the location of error in these models. Acta Crystallogr A. 1991;47:110-119.

28. Pannu NS, Read RJ. Improved structure refinement through Maximim Likelihood. Acta Crystallogr A. 1996;52:659-668.

29. Lawkowski RA, MacArthur MW, Moss DS, Thornton JM. PROCHECK: a programm to check the stereochemical quality of protein structures [abstract]. J Appl Crystallogr. 1993;26:283-291.

30. Vriend G. What if: a molecular modelling and drug design program. J mol Graph. 1990;8:52-56.

31. Kunicki TJ, Orchekowski R, Annis D, Honda Y. Variability of integrin alpha 2 beta 1 activity on human platelets. Blood. 1993;82:2693-2703.

32. Roest M, Sixma JJ, Wu YP, et al. Platelet adhesion to collagen in healthy volunteers is influenced by variation of both alpha(2)beta(1) density and von Willebrand factor. Blood. 2000;96:1433-1437.

33. Weik M, Ravelli RB, Silman I, Sussman JL, Gros P, Kroon J. Specific protein dynamics near the solvent glass transition assayed by radiation-induced structural changes. Protein Sci. 2001;10:1953-1961.

34. Bienkowska J, Cruz MA, Atiemo A, Handin RI, Liddington R. The von Willebrand Factor A3 domain does not contain a metal ion-dependent adhesion site motif. J Biol Chem. 1997;272:25162-25167.

Chapter 5

Structures of Glycoprotein Ibα and its complex with von Willebrand Factor A1 domain

Eric G. Huizinga[*§], Shizuko Tsuji[†§], Roland A.P. Romijn[†], Marion E. Schiphorst[†] , Philip G. de Groot[†], Jan J. Sixma[†] & Piet Gros[*]

[*]*Department of Crystal and Structural Chemistry, Bijvoet Center for Biomolecular Research, Utrecht University, Padualaan 8, 3584 CH Utrecht, The Netherlands*

[†]*Thrombosis and Haemostasis Laboratory, Department of Haematology, Institute of Biomembranes, University Medical Center Utrecht, The Netherlands*

[§] These authors contributed equally

Published in Science, 297, 1176-1179, 2002

Summary

Transient interactions of platelet-receptor glycoprotein Ibα (GpIbα) and plasma-protein von Willebrand Factor (VWF) reduce platelet velocity at sites of vascular damage and play a role in haemostasis and thrombosis. Here we present structures of the GpIbα N-terminal domain and its complex with VWF domain A1. In the complex GpIbα wraps around one side of A1 providing two contact areas bridged by an area of solvated charge interaction. The structures explain the effects of gain-of-function mutations related to bleeding disorders and provide a model for shear-induced activation. These detailed insights into the initial interactions in platelet adhesion are relevant for the development of anti-thrombotics.

Results and Discussion

Transient interactions of platelet-receptor glycoprotein Ibα (GpIbα) and immobilized von Willebrand Factor (VWF) mediate rolling of platelets at sites of vascular damage. Rolling reduces platelet velocity and prolongs the contact time with reactive components of the cell matrix. This facilitates platelet-activation and subsequent integrin-mediated firm attachment [1]. Platelet GpIbα and VWF coexist in the circulation, but do not interact at a detectable level unless shear stress is applied or exogenous modulators like the snake venom botrocetin are added [2]. Four types of congenital bleeding disorders have been defined that are caused by mutations in GpIbα or VWF either enhancing or reducing complex formation. Shear-induced GpIbα-VWF interaction in occluded atherosclerotic arteries or at the surface of ruptured atherosclerotic plaques contributes critically to the onset of arterial thrombosis [3].

GpIbα is the central component of a receptor complex consisting of glycoproteins Ibα, Ibβ, IX and V. It anchors the complex to the cytoskeleton and harbors the VWF-binding function in its ~290 N-terminal residues. The VWF-binding site is exposed well above the platelet surface, being connected to a ~45 nm long highly O-glycosylated stalk [4]. The ~250-kDa VWF protein forms large disulfide-bonded multimers with molecular weights of up to10 MDa. It is found in plasma and the sub-endothelial cell matrix and is released from storage granules when platelets and endothelial cells are activated. A VWF-multimer acts as bridging ligand between platelets and the cell matrix, through collagen binding by its A3 domain and binding to GpIbα by its A1 domain [5].

Although the crystal structure of VWF-A1 is known [6; 7] and there is a large body of mutagenesis data [8-15], the precise interactions between GpIbα and A1, the mechanism of shear-induced activation and the molecular basis of related bleeding disorders are poorly understood. We present crystal structures of the N-terminal domain of GpIbα (residues 1-290) and its complex with the VWF-A1 domain (residues 498-705; VWF residue numbering used starts at the first residue of the mature subunit, addition of 763 converts the numbering to that of preproVWF) (Table 1). We expressed recombinant GpIbα with the mutations N21Q and N159Q to remove N-glycosylation sites. Crystallization of the complex required the use of gain-of-function mutants GpIbα-M239V and A1-R543Q that are associated with platelet-type and type 2B von Willebrand diseases and cause an enhanced affinity for complex formation (Kd = 5.8 nM).

The crystal structure of the von Willebrand factor-binding domain of GpIbα displays an elongated curved shape (figure 1) that is typical for proteins containing leucine-rich repeats (reviewed in [16]). Eight short leucine-rich repeats, seven of which were predicted based on the amino-acid sequence, make up the central region of the molecule. Flanking sequences, which are conserved among numerous extra-cellular proteins including the other members of the GpIb-IX-V complex, cap the leucine-rich repeats. The N-terminal sequence forms a 14-residue β-hairpin delimited by a conserved disulfide bond between Cys4 and Cys17. The tip of the β-hairpin, which we refer to as β-finger, protrudes from the protein surface and is disordered in one of the two molecules in the asymmetric unit. The C-terminal sequence, up to residue 267, contains a 9-residue α-helix and four short 3_{10}-helices. The anionic region beyond residue 267 was not visible in the electron-density and was not modeled. Conserved disulfide bonds between Cys209 and Cys248 and between Cys211 and Cys264 stabilize the irregular fold of the C-terminal region. Residues 227 to 241 project from the concave face of the molecule forming a highly flexible loop that shows disorder in both molecules in the asymmetric unit. Sequence alignment of C-terminal flanking regions [17] shows that the protruding loop is not a conserved feature in this domain-family.

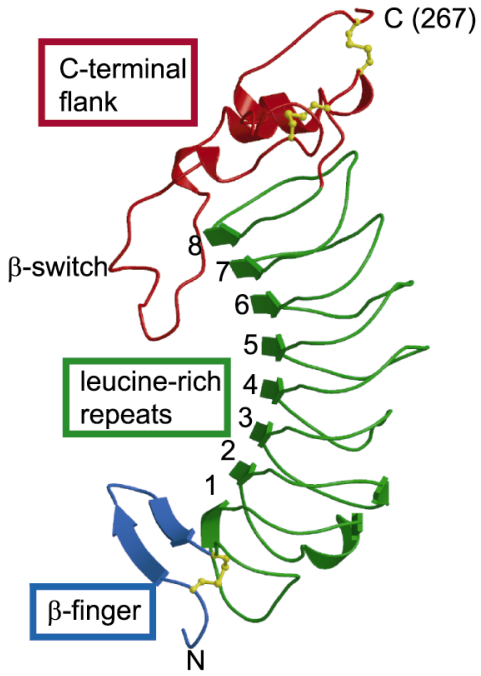

click on this link for rotating image

Figure 1: Structures of the VWF-binding domain of GpIbα and the complex of GpIbα with the A1 domain of VWF. Ribbon representation of GpIbα. The N-terminal β-hairpin, called 'β-finger', is colored blue; the eight leucine-rich repeats are green. The C-terminal flanking region is colored red and contains a disordered loop (residues 227-241), called 'β-switch'. Disulfide bridges are indicated in yellow ball-and-stick representation.

The crystal structure of the complex GpIbα – VWF-A1 shows that the globular A1 domain interacts with the concave face of GpIbα (figure 2). The interaction surface is extended, but discontinuous, comprising two distinct areas of tight interactions (figure 3A). The first and most extensive contact site is located near the top of A1 and buries a solvent accessible surface of ~1700 Å^2. In this contact site leucine-rich repeats 5 to 8 and the C-terminal flank of GpIbα interact with A1 helix α3, loop α3β4 and strand β3 (figure 3A and B). The second and smaller contact site buries a surface of ~900 Å^2 and involves interactions of the N-terminal β-hairpin and the first leucine-rich repeat of GpIbα with loops α1β2, β3α2, and α3β4 at the bottom-face of the A1 domain. As for the native structure of GpIbα, we did not observe electron density for the C-terminal anionic region of GpIbα in the complex. This is surprising since this region affects rolling of GpIbα expressing CHO cells over VWF [18], but is consistent with our observation that the anionic region has no significant effect on binding to VWF-A1.

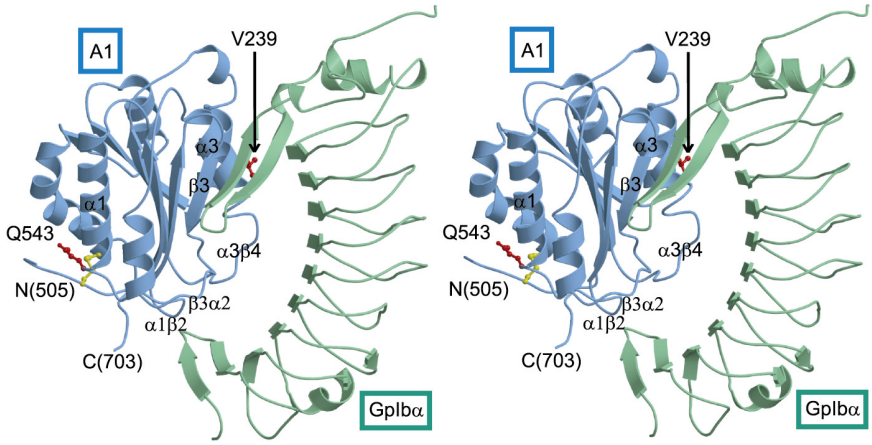

Figure 2: Stereo view of a ribbon representation of the complex GpIbα-A1. GpIbα is shown in green and A1 in blue with mutations GpIbα–M239V and A1–R543Q shown in red and the disulfide bridge in A1 shown in yellow ball-and-stick representation. The β-switch of GpIbα adopts a β-hairpin structure that aligns with the central β-sheet of A1.

click on this link for rotating image

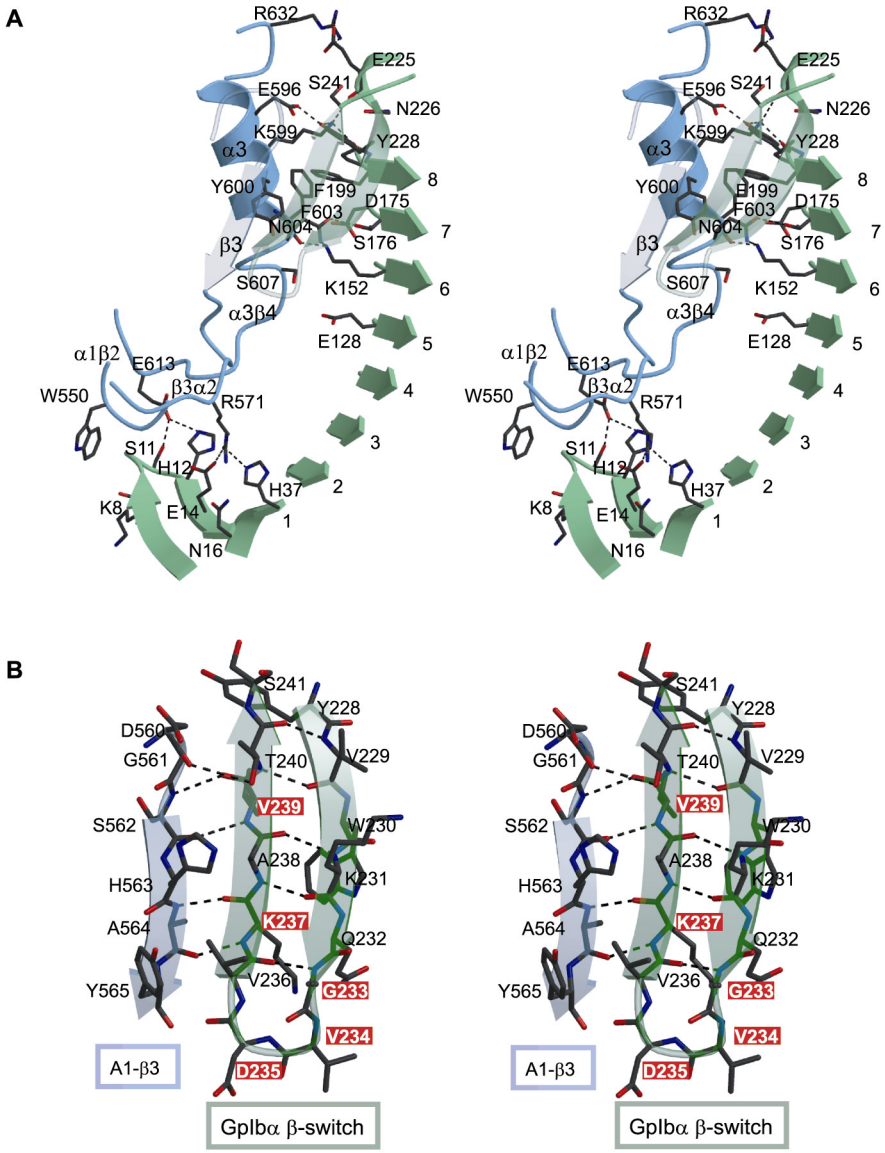

Figure 3: A: Stereo representation of residues at the A1-GpIbα interface, excluding residues located in the β-switch of GpIbα and strand β3 of A1. Residues involved in inter-molecular contacts shorter than 4.0 Å are shown in stick representation; they form two sites of tight contact separated by an area of solvated interactions. Remarkably, Lys549, Trp550 and Arg571 of A1 contacting the β-finger and the first leucine-rich-repeat of GpIbα are disordered showing reduced electron density for their side chains. B: Close-up of the β-switch and its interaction with strand β3 of A1. Main-chain hydrogen bonds are shown by dotted lines. Amino acids known to have gain-of-function mutations related to platelet-type von Willebrand disease have red labels and likely induce β-hairpin formation in the β-switch of GpIbα.

The flexible loop 227-241 in the C-terminal flank of GpIbα undergoes a conformational change upon complex formation. In the complex this loop, that we call the β-switch, forms a 16-residue β-hairpin that extends from residues 227 to 242 and aligns with strand β3 of A1 (residues 562-566) forming a continuous β-sheet shared between the two

molecules (figure 3B). Interestingly, gain-of-function mutations related to platelet-type von Willebrand disease, are all found in the β-switch. The specific mutation M239V that we used to obtain crystals of the complex, enhances binding ~3-fold and is located in the β-switch strand that directly hydrogen bonds to β3 of A1. Val239 provides two intermolecular main-chain hydrogen bonds and its side-chain contacts Tyr600 of helix α3 in A1. Based on the structure similar interactions with methionine in the wild-type protein may be expected. Other known gain-of-function mutations include G233V, that like M239V is detected in patients with platelet-type von Willebrand disease [19; 20], and V234G, D235V and K237V that have been identified by site-directed mutagenesis [14; 15]. Four of the five gain-of-function mutations involve amino-acid substitutions known to stabilize β-hairpin structures by introducing a Cβ-branched residue in the strands (G233V, M239V and K237V) or a glycine residue in the tight turn (V234G)[21]. The mutation M239V increases the association rate three-fold, and hardly affects the dissociation rate, which is consistent with stabilization of the β-hairpin priming the mutant GpIbα for A1-binding. Unclear at this stage is how D235V, at the second position in the tight turn, induces β-hairpin formation and enhances the binding affinity. However, all five mutations support an indirect mechanism by influencing the conformation, because the side chains have either no or few direct contacts to A1 in the complex. Other valine substitutions in this region (K231V, Q232V, A238V and T240V) that reduce binding affinity [15] may be explained in part by steric hindrance (Q232V and A238V) and loss of a hydrogen bond with Asp560 of A1 (T240V). Overall, we conclude that the conformational equilibrium of the β-switch of GpIbα is a critical factor in the precisely balanced affinity of the interacting partners.

Gain-of-function mutations related to type 2B von Willebrand disease cluster at the bottom face of A1 (figure 4) adjacent to the interaction site with the β-finger of GpIbα. Type 2B mutation R543Q that we used in the structure determination of the complex is located 20 Å away from the interaction site. It causes a ~2.5 fold increase in binding affinity of the isolated A1 domain. However, the affinity of the wild-type A1 domain (Kd ~30 nM) is already much higher than the affinity of multimeric VWF, for which we do not detect any binding up to a concentration of 150 nM. Similarly, other studies have indicated that the affinity depends on the length of the A1-containing VWF fragment employed (see e.g. ref. [9]). Therefore, the A1 domain used for crystallization lacks key structural elements that suppress GpIbα binding in multimeric VWF. In the crystal structure of the wild-type domain [7] the N- and C-termini of A1 approach the β-finger interaction site (figure 4), suggesting that longer

terminal peptides could shield the binding site of the β-finger in multimeric VWF. Type 2B mutations likely destabilize a network of interactions observed between the bottom face of A1 and its terminal peptides in the wild-type A1 structure [7], thereby making the binding site accessible. In the complex we indeed observe a displacement of the termini away from the interaction site and a partial disordering of the N-terminus. In comparison, the homologous integrin I-type domains bind their ligands at a different site and the large conformational changes observed upon ligand binding in I-domains [22] do not occur in A1. The mechanism of affinity modulation in the A1 domain is therefore different from that of I-type domains and likely involves conformational changes at the N- and C-termini. Shear stress may induce these changes in immobilized VWF causing activation in the platelet adhesion process.

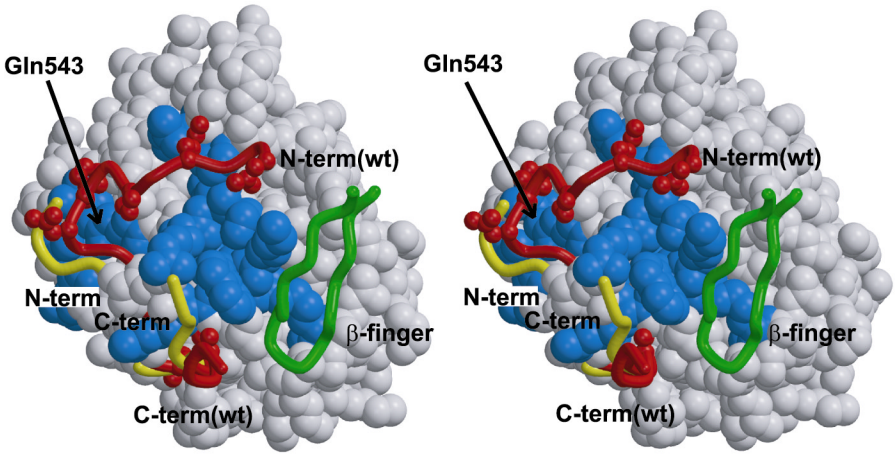

Figure 4: Structural changes at the N- and C-terminal side of VWF-A1. The bottom face of the A1 domain, as observed in the complex with GpIbα, is shown in space-filling representation with the N- and C-terminal peptides shown as Cα-traces in yellow. The position of the β-finger of GpIbα is given by a Cα-trace in green. In red we indicated the Cα-traces of the N- and C-terminal peptides of the uncomplexed, wild-type A1 domain [7]. Residues with known gain-of-function mutations, yielding a type 2B von Willebrand disease phenotype, are either shown in ball-and-stick representation in the (wild-type) N- or C-terminal peptides or colored blue in the space-filling model of the bottom face. In full-length VWF flanking peptides of A1 possibly shield the binding site of the β-finger of GpIbα.

The electrostatic surface-potentials of GpIbα and A1 are characterized by large patches of opposite charge at the GpIbα-A1 interface that induce long-range electrostatic attraction (figure 5). Besides the positively charged patch at the interface, A1 also shows a large negatively charged patch on the opposite side of the domain. Possibly, the asymmetric charge distribution on A1 helps in steering the long-range interactions. Crystal structures of P- and E-selectins bound to sialyl Lewis^X or a sulfated peptide from PSGL-1, components that mediate rolling of leukocytes over inflamed endothelium, also indicated dominant

electrostatic interactions [23]. However, in the GpIbα-A1 complex, residues making up the charge potentials at the interface are not involved in direct contacts, but are either fully or partially solvated. Thus, it appears that the surfaces of A1 and GpIbα are organized for long-range electrostatic attraction avoiding the energetically unfavorable desolvation of charged residues [24] in the formation of the final complex.

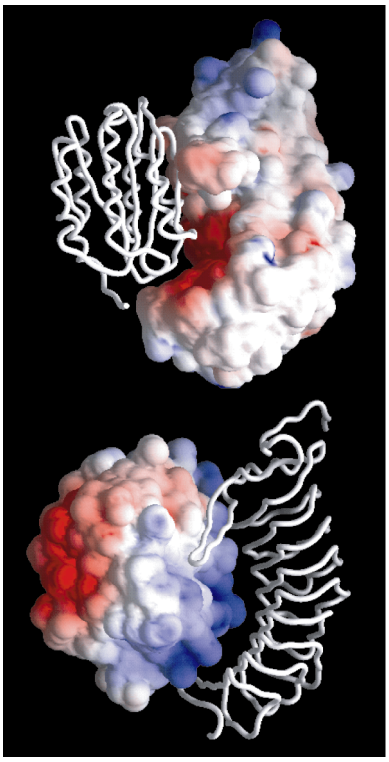

Figure 5: Electrostatic surface potentials of the A1 domain of VWF and GpIbα. Potentials were calculated for the individual molecules. The surface is colored blue for potentials of > 6kT/e and red for potentials of < -6kT/e. The Cα-traces of the partner molecules in the complex are shown in white for clarity. The areas of large electrostatic potentials at the interface of A1 and GpIbα coincide with the region of loose, solvent-mediated contacts between the two molecules. Calculations were performed with GRASP [25].

The Bernard-Soulier syndrome and type 2M von Willebrand disease are characterized by loss of function mutations in GpIbα and VWF-A1, respectively. Loss of function mutations in the VWF-binding domain of GpIbα occur at buried sites (L57F, C65R, L129P and A156V) or in a disulfide bond (C209S) and likely disturb the structural integrity of the domain causing a reduction in binding affinity. Numerous, loss-of-function mutations, detected in von Willebrand disease type 2M patients [8] or identified by site-directed mutagenesis [9-13] scatter throughout the A1 domain. Sixteen loss-of-function mutations involve residues in or directly next to the GpIbα binding site, whereas 10 occur at buried positions inside the A1 domain, and are likely to disrupt the A1 structure or induce conformational changes to A1 incompatible with binding to GpIbα. The remaining 14 mutations are scattered

over the surface outside the observed GpIbα binding site and cannot be explained based on the structure of the A1-GpIbα complex.

Our data suggest that GpIbα and VWF are attracted by long-range electrostatic interactions and indicate two contact sites in the final complex, which present primary targets for development of drugs for the treatment or prevention of arterial thrombosis. Interaction at the larger contact site depends on conformational changes in the β-switch of GpIbα, whereas the second, smaller site requires most likely dislodging of the termini of the A1 domain uncovering the site of interaction. Mutations that cause gain-of-function diseases favor the bound conformation at both contact sites. It is conceivable that under physiological conditions shear stress on immobilized VWF displaces the termini of the A1 domain exposing the second binding site and hence enhances platelet association to the site of vascular damage.

Methods

Protein expression and purification

GpIbα residues 1 to 269 and 1 to 290 preceded by the signal peptide and fused to a C-terminal $(His)_6$ or Arg-$(His)_6$ sequence, respectively, were cloned into expression vector pCDNA3.1. The QuikChange kit from Stratagene was used to introduce mutations N21Q and N159Q, removing two N-glycosylation sites, and mutation M239V, a platelet-type von Willebrand disease mutation. Proteins were expressed in stable BHK cell-lines. BHK cells were cultured in Dulbecco's MEM/ F-12 Ham medium containing 5% fetal calf serum. During protein production serum was replaced by 1% Ultroser G (Gibco). GpIbα fragments were purified from expression medium by Ni^{2+}/NTA chromatography followed by anion exchange (MonoQ) and gel filtration (Superdex 200). Typically, 1 mg of GpIbα could be purified from 1 liter of medium. The protein was concentrated to ~7 mg/ml in the gel filtration buffer (50 mM NaCl, 20 mM Tris/HCl pH 8.0). Anion exchange of wild-type and mutant GpIbα(1-290) proteins yielded four base-line separated peaks. Electro-spray mass spectroscopic analysis showed that these peaks contain GpIbα modified by sulfation at 0, 1, 2 or 3 sites, likely tyrosine residues in the anionic region (data not shown). Fully sulfated GpIbα was used for crystallization experiments.

Wild-type VWF-A1 domain residues 498 to 705 and mutant A1 R543Q were cloned in expression vector pPIC9 and over-expressed in *Pichia pastoris* strain GS115, according to the

Invitrogen manual. After 3 days of induction expression medium was collected and dialyzed against standard buffer (25 mM Tris, 100 mM NaCl, pH 7.8). The protein was purified on heparin Sepharose, followed by gel filtration (Superdex 200). It was dialyzed against standard buffer and concentrated to ~4 mg/ml.

Multimeric recombinant VWF was produced and purified according to a published procedure [26].

Crystallization

Crystals were grown using the hanging-drop vapor-diffusion technique. GpIbα (N21Q, N159Q) crystals were obtained at 28 ^{o}C by mixing 1 µl of protein solution and 1 µl reservoir solution (1.8 M ammonium sulfate, 0.2 M lithium sulfate and 100 mM CAPS pH 8.2). Before flash cooling, crystals were transferred to a cryo-protective solution (25% (w/v) PEG 3000, 200 mM NaCl, 100 mM Tris pH 8.2 and 15% (v/v) glycerol). GpIbα crystals have space group *C2* with cell constants: a = 121.5 Å, b = 54.5 Å, c = 101.8 Å, β = 103.7^{o}, and contain two molecules per asymmetric unit.

Crystals of a complex of GpIbα mutant (N21Q, N159Q, M239V) and A1 mutant (R543Q) were obtained at 4 ^{o}C by mixing 1 µl protein solution containing a 1:1 molar ratio of A1 and GpIbα and 1 µl precipitant solution (10% (w/v) PEG 3000, 200 mM NaCl and 100 mM MES pH 5.5). Before flash cooling crystals were transferred to precipitant solution containing 20 % (v/v) glycerol. Crystals have space group $P6_1$ with cell constants: a = b = 89.8 Å, and c = 124.6 Å, and contain one complex per asymmetric unit.

Structure determination

Data were collected on beam line ID14-2 at the ESRF and on beam line X11 at the EMBL outstation (DESY). Data were processed with DENZO and SCALEPACK [27]. Structures were solved in conjunction by molecular replacement. A model of A1 [7] was placed in the unit cell of the complex using CNS [28]. Solvent flattening with CNS revealed β-strands of GpIbα leucine-rich repeats. A mask was constructed around the putative GpIbα molecule and electron density inside the mask was used for molecular replacement with AMoRe [29]. This identified two molecules in the asymmetric unit of the GpIbα crystal. Improved electron density obtained after density modification and phase extension to 2.5 Å was used for model building with O [30]. The model was refined at 1.8 Å resolution using CNS and then used together with the model of A1 [7] as the starting point for refinement of the GpIbα-A1 complex.

Refinement included bulk solvent correction and calculation of Rfree using 5% of the reflections. Diffraction data and refinement statistics are given in Table I. The structures of GpIbα and the GpIbα-A1 complex have been deposited in the PDB with ID numbers 1M0Z and 1M10, respectively.

Table I.

Data collection and refinement statistics

	GpIbα(ESRF)	GpIbα-A1 (DESY)
Data collection statistics*		
Space group	*C2*	$P6_1$
Unit cell dimensions (Å, °)	a = 121.5, b = 54.5, c = 101.8, β = 103.7	a = b = 89.8, c = 124.6
Resolution (Å)	40.0-1.85 (1.9-1.85)	40.0-3.1 (3.2-3.1)
Completeness (%)	97.8 (80.8)	99.9 (99.9)
Mosaicity (°)	0.4	0.2
Redundancy	3.6 (2.4)	5.8 (5.4)
R_{merge} (%)	7.3 (33.7)	8.7 (48.0)
I/σ_I	16.3 (2.9)	19.3 (3.6)
Refinement statistics		
R_{factor} (%)	18.7	23.4
R_{free} (%)	21.7	29.6
No. of protein atoms	4115 (dimer)	3690
No. of waters	687	0
r.m.s.d. bonds (Å)	0.005	0.009
r.m.s.d. angles (°)	1.3	1.6

* Values in parentheses are for the highest resolution shell.

Biacore analysis

Binding studies were performed on a Biacore 2000 (Biacore AB, Uppsala Sweden). GpIbα monoclonal antibody 2D4 was immobilized on CM5-sensorchips by amine-coupling as instructed by the supplier. A control channel was activated and blocked by using the amine-coupling reagents in the absence of protein. Proteins were dialysed to standard Biacore buffer (150 mM NaCl, 0.005% (v/v) Tween-20 and 25 mM HEPES pH 7.4) and analyzed at 25 °C.

GpIbα (150 nM) was injected for 1 minute, followed by a 2 minute association phase of A1 (5-100 nM) or multimeric recombinant VWF (150 nM). Finally, standard buffer was injected and the dissociation phase was recorded for 5 minutes. The sensor-chip was regenerated by injections of 50 mM triethylamine, 10 mM sodium formate pH 2.0 containing 150 mM NaCl and another injection of 50mM triethylamine. Each interaction was analyzed at five different VWF-A1 concentrations. Data evaluation was performed with Bia evaluation software (Biacore AB) using a 1:1 Langmuir model with baseline drift to compensate for the slow release of GpIbα from 2D4. Control experiments included immobilization of GpIbα *via* His-tag antibody 3D5 (Novagen), which excluded artifacts caused by antibody 2D4, and a comparison of glycosylated and non-glycosylated mutant GpIbα to confirm that glycosylation has no effect on binding.

Acknowledgements

We thank D. Westra and M. Bulsink for contributions to the early stages of the project; P. Lenting and E. Westein for technical assistance with Biacore measurements; H. Deckmyn (Kortrijk, Belgium) for generously supplying monoclonal 2D4; and beam line scientists at the ESRF in Grenoble and the EMBL outstation in Hamburg for assistance during data collection. We acknowledge financial support of the “European Community - Access to Research Infrastructure Action of the Improving Human Potential Programme" to the EMBL Hamburg Outstation, the Dutch Heart Foundation and the council of Medical Sciences of the Netherlands Organization for Scientific Research.

Reference List

1. Savage B, Saldívar E, Ruggeri ZM. Initiation of platelet adhesion by arrest onto fibrinogen or translocation on von Willebrand factor. Cell. 1996;84:289-297.

2. Goto S, Salomon DR, Ikeda Y, Ruggeri ZM. Characterization of the unique mechanism mediating the shear- dependent binding of soluble von Willebrand factor to platelets. J Biol Chem. 1995;270:23352-23361.

3. Goto S. Role of von Willebrand factor for the onset of arterial thrombosis. Clin Lab. 2001;47:327-334.

4. Berndt MC, Shen Y, Dopheide SM, Gardiner EE, Andrews RK. The vascular biology of the glycoprotein Ib-IX-V complex. Thromb Haemost. 2001;86:178-188.

5. Sadler JE. Biochemistry and genetics of von Willebrand factor. Annu Rev Biochem. 1998;67:395-424.

6. Celikel R, Varughese KI, Madhusudan, Yoshioka A, Ware J, Ruggeri ZM. Crystal structure of the von Willebrand factor A1 domain in complex with the function blocking NMC-4 Fab. Nature Struct Biol. 1998;5:189-194.

7. Emsley J, Cruz M, Handin R, Liddington RC. Crystal structure of the von Willebrand factor A1 domain and implications for the binding of platelet glycoprotein Ib. J Biol Chem. 1998;273:10396-10401.

8. Ginsburg D, Sadler JE. von Willebrand disease: a database of point mutations, insertions, and deletions. For the Consortium on von Willebrand Factor Mutations and Polymorphisms, and the Subcommittee on von Willebrand Factor of the Scientific and Standardization Committee of the International Society on Thrombosis and Haemostasis. Thromb Haemost. 1993;69:177-184.

9. Matsushita T, Sadler JE. Identification of amino acid residues essential for von Willebrand factor binding to platelet glycoprotein Ib. Charged-to- alanine scanning mutagenesis of the A1 domain of human von Willebrand factor. J Biol Chem. 1995;270:13406-13414.

10. Cruz MA, Daicovo TG, Emsley J, Liddington RC, Handin RI. Mapping the GpIb binding site in the von Willebrand Factor A1 domain. J Biol Chem. 2000;275:19098-19105.

11. Matsushita T, Meyer D, Sadler JE. Localization of von willebrand factor-binding sites for platelet glycoprotein Ib and botrocetin by charged-to-alanine scanning mutagenesis. J Biol Chem. 2000;275:11044-11049.

12. Vasudevan S, Roberts JR, McClintock RA, et al. Modeling and functional analysis of the interaction between von Willebrand factor A1 domain and glycoprotein Ibα. J Biol Chem. 2000;275:12763-12768.

13. Celikel R, Ruggeri ZM, Varughese KI. Von Willebrand Factor conformation and adhesive function is modulated by an internalized water molecule. Nature Struct Biol. 2000;7:881-884.

14. Tait AS, Cranmer SL, Jackson SP, Dawes IW, Chong BH. Phenotype changes resulting in high-affinity binding of von Willebrand factor to recombinant glycoprotein Ib-IX: analysis of the platelet-type von Willebrand disease mutations. Blood. 2001;98:1812-1818.

15. Dong J, Schade AJ, Romo GM, et al. Novel gain-of-function mutations of platelet glycoprotein IBalpha by valine mutagenesis in the Cys209-Cys248 disulfide loop. Functional analysis under statis and dynamic conditions. J Biol Chem. 2000;275:27663-27670.

16. Kobe B, Kajava AV. The leucine-rich repeat as a protein recognition motif. Curr Opin Struct Biol. 2001;11:725-732.

17. Bateman A, Birney E, Cerruti L, et al. The Pfam protein families database. Nucleic Acids Res. 2002;30:276-280.

18. Dong JJ, Ye P, Schade AJ, et al. Tyrosine sulfation of glycoprotein (GP) Ibalpha: Role of electrostatic interactions in von willebrand factor binding. J Biol Chem. 2001;276:16690-16694.

19. Miller JL, Cunningham D, Lyle VA, Finch CN. Mutation in the gene encoding the alpha chain of platelet glycoprotein Ib in platelet-type von Willebrand disease. Proc Natl Acad Sci U S A. 1991;88:4761-4765.

20. Russell SD, Roth GJ. Pseudo-von Willebrand disease: a mutation in the platelet glycoprotein Ib alpha gene associated with a hyperactive surface receptor. Blood. 1993;81:1787-1791.

21. Blanco F, Ramirez-Alvarado M, Serrano L. Formation and stability of beta-hairpin structures in polypeptides. Curr Opin Struct Biol. 1998;8:107-111.

22. Emsley J, Knight CG, Farndale RW, Barnes MJ, Liddington RC. Structural basis of collagen recognition by integrin α2β1. Cell. 2000;100:47-56.

23. Somers WS, Tang J, Shaw GD, Camphausen RT. Insights into the molecular basis of leukocyte tethering and rolling revealed by structures of P- and E-selectin bound to SLe(X) and PSGL-1. Cell. 2000;103:467-479.

24. Sheinerman FB, Norel R, Honig B. Electrostatic aspects of protein-protein interactions. Curr Opin Struct Biol. 2000;10:153-159.

25. Nicholls A, Sharp KA, Honig B. GRASP: Graphical representation and analysis of surface properties. Biophys J. 1993;64:166-170.

26. Lankhof H, van Hoeij M, Schiphorst ME, et al. A3 domain is essential for interaction of von Willebrand factor with collagen type III. Thromb Haemost. 1996;75:950-958.

27. Otwinowski Z, Minor W. Processing of X-ray diffraction data collected in oscillation mode. Methods Enzymol. 1996;276:307-326.

28. Brünger AT, Adams PD, Clore GM, et al. Crystallography and NMR system: A new software suite for macromolecular structure determination. Acta Crystallogr D. 1998;54:905-921.

29. Navaza J. AMoRe: an automated package for molecular replacement. Acta Cryst. 1994;A50:157-163.

30. Jones TA, Zou JY, Cowan SJ, Kjeldgaard M. Improved methods for building protein models in electron-density maps and the location of errors in these models. Acta Cryst. 1991;A47:110-119.

Chapter 6

Structural basis of von Willebrand Factor Activation for Gplbα binding

Roland A.P. Romijn[§], Shizuko Tsuji[§], Piet Gros[¶], Jan J. Sixma[§] and Eric G. Huizinga[§¶]

[§] Thrombosis and Haemostasis Laboratory, Department of Haematology, University Medical Center and Institute of Biomembranes, HP G03.647, PO box 85500, 3508 GA Utrecht, The Netherlands and

[¶] Bijvoet Center for Biomolecular Research, Department of Crystal and Structural Chemistry, Utrecht University, Padualaan 8, 3584 CH Utrecht, The Netherlands.

Summary

Thrombus formation is initiated by platelet arrest at sites of vascular injury. This process is dependent on von Willebrand Factor (vWF) and requires the interaction of its A1 domain with glycoprotein (Gp) Ibα on the platelet. VWF must be activated before GpIbα binding occurs, either via surface adsorption, vWD type 2B mutations or exogenous agonists.

We have investigated the binding kinetics of wild type- and vWD mutant Arg543Gln-vWF and of wild type- and Arg543Gln-A1 to GpIbα. In contrast to wt-vWF, wt-A1 bound spontaneous to GpIbα indicating that the isolated A1 domain is already activated. The effect of mutation Arg543Gln in the isolated A1 domain is small compared to the effect in vWF.

We have solved three crystal structures of wt-A1 and three crystal structures of Arg543Gln-A1 and compared their conformation with the A1•GpIbα complex, Ile546Val-A1 and published wt-A1 structures. In wt-A1, the N- and C-terminal flanking peptides approach the GpIbα binding site at the bottom of A1. Probably in vWF the peptides overlap the GpIbα binding site. In type 2B-A1 the peptides adopt a different conformation and do not overlap the GpIbα binding site. Probably this conformation resembles vWF under conditions of shear after binding to the vascular matrix.

In conclusion, these crystallographic data confirm the activation mechanism of A1 involving conformational changes in the N- and C-terminal flanking peptides. These conformational changes switch the A1 domain from a low- to a high affinity state by opening the GpIbα binding site at the bottom face of the domain.

Introduction

Von Willebrand factor (vWF) is a multimeric plasma glycoprotein that is essential for platelet adhesion at sites of vascular injury. The primary function of vWF is to form a molecular bridge between collagen from the subendothelial connective matrix of a damaged vessel wall and the platelet receptor glycporitein (Gp) Ib-IX-V complex.

Mature vWF[a] consists of 2050 amino-acid residues in five different domain subtypes in the order D´-D3-A1-A2-A3-D4-B1-B2-B3-C1-C2-CK. After synthesis, vWF dimerisation occurs at the cystine knot (CK) domain and multimerisation at the D3 domain [1]. A vWF multimer can contain up to 80 monomers [2]. Multimerisation of vWF is essential for a normal function, because low vWF multimers have a decreased affinity for their ligands [3]. The A1 domain, spanning residues Cys^{509} - Cys^{695}, contains the GpIbα binding site [4; 5].

In normal haemostasis the vWF-A1 domain does not bind spontaneously to GpIbα. *In vivo*, immobilisation of vWF to the subendothelial connective tissue induces GpIbα binding, especially under conditions of high shear [6]. *In vitro*, binding to GpIbα can be induced by modulators like the toxin botrocetin [7] from *Bothrops jararaca* or the antibiotic ristocetin [8] from *Nocardia lurida*. Botrocetin and ristocetin bind to different regions in A1 [9]. Ristocetin interacts with the C-terminal flanking peptide of A1 [10;11] and mimics shear-induced GpIbα binding [12]. However, the activation mechanism of vWF at a molecular level is a poorly understood process.

Recently we have solved the crystal structure of the A1 domain in complex with the 290 amino-terminal residues of GpIbα that contains the A1-binding site [13]. A1 and GpIbα have an extended, but discontinuous, interaction site. There are two areas of tight interactions. The first interaction site is located near the top of A1 and involves residues in helix α3, loop α3β4 and strand β3. The second interaction site comprises several loops at the bottom-face of A1. We hypothesized that in inactive vWF the second interaction site is blocked by the N- and C-terminal flanking peptides and that GpIbα binding may be induced by a conformational change in these peptides

In patients, so-called von Willebrand disease (vWD) type 2B mutations at the bottom of the A1 domain, or in its flanking peptides, also induce spontaneous GpIbα binding and cause platelet clumping, thrombocytopenia, low plasma vWF levels and a bleeding tendency. A mechanism by which vWD type 2B mutations activate the A1 domain has been proposed

by Celikel *et al.* [14]. In this model, mutation Ile546Val at the bottom of A1 induces a conformational change in hairpin β2β3 that is part of the GpIbα-binding site, but is located close to the top of A1. Although in the A1•GpIbα complex minor conformational changes are observed for loop β2β3, larger conformational changes occur in the N- and C-terminal flanking peptides [13].

In this study we have solved crystal structures of three different crystal forms of either wt-A1 and gain-of-function mutant Arg543Gln-A1, yielding eleven new models. Together with the previously published wt- and type 2B mutant A1 structures this set of structures was used for the analysis of conformational changes in A1 required for activation. Observed conformational changes in the N- and C-terminal flanking peptides explain the activation mechanism of vWF resulting in GpIbα binding.

Methods

Construction of *Pichia pastoris* expressing A1

VWF residues 498 – 705 (VWF residue numbering used starts at the first residue of the mature subunit, addition of 763 converts the numbering to that of preproVWF) containing the A1 domain, were cloned into expression vector pPIC9 (Invitrogen, Breda, The Netherlands). The wt- and Arg543Gln-A1 domains were amplified by PCR from plasmids pNUT-vWFcas and pNUT-vWF-Arg543Gln [15; 16], respectively using primers GGACTCGAGAAAGAGAG-GCTGAAGCT**GACATCTCGGAACCGCCGTTGC** and GCGGCCGCTTA**AGTAGGA-GGAGGGGCTTCAGGGG** (sequences in bold are from vWF, other sequences are from pPIC9) and PWO polymerase (Roche, Almere, The Netherlands). The PCR product was extended by an additional adenine nucleotide using Taq polymerase (Enzyme Technologies, United Kingdom), ligated into pCR2.1-TOPO vector (Invitrogen, Breda, The Netherlands) generating TOPO-A1 and sequenced (Hubrecht laboratories, Utrecht, The Netherlands). TOPO-A1 was digested with restriction enzymes XhoI and NotI and the fragment containing A1 was ligated with XhoI – NotI digested plasmid pPIC9 using Rapid ligase (Roche, Almere, The Netherlands) generating expression vectors pPIC9-vwf498/705 and pPIC9-vwf498/705-Arg543Gln.

[a] Throughout the text: vWF represents multimeric vWF and A1 represents the isolated A1 domain.

The expression vectors were linearised by digestion with BglII or SacI and transformed to *Pichia pastoris* strain GS115. Twenty colonies were picked and grown in 4 ml BMGY medium, containing 1 % yeast extract, 2 % peptone, 100 mM potassium phosphate pH 6.0, 1.34 % yeast nitrogen base, $4*10^{-5}$ % biotin and 1 % glycerol, for 72 hours. Cells were harvested by centrifugation and grown in 4 ml BMMY medium, containing 1 % yeast extract, 2 % peptone, 100 mM potassium phosphate pH 6.0, 1.34 % yeast nitrogen base, $4*10^{-5}$ % biotin and 0.5 % methanol, for an additional 72 hour. Expression medium was collected by centrifugation and A1 expression levels were analysed by ELISA. To this end, expression medium was diluted 10, 100 or 1000 fold in 50 mM carbonate buffer pH 9.6 and coated in microtiter plate wells at 37 ^{o}C for 3 hours. Wells were washed with PBS/0.1% Tween-20, blocked with 1 % protifar (Nutricia, Zoetermeer, The Netherlands) in PBS/0.1% Tween-20 (1/2 h, 37 ^{o}C), washed with running tap-water and incubated with HRP conjugated polyclonal α-vWF (DAKO, Glostrup, Denmark) diluted 1:2500 in PBS/0.1% Tween-20 containing 1 % protifar (1 h, 37 ^{o}C). O-phenylenediamine was used as substrate for detection. Three clones displaying the highest expression were stored in 20 % glycerol stocks at –80 ^{o}C.

Expression and purification of vWF-A1

For large-scale expression of A1, a single colony was inoculated in 6 * 300 ml BMGY medium and grown for 90 h at 30 ^{o}C. Cells were collected by centrifugation, suspended in 6 * 300 ml BMMY medium and grown for 72 h at 30 ^{o}C. Expression medium was collected by centrifugation, filtered (0.22 μm) and dialysed against 20 volumes of a buffer containing 25 mM Tris, 100 mM NaCl, pH 7.8 (o/n, 4 ^{o}C). After filtration A1 was loaded on a 12 ml heparin sepharose column (Amersham Pharmacia Biotech, Roosendaal, The Netherlands). The column was extensively washed with 25 mM Tris, 200 mM NaCl, pH 7.8. and A1 was eluted with 25 mM Tris, 1 M NaCl, pH 7.8. A1 containing fractions were pooled and purified over a HiLoad 16/60 Superdex 200 prep grade column (Amersham Pharmacia Biotech, Roosendaal, The Netherlands) in 25 mM Tris, 250 mM NaCl, pH 7.8. Fractions were analysed by SDS-PAGE, pooled, dialysed against 25 mM Tris, 100 mM NaCl, pH 7.8 (o/n, 4 ^{o}C), concentrated to 4-4.5 mg/ml and stored at –20 ^{o}C. Typically, 6 mg of purified A1 was obtained from 1 l expression medium. The purified and concentrated A1 domain migrated on a non-reducing SDS-PAGE gel as a single band with minor contaminating bands.

Expression, purification and characterisation of wt- and Arg543Gln-vWF

VWF was stably expressed in baby hamster kidney cells overexpressing furin required for proper removal of vWF propeptide [17; 18]. Cells were cultured in serum-free medium. VWF was purified by immuno-affinity chromatography [17] and stored in 50 mM Hepes, 100 mM NaCl pH 7.4 at –20 °C until use. The vWF concentration and multimeric structure were determined by sandwich ELISA [17] and agarose gel electrophoresis [19], respectively.

Expression, purification and characterisation of GpIbα

GpIbα was stably expressed in baby hamster kidney cells that were cultured in serum free medium. GpIbα was purified as described before [13] and migrated as a single 25 kDa band on a non-reducing SDS-PAGE gel.

Surface Plasmon Resonance Analysis

Binding studies were performed using surface plasmon resonance (SPR) in a Biacore 2000 biosensor (Biacore AB, Uppsala Sweden). Monoclonal antibody 2D4 directed against GpIbα was immobilized on a CM5-sensorchip using the amine-coupling kit as instructed by supplier, yielding 3300 reference units (RU) that corresponds with 22 fmol/mm^2 immobilised 2D4. A control channel was activated and blocked using the amine-coupling reagents in the absence of protein. Proteins were dialyzed against standard buffer (150 mM NaCl, 0.005% (v/v) Tween-20, 25 mM Hepes, pH 7.4) and analysed at 25 ^{o}C. For each determination, 350 nM GpIbα was injected at a flow rate of 5 µl/min for 4 minutes (yielding 500 RU, 15 fmol/mm^2), followed by a 2 minute association phase by injection of vWF- or A1 variants (5 – 150nM) at 20 µl/min and a 5 minute dissociation phase. The sensor-chip was regenerated by injections of 50 mM triethylamine, 10 mM sodium formate pH 2.0 containing 150 mM NaCl and another injection of 50 mM triethylamine. The binding of vWF- and A1-variants to GpIbα was evaluated at five concentrations, each determined in triplicate, and analysed with Bia-evaluation software (Biacore AB, Uppsala Sweden) using a 1:1 Langmuir model with baseline drift to compensate for the slow dissociation of GpIbα from 2D4. Binding to GpIbα coated channels was corrected for binding to non-coated channels.

Crystallisation and data collection

A1 crystals were obtained using the hanging-drop vapour-diffusion method at 4 ^{o}C. Small differences in the composition of the precipitant solution resulted in different crystal forms (Table I). Micro-seeding was used to increase crystal-size. The dimensions of the crystals used for data collection ranged from 50 to 200 μm. Crystals were equilibrated in precipitant solution containing 30 – 35 % glycerol and flash-cooled in liquid nitrogen. X-ray diffraction data were collected at the ESRF synchrotron-radiation facility, beam lines ID14-EH2, ID14-EH3 and ID9 (Grenoble, France). Data reduction, merging and scaling were performed with DENZO and SCALEPACK [20]. Diffraction data statistics are summarised in table I.

Structure Determination and Refinement

Structures were solved by molecular replacement using CNS [21] with wt-A1 [22] as a search model. For model refinement, cycles of rebuilding using O [23] and positional and B-factor refinement using CNS were performed until convergence. In some cases non-crystallographic symmetry restraints were applied, but only in the initial stages of refinement. Cross validation was used throughout refinement using a 5% test set of reflections. Refinement used the maximum-likelihood algorithm [24] and bulk-solvent correction was applied. Water molecules were placed in difference electron-density peaks with a peak height of at least 3.0 σ, a distance of 2.7-3.2 Å to a hydrogen-bond donor or acceptor. Water molecules with a B-factor above 100 Å^2 were rejected. Refinement statistics are summarised in table I.

Strong positive electron density peaks observed in A1 structures wt-$P4_12_12$, wt-$P2_1$, RQ-$P4_12_12$ and RQ-$P4_32_12$ were interpreted as cadmium and chloride ions based on peak height and chemical environment (Table I). The cadmium ions mediate important crystal contacts, since crystals that were transferred to EDTA-containing precipitant solution dissolved.

Table I

Diffraction-data and refinement statistics

Crystal and Diffraction data	wild-type A1[c,e]			Arg543Gln-A1[d,f]		
Space group	$P4_12_12$	$P2_1$	$P2_12_12_1$	$P4_32_12$	$P4_12_12$	$P2_12_12_1$
Crystallisation condition	0.1 M Tris pH 8.5, 0.2 M NaCl, 12-16 % PEG8k	0.1 M Tris pH 8.5, 0.1 M NaCl, 9 % PEG8k	0.1 M Tris pH 8.5, 0.2 M Li_2SO_4, 35 % PEG3k, 1.3 mM EDTA	0.1 M Tris pH 7.5, 0.4 M NaCl, 9% PEG8k, 5 mM $CdCl_2$	0.1 M Tris pH 8.5?, 18 % PEG 8k,	0.1 M Tris pH 8.5, 0.2 M Li_2SO_4, 30% PEG 3k, 1.3 mM EDTA
a, *b*, *c* (Å)	75.9,75.9, 93.5	76.8, 60.6, 87.6	50.5, 61.3, 67.6	80.5,80.5,125.3	81.6,81.6,124.2	50.3, 61.6, 67.0
α, β, γ (°)	90, 90, 90	90, 95.1, 90	90, 90, 90	90, 90, 90	90, 90, 90	90, 90, 90
Redundancy	7.1	3.5	7.0	14.1	6.6	6.7
No. of unique reflections	20539	37963	14579	21965	12773	14492
$\langle I \rangle / \langle \sigma(I) \rangle$ [a]	36.1 (5.8)	15.8 (2.2)	17.2 (2.9)	28.7 (7.8)	18 (3.3)	18 (3.6)
Completeness (%)[a]	100 (100)	98 (84)	84 (38)	100 (100)	99.7 (98.7)	99.3 (93.8)
R_{merge} (%)[a,b]	3.6 (37.7)	4.6 (28.4)	8.8 (24.8)	6.9 (30.0)	7.5 (45.4)	7.3 (28.0)
Refinement						
Resolution (Å)	1.95 (2.00-1.95)	2.25 (2.33-2.25)	1.90 (1.94-1.90)	2.2 (2.25-2.20)	2.6 (2.69-2.60)	2.0 (2.07-2.00)
R-factor (%)	18.8	20.1	18.2	21.2	21.9	18.3
R_{free} (%)	22.2	27.5	23.8	26.3	30.5	23.7
r.m.s.d. bond distances (Å)	0.008	0.006		0.005		
r.m.s.d. angles (°)	1.4	1.2		1.2		
Average overall B-factor ($Å^2$)	23.7	38.9	19.1	26.5	52.7	39.8
No. of observed residues[g]	501-704	501-703 (B,D) 499-704 (C,E)	503-703	501-703 (a) 505-705 (b)	506-704 (c) 500-705 (d)	503-701
No. of protein molecules	1	4	1	2	2	1
No. of Cd^{2+} ions	1	4		7	2	
No. of Cl^- ions	1	2		6	1	
No. of SO_4^{2-} ions			2			1
No. of glycerol molecules			1			2
No. of solvent molecules	197	513	220	241	59	181

[a] Numbers in parentheses indicate statistics for highest resolution shells.

[b] $R_{merge} = \sum_i (I_i - \langle I_h \rangle)^2 / \sum_i (I_i)^2$

[c] wt-A1 models are denoted as follows: $P4_12_12$ model is denoted A; $P2_1$ models are denoted B, C, D, E; $P2_12_12_1$ model is denoted F; PDB entry 1oak is denoted G; PDB entry 1auq is denoted H. Additionally, models are denoted wt-$P4_12_12$, wt-$P2_1$, wt-$P2_12_12_1$, wt-1oak and wt-1auq, respectively.

[d] Mutant A1 models are denoted as follows: $P4_32_12$ models are denoted a, b; $P4_12_12$ models are denoted c, d; $P2_12_12_1$ model is denoted e; PDB entry 1FNS (mutant Ile546Val) is denoted f; Arg543Gln-A1 in complex with GpIbα is denoted g. Additionally, models are denoted RQ-$P4_32_12$, RQ-$P4_12_12$, RQ-$P2_12_12_1$, IV-1fns and Arg543Gln-A1•GpIbα, respectively.

[e] Structures have been deposited at PDB accession numbers xxx, yyy, zzz, respectively.

[f] Structures have been deposited at PDB accession numbers aaa, bbb, ccc, respectively.

[g] When more than one model is observed in the asymmetric unit, the models are indicated by characters between parenthesis.

Results and Discussion

Local structural effects of mutation Arg543Gln in A1

The process of A1 activation that results in binding to GpIbα is a poorly understood process. Activation of A1 can be induced by vWD type 2B mutations. In this study we investigated structures of wild type and 2B mutant Arg543Gln-A1 and analysed conformational changes. Both wt- and Arg543Gln-A1 crystallised in three different crystal forms, depending on small differences in crystallisation conditions. X-ray diffraction data were collected to a resolution limit ranging from 1.9 to 2.6 Å and the structures were determined by molecular replacement. Crystallographic and refinement statistics are summarised in table I. As it turned out several crystal forms contain multiple A1 domains in the asymmetric unit yielding a total of 6 atomic models of wt-A1 and five atomic models of Arg543Gln-A1.

The overall structure of all eleven A1 domains determined by us are similar to published structures of A1 [13; 14; 22; 25] and consists of a central six-stranded β-sheet flanked on each side by three α-helices. The N- and C-terminal regions of the domain are connected by a disulphide bond between Cys^{509} and Cys^{695}. We will refer to the Cys^{509}-Cys^{695} loop structure as the body of the domain while the residues on either side of the disulphide-bonded loop will be called the N- and C-terminal flanking peptides.

VWD type 2B mutation Arg543Gln strongly activates vWF [16]. Residue Arg^{543} is located at the end of α-helix 1 close to the bottom face of the domain (figure 1A). Replacement of Arg^{543} by glutamine does not change its backbone conformation. In the mutant the glutamine side chain points in a different direction and interacts with residues Arg^{687} and Asp^{688}. As a consequence, the conformation of these residues and nearby residues Asp^{539} and Met^{540} changes slightly, the largest shift being 1.9 Å for the side-chain of Met^{540}. In five of the six wild-type structures the head-group of Arg^{543} packs against one face of the five-membered ring of the His^{505} side-chain providing favourable van der Waals interactions. This interaction with His^{505} is not possible in the mutant. In four of the five mutant structures His^{505} undergoes a large shift. This shifted conformation is also observed in one wild-type structure. In one mutant structure His^{505} shifts only slightly, but a hydrogen bond to Glu^{542} that is observed in the wild-type structures, is lost. Thus, mutation Arg543Gln destabilises two types of interactions of His^{505} namely van der Waals interactions with the arginine side chain and, indirectly, hydrogen bonding to Glu^{542}.

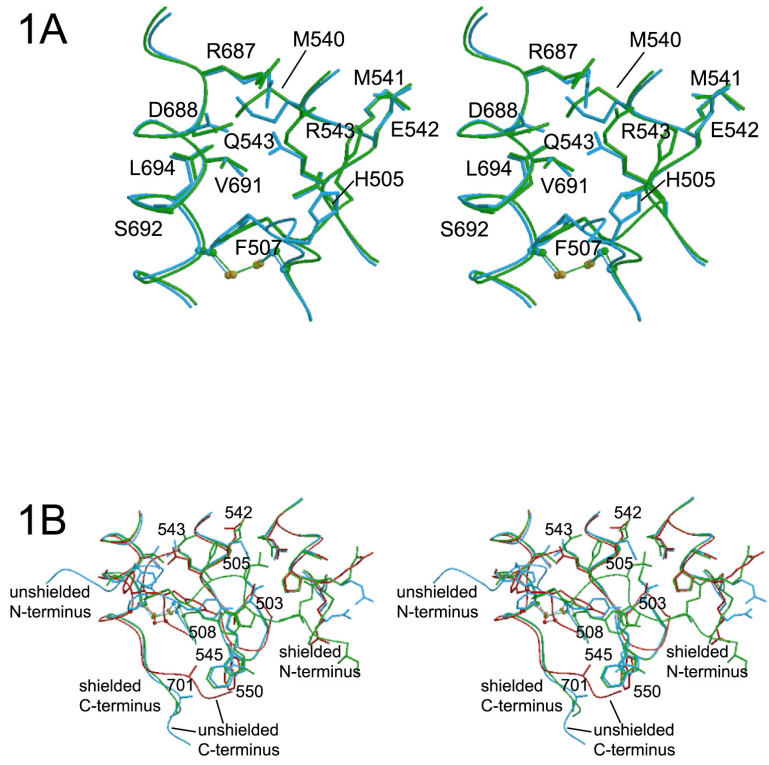

Figure 1: Conformations of the N- and C-terminal flanking peptides. Superposition of different A1 models that are colour coded as follows: wild-type A1, *green*; Arg543Gln-A1, *blue*; A1•GpIbα, *red*. A) Stereographic representation of the A1 domain local to Arg^{543}. In wt-A1 Arg^{543} forms tight van der Waals interactions with His^{505} that is directed in an ideal orientation for hydrogen-bond formation with Glu^{542}. In 2B-A1 the side chain of Gln^{543} is shorter and the polar head-group is now oriented to the interior of the domain. This has no effect on the conformation of the local main-chains, but induces small shifts in the side chains of Met^{540}, Arg^{687} and Asp^{688}. Moreover, the orientation of the Gln^{543} side chain abolishes the positioning of His^{505} to Glu^{542}. B) Stereographic representation of a part of the lower half of the A1 domain showing long-range effects of mutation Arg543Gln. In six of the seven wt-A1 models the N-terminal flanking peptide adopts the shielded conformation and forms many interactions with the body of the domain (see table III). In three out of four Arg543Gln models and in A1•GpIbα the N-terminal flanking peptide adopts the unshielded conformation. The C-terminal flanking peptide adopts the shielded conformation only in three wt-A1 models. Several residues in the body of A1 that interact with the N- and C-terminal flanking peptides are subjected to type 2B mutations. The shielded conformation of the N- and C-terminal flanking peptides suggest that they block the GpIbα binding site in multimeric vWF.
In the shielded conformation of the N-terminal flanking peptide, Pro^{503} stabilises the conformation of Tyr^{508} that directly interacts with loop α1β2. Therefore loop α1β2 may be less stabile in the unshielded conformation (as observed by the significant movement of Tyr^{508}), but it does not adopt a different conformation. This suggests that GpIbα may induce a conformational change in the loop. The diagrams were generated with MOLSCRIPT [34] and RASTED3D [35]

Structural comparison of A1 structures

To analyse the occurrence of long range conformational changes in A1 induced by vWD type 2B mutations we compared all wild-type and mutant crystal structures currently available. In addition to the five wild-type and six mutant structures determined in this study, the comparison included a model of Arg543Gln-A1 from the A1•GpIbα complex [13], the structure of wild-type A1 published by Emsley *et al.* [22] and structures of wild-type A1 and A1 mutant Ile546Val published by Celikel *et al.* [14; 25]. The latter two structures of A1 were crystallised in complex with a Fab-fragment of function inhibiting antibody NMC-4 and lack the N-terminal flanking peptide up to residue 508.

Pair wise superposition of all free A1 models (Table II, first three columns) shows no conformational changes in the α-helices and β-strands, indicating that conformational changes as observed in the α_2 I-domain after collagen binding [26] do not occur in A1 containing a type 2B mutation. Within the body of A1 considerable variation is observed for several loops. However, differences among wild-type models and among mutant models are similar in magnitude as differences between wild-type and mutant models. This suggests that the variation in these loops is due to inherent flexibility and is not a consequence of the mutation. Also comparison of A1•GpIbα with free wt- or mutant A1 structures shows significant differences for the body of the domain, *i.e.* the disulphide bond, loop α1β2 and hairpin β2β3 (Table II, last two columns). The latter two regions interact directly with GpIbα. However, the differences between wt-A1 and A1•GpIbα are not larger than differences between type 2B A1 and A1•GpIbα. This suggests that these differences are introduced by GpIbα binding and not by the mutation.

Table II

Structural variation among mobile loops in wt-A1, vWD-2B A1, and A1•GpIbα (R.m.s.d.[a] values in Å)

Structural element	Residues	wt-A1	2B-A1	wt- *v.s.* 2B-A1	wt-A1 *v.s.* 2B-A1-GpIbα	2B-A1 *v.s.* 2B-A1-GpIbα
Body	509-695	0.38	0.37	0.38	0.56	0.52
N-terminal flanking peptide		2.61	3.28	4.60	4.79	4.23
	509-511	0.33	0.42	0.43	1.77	1.58
α1β2	544-550	0.30	0.38	0.33	1.18	1.21
β2β3	559-563	0.63	0.56	0.61	0.94	0.87
α2α3	584-592	0.61	0.36	0.58	0.66	0.43
α3β4	610-613	0.57	0.47	0.53	0.76	0.77
α5β6	668-671	0.72	0.83	0.75	0.49	0.58
	693-695	0.34	0.28	0.35	1.13	1.05
C-terminal flanking peptide		2.34	1.20	1.93	5.48	3.88

[a] Root mean square deviation in positions (r.m.s.d.) values were calculated using the program LSQMAN [33]. Values (*black)* for the mobile loops are given when the r.m.s.d. for the loop was 1.5 fold increased compared to the overall r.m.s.d.. Not significant values are given in *grey*.

The most prominent structural variation is observed in the flanking peptides. For the N-terminal flanking peptide the root-mean-square deviation in the position of the individual peptides (r.m.s.d.) between wild-type models is significantly smaller than the difference between wt- and 2B A1. Thus for the N-terminal flanking peptide the variation is correlated with the presence of a type 2B mutation. The variation seems not to be correlated for the C-terminal flanking peptide. The differences in the N- and C-terminal flanking peptides in the A1•GpIbα complex is larger than differences among free wt- and free 2B A1 models. This suggests that GpIbα binding to A1 induces additional conformational changes in the N- and C-terminal flanking peptides.

The conformation of the flanking peptides

Conformations of the N-terminal flanking peptides can be divided in two groups based on the observed main-chain conformation at Asp^{506}. In the first group the peptide makes a 90^{o} turn at Asp^{506} and folds over the body of the domain (figure 1B). In this conformation Asp^{498} approaches the GpIbα-binding site at the bottom of A1 within 7 Å. Although this residue itself does not overlap the GpIbα-binding site, one or two additional residues may be sufficient to do so. This conformation will be referred to as the shielded conformation. The shielded conformation dominates in the wild-type structures. It is observed in six out of seven models of wt-A1 and in only one model of Arg543Gln-A1. In the alternative 'open' conformation the N-terminal flanking peptide makes a turn in the opposite direction at Asp^{506} and points away from the GpIbα-binding site. This conformation is observed in three out of four models of Arg543Gln-A1 and in one model of wt-A1. In the open conformation the N-terminal flanking peptide has few interactions with the body of the domain. As a consequence the peptide is more flexible: on average fewer residues are visible in the electron density and the r.m.s.d. is large compared to the shielded conformation (1.73 Å for the open conformation and 0.89 Å for the shielded conformation). The shielded conformation of the N-terminal flanking peptide is stabilised via multiple interactions with the body of the domain (figure 1B, table III). Many of the residues involved in these interactions, either located in the flanking peptide or in the body of the domain, are subject to vWD type 2B mutations. In the A1•GpIbα complex the N-terminal flanking peptide adopts the open conformation. However, its conformation differs from other open conformations, due to an additional shift of the disulphide bond and a concomitant movement of Tyr^{508}. Therefore, binding of GpIbα to A1

involves additional conformational changes that are not induced by the type 2B mutations studied here.

Table III

Interactions of the N- and C-terminal flanking peptides with the body of the A1 domain and the effect of vWD type 2B or 2M mutations

N-terminal flanking peptide				C-terminal flanking peptide			
Residue	Type of vWD	Residue	Type of vWD	Residue	Type of vWD	Residue	Type of vWD
Asp^{498}	2B[a]	Ser^{500}	n.d.	Asp^{696}	normal[a]	Arg^{511}	2B
Ile^{499}	n.d.	Arg^{571}	2M			Ser^{692}	n.d.
		Arg^{573}	normal			Tyr^{693}	n.d.
Ser^{500}	n.d.	Asp^{498}	2B[a]			Leu^{694}	2B
Glu^{501}	2B[a]	Arg^{573}	normal			Ala^{698}	2B
		Pro^{574}	n.d.	Leu^{697}	2B	Ser^{615}	n.d.
		Ser^{575}	n.d.			Tyr^{693}	n.d.
Pro^{502}	n.d.	Leu^{504}	n.d.			Leu^{694}	2B
Pro^{503}	2B	His^{505}	2B			Cys^{695}	2B
		Tyr^{508}	n.d.	Ala^{698}	2B	Arg^{511}	2B
Leu^{504}	n.d.	Glu^{542}	2B[a]			Leu^{512}	n.d.
		Arg^{578}	2B			Leu^{513}	2M
His^{505}	2B	Pro^{503}	2B			Ser^{615}	n.d.
		Phe^{507}	n.d.			Leu^{694}	2B
		Glu^{542}	2B[a]			Cys^{695}	2B
		Arg^{543}	2B			Asp^{696}	n.d.
Asp^{506}	2B[a]	Tyr^{508}	n.d.			Glu^{700}	normal[a]
Phe^{507}	n.d.	His^{505}	2B	Pro^{699}	n.d.	Arg^{511}	2B
		Arg^{543}	2B			Leu^{512}	n.d.
		Asp^{688}	2B[a]			Glu^{613}	2M
		Val^{691}	n.d.			Ser^{615}	n.d.
		Ser^{692}	n.d.			Ala^{701}	2B
Tyr^{508}	n.d.	Pro^{503}	2B	Glu^{700}	n.d.	Arg^{511}	2B
		Asp^{506}	2B[a]			Ala^{698}	2B
		Ser^{510}	n.d.			Pro^{699}	n.d.
		Glu^{542}	2B[a]	Ala^{701}	2B	Pro^{699}	n.d.
		Arg^{543}	2B	Pro^{702}	2M[a]	Leu^{512}	n.d.
		Leu^{544}	n.d.	Pro^{703}	2M[a]		
		Arg^{545}	2B				

n.d.; not discribed in literature.

[a] The phenotype has been assigned although the effect of the mutation was studied in a vWF-variant containing more than one mutation.

The C-terminal flanking peptide protrudes like a stalk from the bottom of A1 (figure 1B). The conformation can roughly be divided in two groups depending on the orientation of the main chain at Glu^{700}. In one group, containing three wild-type and one 2B structure, residues Pro^{702} and Pro^{703} are within 2 and 3 Å, respectively, of the GpIbα-binding site. This

would block GpIbα binding. In analogy to the N-terminal flanking peptide we call this the shielded conformation. In the other conformation, observed in five wt-A1 models and all but one model of mutant A1, the C-terminal flanking peptide is located further away from the GpIbα-binding site due to a rotation of 180 degrees around the Glu^{700} peptide bond. In the A1•GpIbα complex an open conformation is observed.

Since the closed conformation of the N- and C-terminal flanking peptides is observed predominantly, but not exclusively, in free wt-A1 and the open conformation in Arg543Gln-A1, it suggest that both conformations exists in wt-A1 and mutant A1, but that a type 2B-mutation shifts the equilibrium to the open conformation.

The conformation of loop α1β2

Loop α1β2, comprising residues Ile^{544} to Trp^{550}, occupies a central position at the bottom face of the domain. In the shielded conformation this loop contacts the N- and C-terminal flanking peptides via a tight stacking of the side chains of residues Pro^{503}, Tyr^{508}, Arg^{545} and Trp^{550}, and a looser interaction with Ala^{701} (figure 1B). These residues, except Tyr^{508} of which no data are available, are subject to vWD type 2B mutations (Table III). In the A1•GpIbα complex the conformation of loop α1β2 is different compared to the conformation in wt-A1. In addition, loop α1β2 in the complex is mobile and interacts directly with GpIbα, suggesting that it is involved in activation. However, the conformation of loop α1β2 in wt-A1 and 2B-A1 is similar, indicating rather an indirect than a direct role in activation.

The conformation of hairpin β2β3

A closer look at hairpin β2β3 (residues 551-566) was prompted by the hypothesis formulated by Celikel *et al.* that mutation Ile546Val induced a conformational change 28 Å further in the domain in hairpin β2β3 resulting in a higher affinity for GpIbα [14]. Our comparison of a much larger set of structures now shows that hairpin β2β3 adopts a range of conformations (Table II). Part of the observed variability of β2β3 is accounted for binding of cadmium and chloride ions to residues Glu^{557}, His^{559}, Asp^{560}, and His^{563} in several of our structures (Table I) and in the structure of Emsley *et al* [22]. A superposition of all models not affected by ion binding (figure 2) stills shows substantial variation in the conformation of β2β3, in particular for main-chain and side-chain atoms of residues Asp^{560}, Gly^{561}, Ser^{562}, His^{563}. However, the conformation of β2β3 in the Ile546Val- and Arg543Gln-A1 mutants is different from the conformation observed in the A1•GpIbα complex. Clearly, hairpin β2β3 is inherently flexible

and its conformation as observed in the structure of type 2B mutants is not a high-affinity state of the A1 domain. Alternatively, the 2B phenotype of the Ile546Val mutant may involve a conformational change in the N-terminal flanking peptide. However, this could not have been observed in the crystal structure of Ile546Val-A1, since the construct used for crystallisation did not contain the N-terminal flanking peptide.

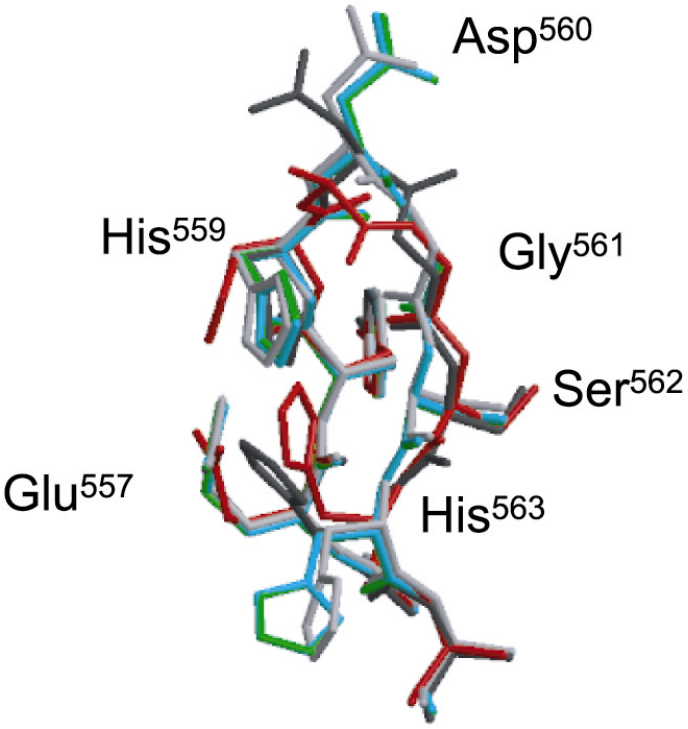

Figure 2: Conformations of hairpin β2β3. Superposition of A1 models wt-P$2_12_12_1$, *green*, wt-1oak, *dark grey*, RQ-P$2_12_12_1$, *blue*, IV-1fns, *light grey*, and A1•GpIbα, *red*. The conformation of hairpin β2β3 in the two wt-A1 models are not identical but differ at residues Asp[560], Ser[562] and His[563]. In addition, the conformation in two vWD type 2B A1 variants of A1 are not similar at these residues and do not resemble the conformation of the hairpin in the A1•GpIbα complex that contains by definition the active conformation.

Binding of the A1 domain and vWF to GpIbα

To investigate if GpIbα binding to the A1 domain is similar as to vWF, we analysed GpIbα-binding by SPR. These results have been summarised before [13], but will be discussed here in detail. Wild-type vWF did not spontaneously bind to GpIbα up to a concentration of 150 nM, but Arg543Gln-vWF did (figure 3). In contrast, wt-A1 bound spontaneously to GpIbα with an affinity of 27 nM. Therefore the wt-A1 domain is already activated. Mutation Arg543Gln in the A1 domain reduced the K_D only 3 fold showing that the effect of the mutation is subtle in A1[498-705]. This observation is in agreement with our crystallographic data, since we observed that only the C-terminal flanking peptide partially overlaps the GpIbα binding site at the bottom of A1. The N-terminal flanking peptide in A1[498-705] approaches, but does not overlap this GpIbα binding site and is therefore not able to prevent GpIbα binding. Probably additional elements in the flanking peptides outside residues 498-705 are required to keep A1 in a low-affinity state as has been demonstrated for other shorter and longer A1-constructs [27;

[28;29;30]. Most likely the N- and C-terminal flanking peptides act in concert, because only

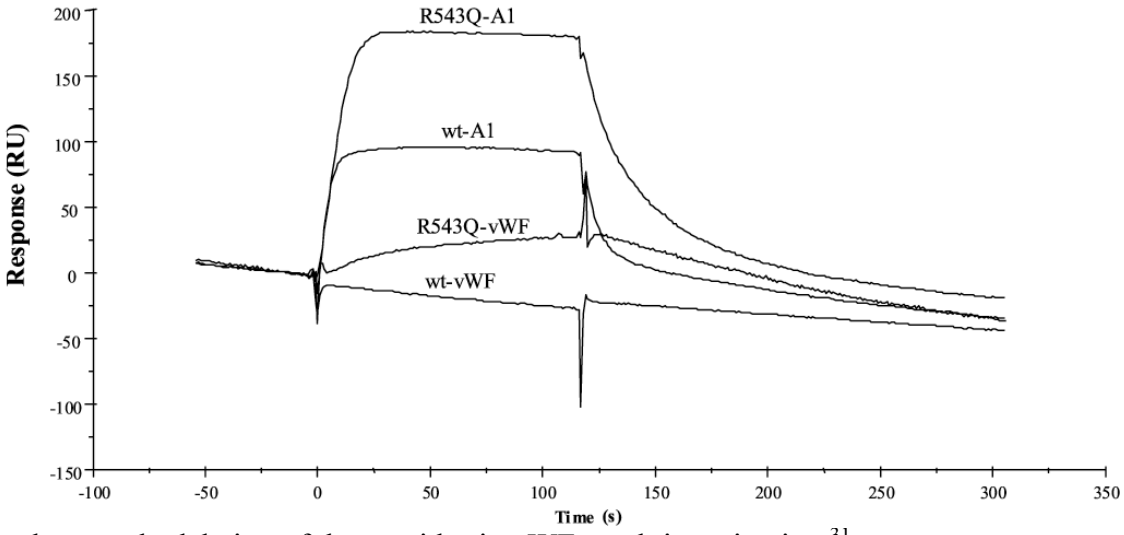

simultaneously deletion of the peptides in vWF result in activation [31].

Figure 3: Binding of multimeric vWF and the isolated A1 domain to immobilised GpIbα was analysed by surface plasmon resonance in a Biacore system. Wild-type A1 bound spontaneously to GpIbα, K_D 27 nM, and mutation Arg543Gln increased the affinity for GpIbα three fold. Wild-type vWF did not bind to GpIbα, suggesting a K_D of at least 5 ? μM. Mutation Arg543Gln in multimeric vWF induced spontaneous binding.

Conclusion

We have investigated structures of wt- and type 2B mutants A1 in relation to GpIbα binding. Conformational changes induced by type 2B mutations within the body of the A1 domain were not observed. However, conformational changes were observed for the N- and C-terminal flanking peptides. In wt-A1 the peptides are directed to the GpIbα binding site at the bottom of A1, suggesting that these peptides overlap the binding site in vWF. In type 2B A1 the peptides are directed differently and probably do not overlap the binding site in type 2B vWF. The importance of the N- and C-terminal flanking peptides in vWF-activation is underlined ristocetin, which interacts with the N- and C-terminal flanking peptides [9; 32]. Ristocetin-induced activation resembles shear-induced activation [12].

Our crystallographic analysis supports a mechanism for activation of vWF as depicted in figure 4. In normal circulation the N- and C-terminal flanking peptides shield the GpIbα – β-finger binding site at the bottom of A1 and vWF has a low-affinity conformation. Pathological shear forces acting on vWF in occluded arteries or drag forces generated by the blood flow acting on immobilised vWF pulls the flanking peptides away by a hinge motion at residues Asp^{506} and Glu^{700} that exposes the GpIbα binding site. VWD type 2B mutations

likely affect the equilibrium between the shielded and open conformation and switch vWF from the low- to the high-affinity state.

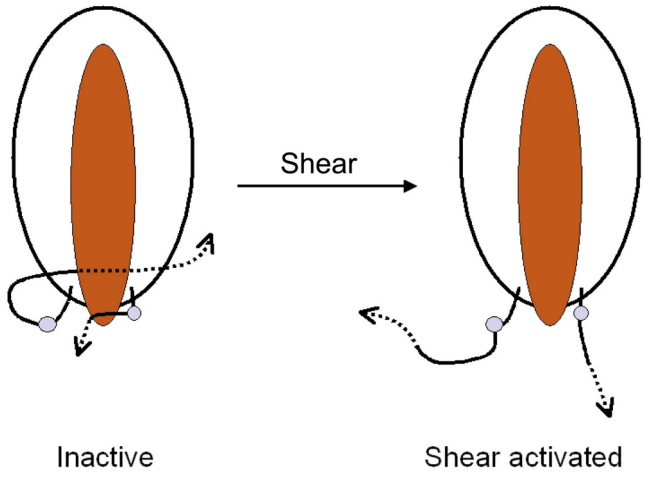

Figure 4: Mechanism of vWF-A1 activation. In vWF both the N- and C-terminal flanking peptides shield the GpIbα – β-finger binding site and vWF adopts its low-affinity state. Due to shear activation or a vWD type 2B mutation, the N- and C-terminal flanking peptides are rotated around a hinge (Asp^{506} and Glu^{700}, respectively, indicated by the blue circles). This opens the GpIbα-binding site and switches A1 to the high-affinity state.

Acknowledgements

We would like to thank Prof. Dr. H. Deckmyn (Kortrijk, Belgium) for generously supplying monoclonal 2D4. We also thank the staff at beam lines ID14-EH2, ID14-EH3 and ID9 of the ESRF in Grenoble for their assistance in data collection.

Reference List

1. Verweij CL, Hart M, Pannekoek H. Expression of variant von Willebrand factor (vWF) cDNA in heterologous cells: requirement of the pro-polypeptide in vWF multimer formation. EMBO J. 1987;6:2885-2890.

2. Voorberg J, Fontijn R, Van Mourik JA, Pannekoek H. Domains involved in multimer assembly of von willebrand factor (vWF): multimerization is independent of dimerization. EMBO J. 1990;9:797-803.

3. Fischer BE, Kramer G, Mitterer A, et al. Effect of multimerization of human and recombinant von Willebrand factor on platelet aggregation, binding to collagen and binding of coagulation factor VIII. Thromb Res. 1996;84:55-66.

4. Sixma JJ, Schiphorst ME, Verweij CL, Pannekoek H. Effect of deletion of the A1 domain of von Willebrand factor on its binding to heparin, collagen and platelets in the presence of ristocetin. Eur J Biochem. 1991;196:369-375.

5. Fujimura Y, Titani K, Holland LZ, et al. von Willebrand Factor: A reduced and alkylated 52/48-kDa fragment beginning at amino acid residue 449 contains the domain interacting with platelet glycoprotein Ib. J Biol Chem. 1986;261:381-385.

6. Savage B, Saldívar E, Ruggeri ZM. Initiation of platelet adhesion by arrest onto fibrinogen or translocation on von Willebrand factor. Cell. 1996;84:289-297.

7. Andrews RK, Booth WJ, Gorman JJ, Castaldi PA, Berndt MC. Purification of botrocetin from *Bothrops jararaca* venom. Analysis of the botrocetin-mediated interaction between von Willebrand factor and the human platelet membrane glycoprotein Ib- IX complex. Biochemistry. 1989;28:8317-8326.

8. Bardsley B, Williams D.H., Baglin TP. Cleavage of rhamnose from ristocetin A removes its ability to induce platelet aggregation. Blood Coagulation & Fibrinolysis 1998; 9(3), 241-244.

9. Girma JP, Takahashi Y, Yoshioka A, Diaz J, Meyer D. Ristocetin and botrocetin involve two distinct domains of von Willebrand factor for binding to platelet membrane glycoprotein Ib. Thromb Haemost. 1990;64:326-332.

10. Azuma H, Sugimoto M, Ruggeri ZM, Ware J. A role for von Willebrand factor proline residues 702-704 in ristocetin-mediated binding to platelet glycoprotein Ib. Thromb Haemost. 1993;69:192-196.

11. Berndt MC, Du X, Booth WJ. Ristocetin-dependent reconstitution of binding of von Willebrand factor to purified human platelet membrane glycoprotein Ib-IX complex. Biochemistry. 1988;27:633-640.

12. Dong JF, Berndt MC, Schade A, McIntire LV, Andrews RK, Lopez JA. Ristocetin-dependent, but not botrocetin-dependent, binding of von willebrand factor to the platelet glycoprotein Ib-IX-V complex correlates with shear-dependent interactions. Blood. 2001;97:162-168.

13. Huizinga EG, Tsuji S, Romijn RAP, Sixma JJ, Gros P. GpIb crystal structure. Submitted to Science. 2002

14. Celikel R, Ruggeri ZM, Varughese KI. Von Willebrand Factor conformation and adhesive function is modulated by an internalized water molecule. Nature Struct Biol. 2000;7:881-884.

15. Van der Plas RM, Gomes L, Marquart JA, et al. Binding of von Willebrand Factor to Collagen type III: Role of specific amino acids in the collagen binding domain of vWF and effects of neighbouring domains. Thromb Haemost. 2000; 84, 1005-1011.

16. Lankhof H, Damas C, Schiphorst ME, et al. Functional studies on platelet adhesion with recombinant von Willebrand factor type 2B mutants R543Q and R543W under conditions of flow. Blood. 1997;89:2766-2772.

17. Lankhof H, van Hoeij M, Schiphorst ME, et al. A3 domain is essential for interaction of von Willebrand factor with collagen type III. Thromb Haemost. 1996;75:950-958.

18. Graham F, van der Eb A. A new technique for the assay of infectivity of human adenovirus 5 DNA. Virology. 1973;52:456.

19. Lawrie AS, Horser MJ, Savidge GF. Phast assessment of vWF:Ag multimeric distribution. Thromb Haemost. 1990;59:369.

20. Otwinowski Z, Minor O. Processing of X-ray diffraction data collected in oscillation mode. Methods Enzymol. 1996;276:307-326.

21. Brünger AT, Adams PD, Clore GM, et al. Crystallography and NMR system: A new software suite for macromolecular structure determination. Acta Crystallogr D. 1998;54:905-921.

22. Emsley J, Cruz M, Handin R, Liddington RC. Crystal structure of the von Willebrand factor A1 domain and implications for the binding of platelet glycoprotein Ib. J Biol Chem. 1998;273:10396-10401.

23. Jones TA, Zou JY, Cowan SW, Kjeldgaard M. Improved methods for the building of protein models in electron density maps and the location of error in these models. Acta Crystallogr A. 1991;47:110-119.

24. Pannu NS, Read RJ. Improved structure refinement through Maximim Likelihood. Acta Crystallogr A. 1996;52:659-668.

25. Celikel R, Varughese KI, Madhusudan, Yoshioka A, Ware J, Ruggeri ZM. Crystal structure of the von Willebrand factor A1 domain in complex with the function blocking NMC-4 Fab. Nature Struct Biol. 1998;5:189-194.

26. Emsley J, Knight CG, Farndale RW, Barnes MJ, Liddington RC. Structural basis of collagen recognition by integrin α2β1. Cell. 2000;100:47-56.

27. Sugimoto M, Dent J, McClintock R, Ware J, Ruggeri ZM. Analysis of structure-function relationships in the platelet membrane glycoprotein Ib-binding domain of von Willebrand's factor by expression of deletion mutants. Journal of Biological Chemistry 1993; 268(16), 12185-12192.

28. Miura S, Li CQ, Cao Z, Wang H, Wardell MR, Sadler JE. Interaction of von Willebrand Factor domain A1 with platelet glycoprotein Ibα-(1-289). Slow intrinsic binding kinetics mediate rapid platelet adhesion. J Biol Chem. 2000;275:7539-7546.

29. Cruz MA, Handin RI, Wise RJ. The interaction of the von Willebrand factor-A1 domain with platelet glycoprotein Ib/IX. The role of glycosylation and disulfide bonding in a monomeric recombinant A1 domain protein. J Biol Chem. 1993;268:21238-21245.

30. Miyata S, Ruggeri ZM. Distinct structural attributes regulating von Willebrand factor A1 domain interaction with platelet glycoprotein Ibα under flow. J Biol Chem. 1999;274:6586-6593.

31. Nakayama T, Matsushita T, Dong Z, et al. Identification of the regulatory elements of human von Willebrand factor for binding to platelet GPIb. Importance of structural integrity of the regions flanked by CYS509-CYS695 disulfide bond. J Biol Chem. 2002.

32. Hilbert L, Gaucher C, Mazurier C. Effects of different amino-acid substitutions in the leucine694-proline708 segment of recombinant von Willebrand factor. Br J Haematol. 1995;91:983-990.

33. Gerard J.Kleywegt. LSQMAN. 1999.

34. Kraulis P. Molscript: a program to produce both detailed and schematic plots of protein structures. J Appl Crystallogr. 1991;25:649-950.

35. Merritt EA, Bacon DJ. Raster3D: photorealistic molecular graphics. Methods Enzymol. 1997;277:505-524.

Chapter 7

General discussion

Haemostatic plug formation at sites of vascular injury is required to stop bleeding. This process is started by platelet adhesion and aggregation and is followed by fibrin formation. Platelet adhesion and aggregation requires the subendothelial matrix, von Willebrand Factor (vWF), platelet receptors glycoprotein (Gp) Ib-IX-V complex, GpVI, integrins $\alpha_2\beta_1$, $\alpha_{2b}\beta_3$ and fibrinogen.

Adhesion of platelets at sites of vascular damage is initiated by binding of the vWF A3 domain to the subendothelial matrix, followed by rolling and tethering of platelets over this immobilised vWF. The latter process requires the A1 domain of vWF and GpIbα on the platelet. Rolling reduces the velocity of the platelets, a process that is also mediated by GpVI and integrin $\alpha_2\beta_1$. Now the platelets become firmly attached and activated. This allows additional platelets to interact with these initial immobilised platelets; the process of thrombus growth is initiated. Platelet-platelet interactions within the thrombus are mediated by the GpIb-IX-V complex, integrin $\alpha_{2b}\beta_3$ and vWF and fibrinogen. Finally fibrinogen is converted to fibrin, giving the haemostatic plug its final strength.

Von Willebrand Factor is stored in specific organelles in platelets and endothelial cells and it circulates free in plasma. Because vWF and platelets both circulate free in plasma, vWF should not bind spontaneously to platelets. To this end, vWF needs to be activated. The activation mechanism is not understood, but activation can be achieved in several ways.

1) Binding of vWF to the subendothelial matrix, in particular to collagen [1].
2) Binding of exogenous ligands to vWF, for example the antibiotic ristocetin-A [2] or snake toxins botrocetin [3] or bitiscetin [4].
3) Von Willebrand Disease (vWD) type 2B mutations in the A1 domain [5].
4) Platelet-type vWD mutations in GpIb [6].

The studies in this thesis were conducted to investigate the above processes. In particular, we investigated at a molecular level (i) the binding of the A3 domain to collagen type III, (ii) the structure of the A1•GpIbα complex and (iii) conformational changes that activate the A1 domain for binding to GpIbα.

Binding of vWF to collagen.

Insight at the molecular level how vWF immobilises platelets on the subendothelial matrix may be useful to develop new anti-arterial thrombotic compounds. To this end, we investigated the interaction of the A3 domain with collagen type III. These results are described in **chapters 2, 3 and 4**. Based on the homology with integrin I-domains, which bind collagen at the top-face of the domain, several groups, including ours, have introduced mutations at the top face of A3. However, these mutations did not reduce collagen binding suggesting that the collagen-binding site in A3 should be located somewhere else. To obtain information about the approximate location of the collagen-binding site, we solved the crystal structure of the A3 domain in complex with a Fab fragment of function inhibiting antibody, RU5 **(chapter 2)**. We identified the RU5-epitope at the front- and bottom face of A3. Subsequent mutations introduced in and around the RU5 epitope indeed resulted in a reduced collagen-binding. The collagen-binding site in A3 has now been mapped solely to the front face of the domain. Based on the quantitative effects of the mutations in collagen binding, we hypothesise that residues in the lower part of the collagen-binding site are essential in collagen binding, whereas residues in the upper part are involved but not essential in collagen binding. Since the collagen-binding site in the A3-domain contains negatively charged and hydrophobic amino-acid residues, it is evident that A3 binds to positively charged and hydrophobic residues within a collagen triple-helix. The front face of the A3 domain is rather flat and specific collagen sequences that bind to vWF are unknown. Therefore an automated procedure to dock a collagen molecule failed. Manually we identified a range of orientations of the engagement of a collagen triple helix on the A3 domain (figure 1).

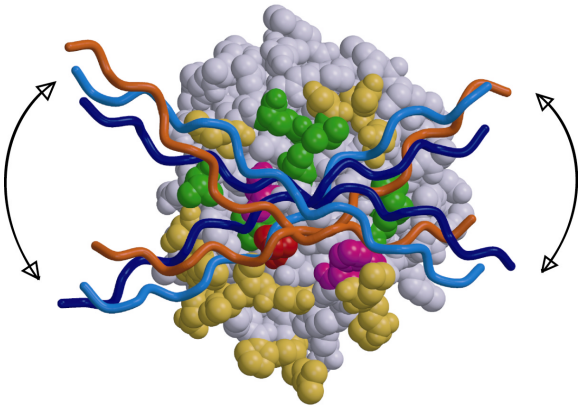

Figure 1: Binding-orientations of a collagen triple helix to the vWF-A3 domain. The front-face of the A3 domain is shown. Residues in *magenta* are essential in collagen binding, residues in *green* are involved but not essential in collagen binding, and residues in *yellow* are not involved at all. The collagen molecule is close to Pro^{981}, shown in *red*, but does not interact with it. Two collagen molecules that enclose the range of orientations for the A3-collagen interaction are shown and the ange is indicated by the arrows.

Schneppenheim *et al.* described several patients with a mutation in the A3 domain that inhibited collagen binding in a solid-state collagen-binding assay [7]. Surprisingly, the patients

are without bleeding problems. However, the mutated residues co-localise with the region of A3 that is involved, but not essential for collagen binding. On the other hand, mutations in the region that is essential in collagen binding may give bleeding problems, but these mutations are not yet identified in patients.

Ribba *et al.* described two related patients suffering from mild bleeding problems, with a mutation in the A3 domain [8]. Residue Ser^{968} is mutated to threonine. Ser^{968} is not solvent exposed, but is buried under the collagen binding site. Therefore a direct effect in collagen binding seems unlikely. In the study described in **chapter 4** we solved the crystal structure of A3 with this mutation. Interestingly, we did not observe any conformational changes in A3. As we have described in chapter 2, two loops at the lower part of the front face of A3 are rather mobile, suggesting an induced-fit model for the binding of A3 to collagen. Ser^{968} is close to one of these loops and we hypothesised that the mutation shifts the equilibrium to the low-affinity conformation and thereby reduces the affinity of A3 for collagen.

For the α_2-I domain it has been shown that collagen binding induces conformational changes within the domain. To investigate if conformational changes occur in A3 upon collagen binding, co-crystallisation experiments should be performed of A3 in complex with a short collagen-triple helix. However, it is still not known which collagen sequence (and probably it is not a single sequence but multiple) binds to A3 with high affinity. This may be investigated by several approaches: (i) monoclonal antibodies raised against collagen type III may inhibit binding of vWF to collagen. Via phage-display-technology the epitope of the antibody can be determined, (ii) cross-linking of collagen-bound vWF and subsequent digestion of the vWF-collagen complex. Via N-terminal protein sequencing the specific collagen sequences may be identified.

It has been argued that *in vivo* the A3 domain is not involved in immobilizing platelets to the vessel wall, because patients with a mutation in the collagen-binding site do not have a bleeding problem [7]. However, we have shown that these mutated residues are located in the upper part of the collagen-binding site that is involved, but not essential in collagen binding. Recently the relevance of the binding of A3 to collagen *in vivo* has been demonstrated by injection of monoclonal antibodies directed against the A3 domain in baboons [9]. This resulted in an elongated bleeding time. To tackle these discrepancies further, bleeding-time experiments in vWF knock-out mice should be performed after infusion with either mouse wild-type vWF or mouse vWF lacking the A3 domain.

The A1•GpIbα complex and conformational changes in A1.

VWF becomes activated when it is immobilised to a surface. As mentioned above, the activation-mechanism is not understood. Most likely it requires conformational changes in the A1 domain. It is generally believed that these conformational changes are similar to the conformational changes induced by vWD type 2B mutations.

To address this problem we solved a crystal structure of GpIbα and of GpIbα in complex with the A1 domain (**chapter 5** and figure 2). The leucine-rich repeats of GpIbα adopt a horse-shoe like structure that is sandwiched on either side by flanking elements. The N-terminal flanking structure contains the so-called β-finger that protrudes from the domain. The C-terminal flanking structure contains the so-called β-switch, which is structurally disordered, and is followed by the anionic region. In the A1•GpIbα complex we identified two sites in A1 that tightly interact with GpIbα. The first interaction site is at the upper part of A1 and involves residues of hairpin β2β3 and nearby residues. This interaction site binds to the GpIbα – β-switch and several other GpIbα residues in the vicinity of the β-switch. When the β-switch interacts with the A1 – β2-β3 hairpin, the β-switch undergoes a conformational change and adopts a β-hairpin conformation. Since platelet-type vWD mutations are located in the β-switch and involve mutations that favour β-strand formation, it is likely that these mutations induce the β-hairpin structure in the β-switch and thereby activate GpIbα. The second GpIbα binding site in A1 is located at the lower part of the domain, close to the region in A1 that contains the type 2B mutations. This region interacts with the GpIbα β-finger.

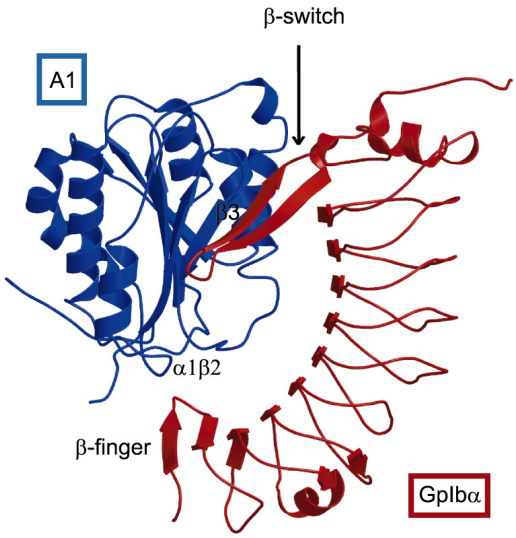

Figure 2: Crystal structure of the A1•GpIbα complex. A1 is shown in *blue* and GpIbα is shown in *red*. GpIbα has two main interaction sites within A1. The β-finger interacts with several loops, including loop α1β2, at the bottom of A1. The β-switch interacts with strand β3 of hairpin β2β3 and several other residues at the top of A1. Several long-range charge-charge interactions between the GpIbα LRRs and the body of A1 provide an additional interaction site.

In the past, two structures of wt-A1 and one structure of vWD type 2B mutant Ile546Val have been published [10-12]. In the study described in **chapter 6** we solved the structure of three different crystal forms of wt-A1$^{498-705}$, yielding six models, and three different crystal forms of type 2B mutant Arg543Gln-A1, yielding five models. In all wt- and type 2B A1 models the overall fold of the body of the domain was similar. In contrast, the N- and C-terminal flanking peptides adopted a different conformation in type 2B mutant Arg543Gln-A1 compared to the conformation in wild-type A1. In most of the wt-A1 models the N- and C-terminal flanking peptides are directed towards the GpIbα – β-finger binding site suggesting that in multimeric vWF they overlap with the β-finger binding site. This is the so-called shielded conformation. In most of the Arg543Gln-A1 models the N- and C-terminal flanking peptides are pointed in a different direction due to a hinge motion around Asp^{506} and Glu^{700}, respectively, thereby opening the β-finger binding site. This motion of the flanking peptides could activate the A1 domain for GpIbα binding. It is likely that shear activates A1 via a similar mechanism, because vWF that is immobilised via its A3 domain may "sense" the forces generated by the flowing blood. As a result, vWF may partially unwind that induces the conformational change in the N- and C-terminal flanking peptides of the A1 domain.

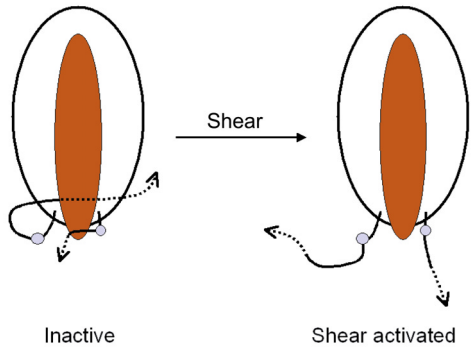

Figure 3: Schematic representation of A1 activation. In inactive vWF the N- and C-terminal flanking peptides of A1 fold over the body of the domain and shield the β-finger binding site. Activation induces a motion around two hinges (indicated by the *blue* circle) that opens the binding site.

Based on our observations we disagree with the hypothesis of Celikel *et al.* [12] who postulated that A1 is activated due to a conformational change in the β2β3 hairpin of A1. In our structural analysis we observed conformational flexibility of hairpin β2β3 that is not correlated with the presence of a type 2B mutation. Celikel *et al.* were not able to observe a conformational change in the N-terminal flanking peptide, because these residues were absent in their A1-construct.

The exact number of residues in the N- and C-terminal flanking sequences that are required to prevent spontaneous GpIbα-binding is still unknown. Residues upstream of Asp^{498}

and downstream of Thr^{705} are required to suppress GpIbα binding, because various A1-constructs with longer N-and C-terminal flanking peptides do not bind spontaneously to GpIbα, whereas $A1^{498-705}$ does. It is also known that *O-linked* glycan residues are required to prevent spontaneous GpIbα binding, because non-glycosylated (*i.e.* bacterial) or desialated A1 fragments bind spontaneously to GpIbα, whereas identical glycosylated A1 fragments do not. It is, however, still not known which residues require *O*-glycosylation. To address the above problems, an A1-construct should be developed that is fully glycosylated and does not bind spontaneously to GpIbα. Next, the number of residues in the N- and C-terminal flanking peptides should be systematically decreased and *O-linked* glycosylation sites should be specifically removed. Additionally, the A1 construct which does not interact spontaneously with GpIbα should be crystallised to study the interactions of the N- and C-terminal flanking peptides with the body of the domain at a molecular level.

Binding of vWF to a surface like glass, collagen or endothelial cell matrix triggers binding of GpIbα on the platelet to vWF. As is described in chapters 5 and 6, activation of vWF involves conformational changes in the N- and C-terminal flanking peptides of the A1 domain. These conformational changes may be induced by binding of the A3-domain to collagen, or by hydrodynamic forces generated by the flowing blood. In addition, it can not be excluded that GpIbα mediated binding of platelets to immobilized vWF is an effect of the increased local vWF concentration. Therefore Biacore-experiments should be performed at multiple flow-rates in which different vWF-densities are immobilised via collagen or via a monoclonal antibody to the sensor chip.

In summary, our investigations identified the collagen-binding site on the vWF-A3 domain. Based on the surface characteristics of the collagen-binding site, a hypothesis of the nature of the collagen triple helix to which A3 will bind has been made. The identification of specific collagen sequences that interact with A3 is subject for future research. Crystal structures of GpIbα, A1•GpIbα, wt- and R543Q-A1 have been solved. Based on these structures we hypothesised that the N- and C-terminal flanking peptides of A1 shield one of the two GpIbα binding sites in A1 and thereby prevent GpIbα binding. A1-activation involves a conformational change in these flanking peptides. The exact number of residues in the N- and C-terminal flanking peptides that shield A1 completely is subject for further research.

In conclusion, we have gained insight in the collagen-vWF-GpIbα interactions at a molecular level. It has not escaped our notice that these results are of significant value for the development of new drugs against arterial thrombosis.

Reference list

1. Savage B, Almus-Jacobs F, Ruggeri ZM. Specific synergy of multiple substrate-receptor interactions in platelet thrombus formation under flow. Cell. 1998;94:657-666.

2. Scott JP, Montgomery RR, Retzinger GS. Dimeric ristocetin flocculates proteins, binds to platelets, and mediates von Willebrand factor-dependent agglutination of platelets. J Biol Chem. 1991;266:8149-8155.

3. Usami Y, Fujimura Y, Suzuki M, et al. Primary structure of two-chain botrocetin, a von Willebrand factor modulator purified from the venom of *Bothrops jararaca*. PNAS. 1993;90:928-932.

4. Obert B, Houllier A, Meyer D, Girma JP. Conformational changes in the A3 domain of von Willebrand factor modulate the interaction of the A1 domain with platelet glycoprotein Ib. Blood. 1999;93:1959-1968.

5. Ginsburg D, Sadler JE. von Willebrand disease: a database of point mutations, insertions, and deletions. For the Consortium on von Willebrand Factor Mutations and Polymorphisms, and the Subcommittee on von Willebrand Factor of the Scientific and Standardization Committee of the International Society on Thrombosis and Haemostasis. Thromb Haemost. 1993;69:177-184.

6. Miller JL. Platelet-type von Willebrand disease. Thromb Haemost. 1996;75:865-869.

7. Schneppenheim R, Obser T, Drewke E, et al. Isolated Molecular Defects of Von Willebrand Factor Binding to Collagen Do Not Correlate with Bleeding Symptoms [abstract]. Blood. 2001.

8. Ribba AS, Loisel I, Lavergne JM, et al. Ser968Thr mutation within the A3 domain of von Willebrand factor (VWF) in two related patients leads to a defective binding of VWF to collagen. Thromb Haemost. 2001;86:848-854.

9. Wu D, Vanhoorelbeke K, Cauwenberghs N, et al. Inhibition of the von Willebrand (VWF)-collagen interaction by an antihuman VWF monoclonal antibody results in abolition of in vivo arterial platelet thrombus formation in baboons. Blood. 2002;99:3623-3628.

10. Emsley J, Cruz M, Handin R, Liddington RC. Crystal structure of the von Willebrand factor A1 domain and implications for the binding of platelet glycoprotein Ib. J Biol Chem. 1998;273:10396-10401.

11. Celikel R, Varughese KI, Madhusudan, Yoshioka A, Ware J, Ruggeri ZM. Crystal structure of the von Willebrand factor A1 domain in complex with the function blocking NMC-4 Fab. Nature Struct Biol. 1998;5:189-194.

12. Celikel R, Ruggeri ZM, Varughese KI. Von Willebrand Factor conformation and adhesive function is modulated by an internalized water molecule. Nature Struct Biol. 2000;7:881-884.

Hoofdstuk 8

Samenvatting in het Nederlands

Inleiding

Het stoppen van een bloeding bestaat uit twee processen: bloedstelping en bloedstolling. Tijdens de bloedstelping worden bloedplaatjes aan de beschadigde vaatwand gebonden en ontstaat de plaatjesprop. Bloedstolling is het proces van fibrinevorming, dat de plaatjesprop zijn uiteindelijke sterkte geeft. Het in dit proefschrift beschreven onderzoek betreft een onderdeel van de **bloedstelping**.

Binding van bloedplaatjes aan een beschadigde vaatwand is een complex proces en is afhankelijk van componenten uit de vaatwandmatrix, waaronder collageen, verschillende receptoren op het bloedplaatje, waaronder GpIb-IX-V, GpVI, $\alpha_2\beta_1$ en $\alpha_{2b}\beta_3$, en plasma-eiwitten zoals von Willebrand factor en fibrinogeen. In dit proefschrift worden onze studies naar **Von Willebrand factor** beschreven.

Von Willebrand factor, vWF, is een multimeer eiwit dat aan collageen op de plaats van de beschadiging in de vaatwand bindt. Vervolgens vinden er veranderingen in de structuur van vWF plaats waardoor vWF ook aan receptor GpIb-IX-V op het bloedplaatje kan binden. Nu is het bloedplaatje geïmmobiliseerd op de plaats van de beschadigde vaatwand. De binding tussen het geïmmobiliseerde bloedplaatje en de vaatwand wordt versterkt door interacties van plaatjes receptoren GpVI en $\alpha_2\beta_1$ met collageen. Vervolgens binden andere bloedplaatjes aan de eerste laag plaatjes via interactie van plaatjes receptor $\alpha_{2b}\beta_3$ met fibrinogeen en vWF uit het plasma en ontstaat de plaatjesprop. **De binding van vWF aan collageen en GpIb-IX-V** zijn de specifieke onderwerpen van dit proefschrift.

Resultaten

In **hoofdstuk één** wordt een algemene inleiding over bloedstelping gegeven. Primair wordt de aandacht gelegd op **von Willebrand Factor** (vWF). Beschreven wordt hoe en waar vWF gesynthetiseerd wordt en waar het gelokaliseerd is in het lichaam. Verder wordt beschreven uit welke domeinen vWF is opgebouwd en wat de functie deze domeinen is. Specifiek wordt ingegaan op de A1 en A3 domeinen.

In **hoofdstuk twee en drie** zijn de experimenten beschreven waarmee de collageen bindingsplaats op het A3 domein is gelokaliseerd. In analogie met homologe I-domeinen, die

collageen binden aan de bovenkant van het domein, waren in het verleden aan de bovenkant van het A3 domein mutaties geïntroduceerd. Echter, collageen binding van deze mutanten was normaal waardoor geconcludeerd kon worden dat collageen niet aan de bovenkant van A3 bindt. Om de collageen bindingsplaats op het A3 domein grof te bepalen hebben we de kristal structuur van A3 in complex met het Fab-fragment van monoclonaal antilichaam RU5 bepaald. RU5 remt de binding van vWF aan collageen waardoor het waarschijnlijk is dat het epitoop van RU5 en de collageen bindingsplaats (partieel) overlappen. In de kristal structuur van het A3•RU5 complex was duidelijk dat RU5 aan de voor- en onderzijde van A3 bindt en niet aan de bovenkant. Op basis van deze structuur hebben we 27 aminozuren geïdentificeerd die betrokken zouden kunnen zijn in collageen binding. Deze aminozuren hebben we gemuteerd. Een aantal van deze mutanten bezit een verlaagde affiniteit voor collageen, wat inhoudt dat de gemuteerde aminozuren zeer waarschijnlijk betrokken zijn bij de collageen binding. Op basis hiervan hebben we geconcludeerd dat de collageen bindingsplaats aan de voorkant van het A3 domein ligt. Uit de experimenten bleek tevens dat de aminozuren in de onderste helft van de collageen bindingsplaats essentieel zijn voor de collageen binding, terwijl aminozuren in de bovenste helft slechts additioneel betrokken zijn. Een hypothetisch model van de binding van collageen aan A3 is gegeven in figuur 1.

Collageen residuen die aan A3 binden zijn nog niet geïdentificeerd. Nu de collageen bindingsplaats op het A3 domein gelokaliseerd is kunnen we op basis van de karakteristieken van de bindingsplaats een uitspraak doen over collageen sequenties die aan A3 binden. Op basis hiervan is het waarschijnlijk dat hydrofobe- en positief geladen collageen sequenties aan A3 binden.

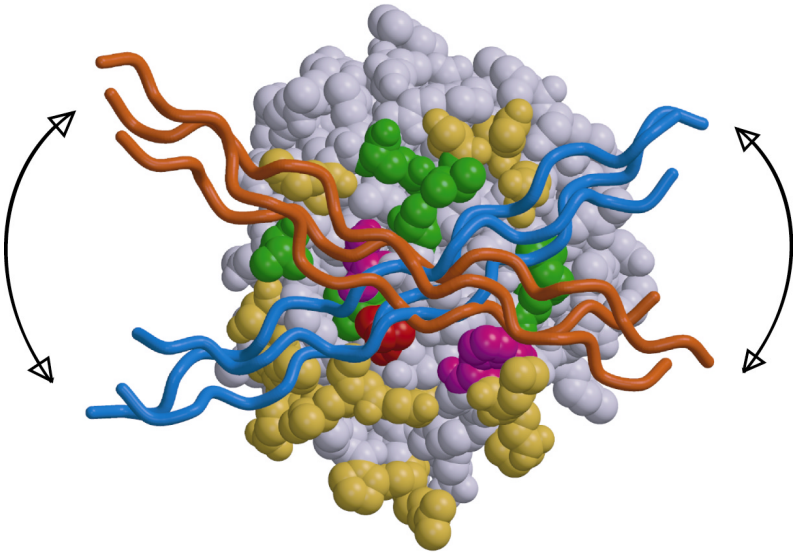

Figuur 1. De collageen bindingsplaats op het vWF-A3 domain. Ruimtelijk model van de voorkant van het vWF-A3 domein. Residuen in *roze*, Asp^{979}, Ser^{1020} en His^{1023}, zijn essentieel voor de collageen binding en residuen in *groen*, Ile^{975}, Thr^{977}, Val^{997}, Glu^{1001} en Arg^{1016}, zijn betrokken bij de collageen binding, maar zijn niet essentieel. Residuen in *geel* hebben geen interactie met collageen. Residuen in *grijs* hebben we niet gemuteerd. Pro^{981}, in *rood*, bindt niet aan collageen, maar als het wordt gemuteerd naar een histidine, remt het de collageen binding via sterische hindering.
Twee collageen moleculen zijn weergegeven in blauw en bruin welke de range van mogelijke oriëntaties aangegeven hoe collageen aan A3 kan binden.

Onderwerp voor verdere studie is de identificatie van collageen sequenties die aan A3 binden en het bepalen van de kristalstructuur van een A3•collageen complex.

In **hoofdstuk vier** is de kristal structuur van het A3 domein beschreven dat mutatie Ser968Thr bevat. Deze mutatie is gevonden bij een patiënt met een bloedingsneiging. Aminozuur Ser^{968} is echter niet gelokaliseerd aan het oppervlak van A3, maar net onder de collageen bindingsplaats. Daardoor is een directe rol voor Ser^{968} in collageen binding niet waarschijnlijk. Mutatie Ser968Thr veranderde niet zichtbaar de conformatie van het A3 domein. Echter, uit de vergelijking van vele A3 kristalstructuren bleek dat de collageen bindingsplaats van A3 meerdere conformaties kan aannemen. Hoewel er geen directe experimentele aanwijzingen zijn, veronderstellen we dat een aantal conformaties wel in staat is om collageen te binden en andere conformaties niet. Waarschijnlijk heeft de mutatie invloed op de ratio van de actieve- en de niet-actieve conformatie en wordt het evenwicht verschoven naar de niet-actieve conformatie.

Het A1 domein van vWF bindt aan de receptor GpIb-IX-V op het bloedplaatje. In het onderzoek zoals beschreven in **hoofdstuk vijf** werd de kristal structuur van het A1-bindende deel van GpIb-IX-V, de 290 N-terminale residuen van de GpIbα subunit, bepaald (zie figuur 2). Tevens werd de structuur bepaald van A1 in complex met dit deel van GpIbα. Het vWF-A1 domein heeft twee bindingsplaatsen voor GpIbα. Eén bindingsplaats is gelokaliseerd aan de bovenkant van het A1 domein en bevat aminozuren die op basis van mutatiestudies al eerder waren geïdentificeerd. Dit deel van A1 bind aan de zogenaamde β-swich op GpIbα. Onverwacht was de tweede bindingsplaats voor GpIbα aan de onderkant van A1 dat interactie heeft met de β-finger van GpIbα. Verder zijn er verschillende lange-afstand lading interacties van residuen in de β-strands van de GpIbα leucine-rich-repeats met A1.

Patiënten met een zogenaamde “Platelet-type von Willebrand Disease” mutatie in GpIbα hebben een bloedingsneiging doordat GpIbα spontaan aan vWF bindt. Hierdoor ontstaan plaatjes-aggregaten die geklaard worden in de milt. De GpIbα en A1•GpIbα-complex structuren verklaren deze spontane vWF-GpIbα interactie. Deze mutaties komen namelijk voor in de zogenaamde β-switch van GpIbα die niet geordend is in vrij GpIbα, maar een β-hairpin conformatie heeft in het A1•GpIbα complex. De mutaties promoten de β-hairpin conformatie waardoor GpIbα spontaan aan A1 kan binden.

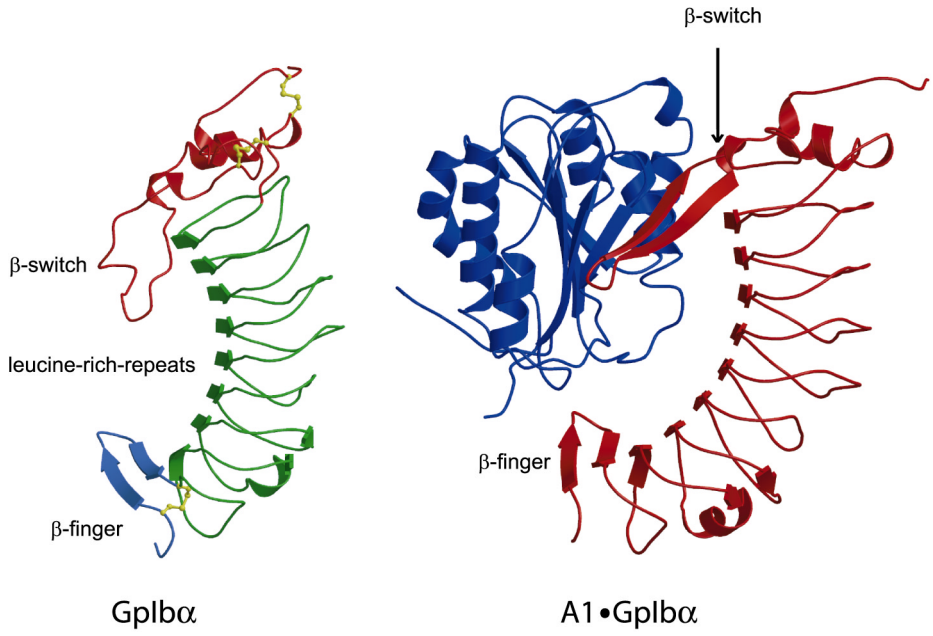

Figuur 2. Kristal structuren van GpIbα en A1•GpIbα. De β-switch in vrij GpIbα heeft een wanordelijke structuur. Echter, als GpIbα aan A1 bindt ondergaat de β-switch een conformatieverandering naar een β-hairpin structuur. De β-switch en andere locale GpIbα residuen binden aan de bovenkant van A1. De β-finger bindt aan de onderkant van A1 vlak bij het gebied in A1 waar de activerende 2B mutaties liggen. Residuen in de β-strands van de leucine-rich-repeats van GpIbα hebben lange afstand lading interacties met A1.

In normale situaties bindt het A1 domein van vWF niet spontaan aan GpIbα. Von Willebrand Factor moet eerst worden geactiveerd. Activering vindt plaats doordat vWF aan de vaatwand bindt. Er zijn patiënten met een zogenaamde von Willebrand Disease type 2B mutatie in het A1 domein waardoor vWF spontaan aan GpIbα bindt zonder dat vWF aan de vaatwand gebonden is. Deze patiënten hebben een laag vWF- en plaatjes niveau in hun bloed. Dit leidt tot bloedingen met allerlei complicaties. In **hoofdstuk 6** is deze activering bestudeerd. De kristalstructuren van wild-type A1 en van A1 met type 2B mutatie Arg543Gln werden bepaald. De enige conformatie verschillen werden waargenomen in de flankerende peptiden van A1. In wild-type A1 zijn deze peptiden georiënteerd in de richting van de GpIbα bindingsplaats en overlappen ze waarschijnlijk de GpIbα bindingsplaats in multimeer vWF. In Arg543Gln-A1 hebben de peptiden een andere oriëntatie welke niet kan overlappen met de GpIbα bindingsplaats. Op basis hiervan is de hypothese opgesteld zoals in figuur 3 weergegeven is. Niet geïmmobiliseerd vWF bevat een inactive conformatie doordat de flankerende peptiden de GpIbα bindingsplaats overlappen. Vaatwand-gebonden vWF is onderhevig aan hydrodynamische krachten van de bloedstroom waardoor de flankerende

peptiden van A1 als het ware van het domein worden losgetrokken en de GpIbα bindingsplaats geëxposeerd wordt.

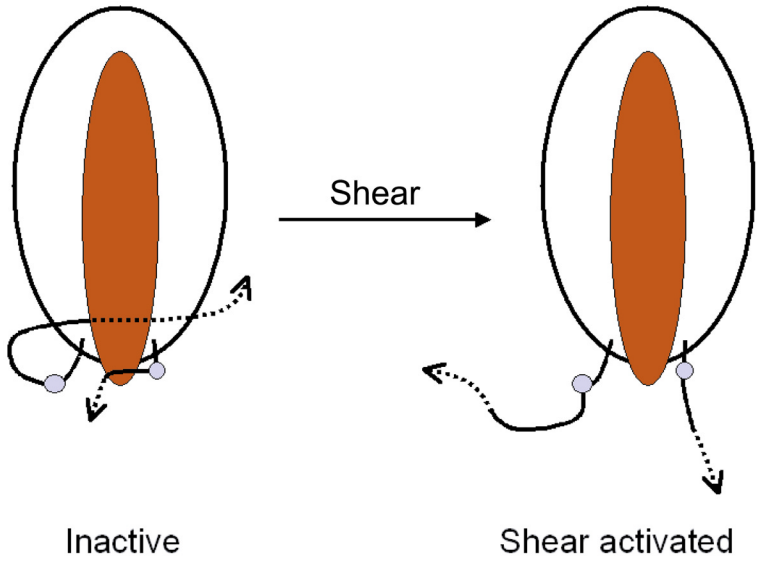

Figuur 3. Activatie-mechanisme van het vWF-A1 domein. In *rood* is de GpIbα bindingsplaats op A1 weergegeven. In inactief A1 overlappen de flankerende peptiden de GpIbα bindingsplaats. Door activatie worden de peptiden anders georiënteerd door een rotatie om een bepaald residue, aagegeven door de *blauwe* cirkel, aan de basis van de peptiden. Hierdoor wordt de GpIbα bindingsplaats geëxposeerd en kan GpIbα binden.

Onderwerpen voor verder onderzoek zijn: (i) het minimum aantal residuen in de flankerende peptiden in A1 dat nodig is om spontane GpIbα binding van geïsoleerd A1 te voorkomen en (ii) verdere bestudering van het activeringsmechanisme met als vraagstelling of activering plaats vindt doordat vWF geïmmobiliseerd wordt, of dat collageen conformatie veranderingen induceerd.

Conclusie

Von Willebrand Factor (vWF) is een essentieel eiwit voor de vorming van de haemostatische plug; vWF bindt bloedplaatjes via hun receptor GpIb-IX-V aan collageen op de plaats van vaatwandbeschadiging. Disfunctionering van collageen – vWF – GpIb-IX-V–as kan bloedingsneiging of arteriële trombose tot gevolg hebben. Het onderzoek zoals beschreven in dit proefschrift heeft inzicht verschaft op moleculair niveau in de interacties van vWF met zowel collageen als met GpIbα. Deze gegevens kunnen van belang zijn voor de ontwikkeling van medicijnen tegen arteriële trombose.

Hoofdstuk 9

Film in het Nederlands

 gebruik deze link om de film te starten (click on this link to start the movie)

Dankwoord

Ziezo, het proefschrift is dan eindelijk klaar.

Daarom wil ik een aantal mensen bedanken die mij al die jaren op het lab. en daarbuiten hebben bijgestaan. Jan Sixma, mijn promotor, bedankt voor alle enthousiasme en kennis die je de afgelopen vier jaren hebt over gebracht. Nu ik – als je laatste AIO – het vWF-project heb afgesloten, kun je rustig van een welverdiende oude dag gaan genieten. Piet Gros, tweede promotor, je bent waarschijnlijk voorlopig nog niet van mij af, want kristallografie is een mooi vak. Eric Huizinga, co-promotor, bedankt voor alle inspiratie en toewijding je mij hebt gegeven. Winnifred Wuyster, dankzij jou zijn hoofdstukken twee en drie mogelijk geworden! Iedereen van lab 1, Marion, Shizuko, Martin IJ, Martin B, Martijn, Douwe, Chantal, Hanneke, Domenico, Ya-Ping, Wilco, lab 2, lab 3, kristallograven, Barend, Lucy, Mitja, Sjors, Classien, Annika, en alle anderen die ik onbewust ben vergeten: jullie waren en zijn fijne collega's.

Verder gaat mijn grote dank uit naar jullie, mijn ouders en schoonmoeder, want jullie hulp was echt geweldig.

Monique, je hebt altijd gezegd dat er meer in het leven is dan wetenschap alleen. Nu mijn proefschrift dan klaar is hebben we daar eindelijk meer tijd voor. Peter, Sander en ……. Pappa is er voor jullie!

Roland

Curriculum vitae

De schrijver van dit proefschrift werd geboren op 12 februari 1971 te Tiel. Het MAVO diploma werd in 1988 behaald aan de Dominicus MAVO te Tiel en het HAVO diploma in 1990 aan de Rijksscholen Gemeenschap eveneens te Tiel. In 1994 werd het HBO-diploma Chemie, afstudeerrichting biochemie, behaald aan de Hogeschool van Utrecht. Tijdens deze studie werd een één-jarige stage volbracht bij Gist-brocades te Delft. Hierna werd de verkorte opleiding scheikunde begonnen aan de Universiteit Utrecht met een biochemisch hoofdvak bij de vakgroep "Centrum voor Biomembranen en Lipide Enzymologie" onder leiding van Prof. Dr. B. de Kruijff. In 1996 werd het diploma behaald.

Van september 1996 tot en met november 1997 was hij werkzaam als analist bij diverse vakgroepen aan de Universiteit Leiden.

Van december 1997 tot en met februari 2002 was hij werkzaam als onderzoeker-in-opleiding bij het Laboratorium voor Thrombose en Haemostase van het Universitair Medisch Centrum Utrecht (onder leiding van Prof. Dr. J.J. Sixma) en de Sectie Kristal- en Structuurchemie van het Bijvoet Centrum voor Biomolecular Research, faculteit scheikunde, Universiteit Utrecht (onder leiding van Prof. Dr. P. Gros) alwaar het in dit proefschrift beschreven onderzoek werd uitgevoerd.

Vanaf maart 2002 werd begonnen aan een project om een assay op te zetten om de activiteit van het von Willebrand Factor cleaving protease in (TTP)-patiënten te bepalen. Dit onderzoek vindt eveneens plaats bij het Laboratorium voor Thrombose en Haemostase.